Report

2016 Technology Demonstration Workshop (TDW) on Gamma Imaging-External

Summary: *This document is an edited version of the restricted technical report SG-EX-14311 Technology Demonstration Workshop on Gamma-Ray Imaging prepared by the Joint Research Centre, the European Commission's in-house science service. The scientific output expressed does not imply a policy position of the European Commission. This document summarizes the results from the IAEA's Technology Demonstration Workshop (TDW) on gamma imaging held at the IAEA 19-23 October 2015. This technical report was originally prepared by Mr. A. Rozite.*

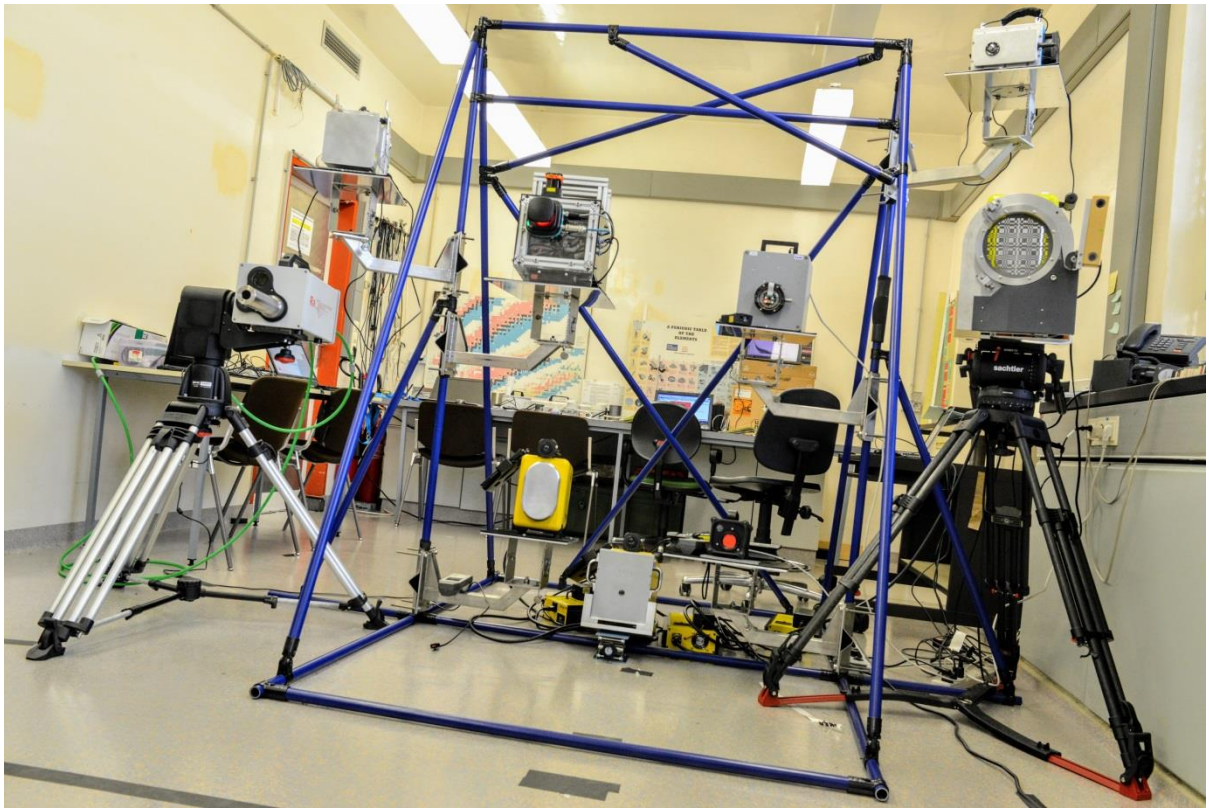

Figure 1 - Gamma Imaging systems being tested

Table of Contents

1 Purpose and Scope 5
2 Executive summary 5
3 Background 7
4 Participating systems at the workshop 11
4.1 GeGI 15
4.2 HEMI 18
4.3 HiSpect 19
4.4 iPIX 20
4.5 N-Visage 21
4.6 ORNL HPGe Imager 21
4.7 Polaris-H 24
4.8 RadSearch 26
5 Experiments 28
5.1 Experiment 1: Sensitivity 30
5.1.1 Comparison of spectra and images measured 30
5.1.2 Summary of the results 37
5.2 Experiment 2: Overnight Localization 40
5.2.1 Comparison of the results 41
5.2.2 Summary of results 43
5.3 Experiment 3: Sensitivity to Nuclear Materials 44
5.3.1 Plutonium measurements 44
5.3.2 Uranium measurements 52
5.3.3 Simultaneous U and Pu measurements 60
5.4 Experiment 4 and 5: Angular Resolution 70
5.5 Experiment 6: Extended Source 83
5.6 Experiment 7a: False Alarm Rate 88
5.7 Experiment 7b: High Background 91
5.8 Experiment 8a: Angular Resolution for Extended Sources 100
5.8.1 Experiment E8 – extended HEU sources 100
5.8.2 Experiment E8 – HBPu sources 101
5.9 Experiment 8b: Glovebox Scenarios 102
5.9.1 Low-activity scenario 102
5.9.2 High-activity scenario 103
5.9.3 Fumehood high activity scenario 104
6 Performance vs. Contextual Usage Scenarios 105
7 Conclusion 117
7.1 Conclusion to measurement campaign 119
8 References 122
9 Technical Contacts 123
10 Document Revision History 123

1 Purpose and Scope

Purpose: Technology Demonstration Workshop (TDW) on gamma imaging was organized by the IAEA at the IAEA's Seibersdorf laboratories from 19 to 23 October 2015. The goal of workshop was to evaluate technologies utilized in gamma imaging systems and to complete a status review of the currently available methods and perspectives of the development of this emerging field with an emphasis to nuclear safeguards.

Scope: This report is intended to document and inform interested (external) parties of the results of the workshop.

2 Executive summary

During the past decade, major improvements in growth of compound semiconductor crystals for radiation detectors and in segmentation of high-purity germanium detectors, as well as a deep understanding of the advantages of using of semiconductor detectors in the context of coded-aperture and Compton imaging occurred.

This document summarizes research and development results, which were demonstrated at the workshop by participants on the creation of new generation of gamma-ray imagers applicable for nuclear safeguards and other closely related applications.

At the workshop the following eight gamma ray imagers were presented:

- GeGi – Compton/pinhole imager based on HPGe detector
- HEMI – Compton 3D volumetric imager based on room temperature CZT detectors
- HiSpect – coded-mask imager based on room temperature CZT detectors
- iPIX– coded-mask imager based on room temperature CdTe detector
- ORNL HPGe Imager – coded-mask imager based on HPGe detector
- N-Visage– proximity 3D volumetric imager based on room temperature CZT detector
- Polaris-H – Compton imager based on room temperature CZT detector
- RadSearch – 2D scanner based on LaBr3 detector

Two mature imaging technologies, coded-mask or Compton imaging, are deployed in six systems. Five systems are based on segmented semiconductor detectors and four systems are based on 3D position sensitive detectors.

The goal of the workshop was to evaluate technologies utilized in gamma-ray imaging systems and make a review and conclusion about current status and perspectives of the development of this emerging field with an emphasis to nuclear safeguards. In order to achieve this goal, different types of static measurements with radioactive sources and nuclear materials were conducted.

The following eight experiments were conducted with the systems:

- Experiment 1 – Measurements of sensitivity in wide energy range of imager operation
- Experiment 2 – Overnight localization and identification of weak source in the presence of a masking source
- Experiment 3 – Measurements of sensitivity to nuclear materials, time to detect, identify and localize nuclear materials

- Experiment 4 – Angular resolution
- Experiment 5 – Field of view
- Experiment 6 – Localization performance for extended source
- Experiment 7 (a) – False alarm rate
- Experiment 7 (b) – High-background masking scenario
- Experiment 8 (a) – Angular resolution for extended sources
- Experiment 8 (b) – Glove box scenarios

In addition, dynamic measurements have been made to reveal performance characteristics of 3D volumetric Compton imager.

Compared to conventional gamma-ray spectrometry imaging of a radioactive source, it is done at a cost of losing some sensitivity. For example, in Compton imaging only a fraction of full-energy peak events are suitable for imaging purposes and in coded aperture imaging just a portion of photons reach the detector due to absorption in the mask material; moreover sufficient statistics is needed to create shadow of mask pattern projected on the detector. In other words, source localization time in the form of image may take minutes compared to seconds required to achieve the necessary number of standard deviations in a full energy range or in full-energy peak, which may be referred to detection or identification time in conventional gamma-ray spectrometry. However, statistical principles of data processing are quite similar.

Therefore, tests under experiments 1 and 3 were focused on the estimation of total sensitivity and sensitivity in full-energy peaks. Experiments were conducted with Am 241, Cs-137 and Co-60 to cover wide energy range of imager operation and with HBPu, LBPu, HEU and LEU to evaluate sensitivity to nuclear materials.

Four gamma-ray imagers presented at the workshop, are based on 3D position sensitive semiconductor radiation detectors, which makes the application of combined coded aperture/Compton imaging methods possible. Sensitivity measurements, allowed the IAEA to evaluate and compare the suitability of gamma-ray imagers for both imaging modes.

Test under Experiment 2 and 7 (b) have revealed, the importance of having spectrometric information for coded-aperture imaging, in order to enhance imaging capabilities, which is achieved by imaging the events from the selected region of interest in the spectrum. In Compton imaging full-energy peak events are imaged, therefore Compton imager shall be spectrometric.

As soon as nuclear materials such as, HEU and LBPu are characterized by relatively low energies of emitted photons coded-aperture imaging, it could be considered as a necessary mode of imager operation for the tasks associated with activities of nuclear safeguards.

Angular resolution and field of view of coded aperture imaging is is impacted by the choice of a mask pattern, by the distance between mask and a detector, and by the spatial resolution of the detector. Therefore, basic tests under experiments 4 and 5 were aimed to reveal performance of coded-aperture imagers and in particular to evaluate level of segmentation of semiconductor radiation detectors, whether it is appropriate to address safeguards tasks or not.

Tests under Experiment 6 have demonstrated, an advantage of using mask-anti mask imaging method for imaging of a pattern of extended sources, which is widely distributed across the field of view.

Tests under Experiment 7 (b) and Experiment 8 (b), have demonstrated advantage of having combined coded-aperture/Compton imager.

Tests under Experiment 2 and 8 (a), have demonstrated independence of gamma-ray imagers in their ability to detect and localize radioactive source from necessity in having background measurements.

As a result of the analysis of experimental results, it can be concluded that new generation of gamma-ray imagers possess the following essential features already demonstrated by participants at this workshop:

- Application of semiconductor radiation detectors
- High-level of segmentation of CdTe, CZT and HPGe detectors
- Application of 3D position sensitive semiconductor detectors
- Combination of coded-mask/Compton imaging methods
- Performing dynamic gamma-ray imaging – 3D volumetric Compton imager has been successfully demonstrated.

3 Background

Photons emitted by nucleus as a result of decay or spontaneous fission, are not visible by the human eye. The primary concept behind any gamma-ray imaging system is in visualization of the distribution of radioactive sources in space. This goal is achieved by different imaging methods and at the final step, by overlaying obtained gamma-ray image with the visual image of the inspected object.

Historically, gamma-ray imaging has been pioneered in other fields, and now, Compton and coded-mask methods have been proposed for nuclear safeguards.

For applications which are close to nuclear safeguards by their nature, transportable instruments such as, Gamma-Visor [1] and CARTOGAM [2] have been developed and deployed at nuclear facilities in the past. The latter one was successful in terms of commercialization, and both went through two evolutionary steps, initially a pinhole was used to generate gamma-ray image and then a single aperture was replaced by coded-mask [3][4]. In these systems application of array of scintillation radiation detectors, allowed to create gamma-ray images within certain field of view using single measurement and achieving good spatial resolution.

Another approach has been implemented in the development of gamma-ray scanner [5], based on well collimated radiation detector, which can be focused on a particular area by means of automated positioning mechanism. An imaging area can be divided into consequent scan elements. Spectrum of each scan element can be recorded. Depending on the variations of amplitude of signal between scanning elements gamma-ray image of the whole area can be created, but many measurements are needed.

Modern gamma-ray imaging systems are progressing to small, portable and preferably hand-held systems. As soon as no visual information on source distribution in space is available for the operator prior to gamma-ray imaging, the device shall have relatively wide field of view in order to minimize the number of measurements during the search for the source. In the meantime, the instrument should have good spatial resolution to find anomalies in the radiation field, which may be created by several sources or by an extended source. Inherent property of the instrument, should have the ability to

identify source type. Detection efficiency in combination with used imaging methods, should allow the operator to perform his analysis tasks within a reasonable timeframe, typically minutes for non-complex task, such as localization of point source, which creates a dose-rate at an imager position comparable to the fraction of background dose rate.

Imaging is done at a cost of losing some sensitivity, it could be illustrated by a pinhole imaging method (Figure 2), where a passive screen with a single aperture in the centre is placed between the detector and the source of radiation. Material, density and thickness of the screen are selected so radiation could typically pass only through the hole in the screen. Radiation passing through this hole is projected on the detector and an inverted gamma-ray image of the source pattern is generated. Position sensitive detectors, shall be used to generate an image. Location of the radiation pattern on a detector reflects the location of the source in space. Signal measured by the detector is less intense compared to the signal, which could be measured in case, if there would be no passive screen in front, but at a cost of losing detection efficiency, imaging capability is obtained.

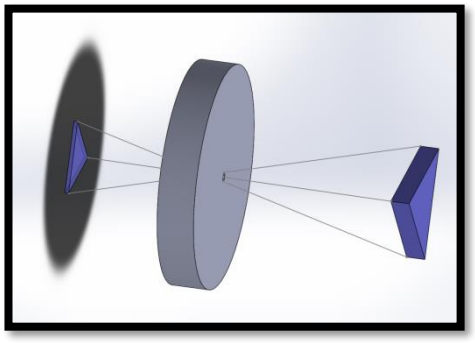

Figure 2. Illustration of pinhole imaging method

Sensitivity of pinhole imagers could be improved by using a coded-mask[6][7], where radiation could pass through multiple apertures, which form a certain pattern. Open area of a mask could reach 50%. Radiation passing through the mask creates a shadow on the surface of position sensitive detector (Figure 3).. Multiple sources will create a common shadow, which has to be subdivided in multiple shadows or in other words de-convoluted; therefore, a special mask pattern shall be used. Results can be improved by using a mask/anti-mask procedure. Anti-mask has an inverted pattern of apertures compared to the mask, so the measurement cycle composed from two measurements should be done.

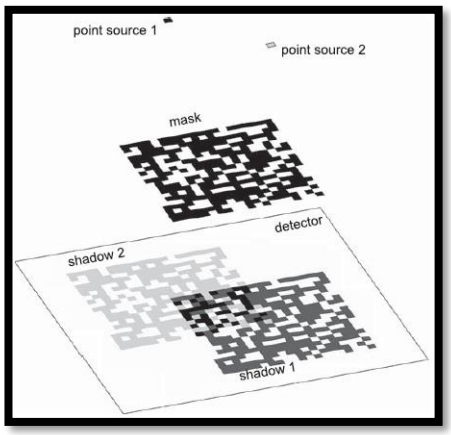

Figure 3. Illustration of coded-mask imaging method [8]

Coded aperture imaging, is more effective for low energies than high energies, since high energy photons may tend to pass through the mask [8].

Since Compton scattering is predominant photon energy, the absorption process is already at energies of photons of several hundred keV even for high-Z detector materials, another imaging method which can be used is Compton imaging.

In Compton imaging, two position sensitive detectors could be used. As shown in Figure 3 below [8], a photon scatters in the first detector and is absorbed in the second detector. Using energy and position measurements, the scattering angle of the photon can be estimated, and its original source location can be isolated to a cone with a vertex at the first measurement point. The intersection of many such rings (Figure 4), produced by a single source, projected on to an imaging plane, identifies the position of that source [8].

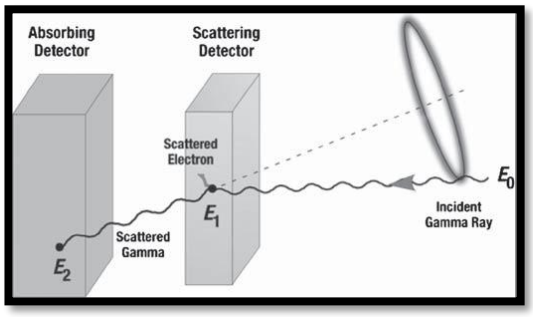

Figure 4. Illustration of Compton imaging method [8]

Compton imaging and coded aperture are most effective in different energy ranges, it is natural to consider the application of both modalities, when seeking to image sources, which range in energy from 100 keV to 2.5 MeV [8].

Another imaging method under development in one of the systems is the usage of active coded mask and potentially combination of two imaging modes; Photons which interact in both an active mask element and the absorbing back detector are treated as Compton imaging events, while photons interacting only in the back detector are treated as coded aperture events [8]. This is of interest for

many applications including nuclear safeguards to perform dynamic gamma-ray imaging. Gamma-ray imaging and detection technologies are summarized in Table 3 and Table 4.

4 Participating systems at the workshop

The following (Table 1, Table 2, Table 3, and Table 4) summarize the technical specifications of each system that was demonstrated at the workshop.

Table 1. Description of gamma-ray imagers

Gamma imaging system	Dimensions	Weight
GeGI	31 x 15 x 23 cm	14 kg
HEMI	28 x 18 x 18 cm	4.5 kg
HiSpect	20 x 21 x 23 cm	8 kg
iPIX	19 x 11 x 11 cm	2.5 kg
N-Visage	Prototype	Prototype
ORNL HPGe Imager	31 x 15 x 23 cm	14 kg
Polaris-H	21 x 19 x 13 cm	4 kg
RadSearch	66 x21 x 18 cm	44 kg (with tripod)

Table 2. Field of view, energy range of operation and energy resolution of imagers

Imager	Field of view, degrees	Imaging energy range of operation, keV	Energy resolution at 662 keV, %
GeGI	4π (Compton) 60° (pinhole)	140 – 3000 (Compton) 30 – 600 (pinhole)	0.28 (E1M2)
HEMI	4π	250 - 3000	3.7 (E1M2) for coincident events
HiSpect	35°	30 - 1300	2.0
iPIX	41.4° – 44.8°	30 - 1200	N/A
N-Visage	4π	30 - 1800	N/D
ORNL HPGe Imager	12° - 110° (coded-mask) 4π (Compton)	30 – 650 (coded-aperture) 650 – 2050 (Compton)	0.28
Polaris-H	4π	250 - 8000	1.0
RadSearch	4° (single scan) 4π (multiple scans)	30 - 2000	3

Table 3. Summary of imaging technologies utilized in gamma-ray imagers

Imager	Detector type	Imaging technology 1	Imaging technology 2	Imaging technology 3

Imager	Detector type	Imaging technology 1	Imaging technology 2	Imaging technology 3
GeGI	Semiconductor	Compton imaging	Pinhole imaging	
HEMI	Semiconductor	Compton imaging	3D Volumetric Compton imaging	Active coded-aperture imaging
HiSpect	Semiconductor	Coded-aperture imaging		
iPIX	Semiconductor	Coded-aperture imaging		
N-Visage	Semiconductor	3D proximity imaging		
ORNL HPGe Imager	Semiconductor	Coded-aperture imaging	Compton imaging	
Polaris-H	Semiconductor	Compton imaging		
RadSearch	Scintillation	2D scanning*		

** By bold are marked technologies which are fully implemented*

Table 4. Summary of detection technologies utilized in gamma-ray imagers

Imager	Detector material	Detector type	Detector size	Number of detector sensing elements
GeGI	HPGe	3D position sensitive	90 x 10 mm	16 x 16 orthogonal strips
HEMI	CZT	Two arrays based on 96 single crystal detectors	32 x 1 cm^3 – front plane 64 x 1 cm^3 – back plane	96 coplanar grid CZT detectors
HiSpect	CZT	3D Position sensitive	40 x 40 x 5 mm	16 x 16 pixels
iPIX	CdTe	2D Position sensitive	14 x 14 x 1 mm	256 x 256 pixels
N-Visage	CZT	Single crystal	10 x 10 x 5 mm	1
ORNL HPGe Imager	HPGe	3D position sensitive	90 x 10 mm	16 x 16 orthogonal strips
Polaris-H	CZT	3D position sensitive	20 x 20 x 15 mm	11 x 11 pixels
RadSearch	$LaBr_3$	Single crystal	Ø25.4 x 25.4 mm	1

Table 5. Summary of software features of gamma-ray imagers which could be essential for operator

Software features	GeGI	HEMI	HiSpect	iPIX	N-Visage	ORNL HPGe Imager	Polaris-H	RadSearch
Is it possible to acquire an overall spectra of the entire target	**Yes**	**Yes**	**Yes**	**No**	**Yes**	**Yes**	**Yes**	**Yes**
Isotope and energy ROI, is it possible to:								
Select a specific isotope (and study the spectra/count profile on the image)	**Yes**	**Yes**	**No**	**No**	**No**	**Yes**	**Yes**	**Yes**
Select a several isotopes (and study the spectra/count profile on the image)	**No**	**Yes**	**No**	**No**	**No**	**Yes**	**Yes**	**Yes**
Select 1 ROI in the energy (and study the spectra/count profile on the image)	**Yes**	**Yes**	**Yes**	**No**	**Yes**	**Yes**	**Yes**	**Yes**
Selects several ROI in the energy (and study the spectra/count profile on the image)	**Yes**	**Yes**	**Yes**	**No**	**No**	**Yes**	**Yes**	**Yes**
See the spectra associated with a specific zone of the image	**Yes**	**No**	**No**	**No**	**No**	**Yes**	**No**	**No**
Acquisition grouping and reconstitution, is it possible to:								
"Combine/cumulate" counts from different measurements (for example if we have two 30-minute acquisitions, is it possible to merge them into one 1-hour measurement?)	**No**	**No**	**Yes**	**No**	**No**	**Yes**	**No**	**No**
Make "backward reconstitution" from a long acquisition (for example if we have 1-hour acquisition, is it possible to see the picture as after 10 minutes from the beginning?)	**No**	**Yes**	**Yes**	**Yes**	**Yes**	**Yes**	**Yes**	**No**
Result export, is it possible to:								
Export overlaid image and visual/gamma images separately?	**Yes**	**Yes**	**Yes**	**Yes**	**Yes**	**Yes**	**Yes**	**Yes**
Is the output spectra format is human readable or compatible with some standard spectra viewing software?	**Yes**	**No**	**Yes**	**No**	**No**	**Yes**	**Yes**	**Yes**
Is it possible to program the camera to take automatic scheduled measurements?	**Yes**	**No**	**No**	**Yes**	**No**	**Yes**	**Yes**	**Yes**

4.1 GeGI

HPGe detectors are a good choice for a Compton camera, not only because of the energy resolution, but that they can be made relatively large, providing good detection efficiency. A break-through in the detector technology was the introduction of the planar HPGe detectors using the amorphous germanium contact technology [12]. This technology has replaced the difficult to segment lithium diffused p+ contacts, and in some instances even the standard boron implanted n+ contacts, so that high levels of electrode segmentation have become reliable.

There is an objective difficulty towards making hand-held HPGe-based gamma-ray imager, which is associated with necessity in cryogenic cooling of HPGe detector. During past decade, miniature Stirling-cycle cryocoolers suitable for HPGe detector cooling, became available from various vendors. Currently, HPGe detectors could be cooled down to operating temperature using compact cryocoolers with cooling power ranging from couple of watts up to dozens of watts at 80K.

For this instrument, a cryocooler has been selected so it could provide fast cool down time from room to operating temperature even for large volume HPGe detector.

The system tested during the workshop is the GeGi-4 (a fifth generation has in the meantime been released, with a smaller footprint). GeGI is based on segmented HPGe detector having diameter 90 mm and thickness 10 mm. HPGe detector is cooled by means of Stirling-cycle cryocooler. Detector cryostat is sealed with metal gaskets; the vacuum support system is based on hydrogen/water getter pumps and on the ion pump for removal of non-active gases. The Ion pump can be switched on independently from a cryocooler. Cool-down time of a HPGe detector from room to operating temperature demonstrated at the workshop was three hours.

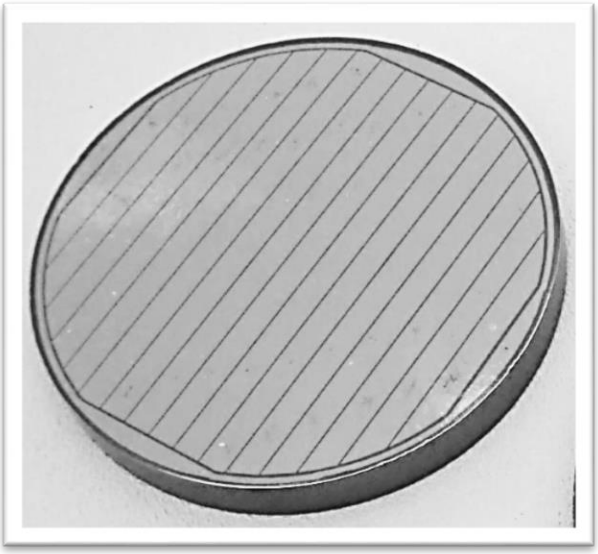

Figure 5. Segmented HPGe detector in the holder [17]

HPGe detector is 3D position sensitive. X, Y – position of photon energy deposition in detector is measured by 16x16 orthogonal strips. Strip pitch is 5 mm and gap is 0.5 mm [15]. Z position is measured using differences in time arrival of charge carriers to electrodes.

First mode of operation of an imager is a Compton mode. In this mode, energy spectrum is measured in the whole energy range, full energy peaks are identified and radioactive source emitting photons with energies ranging from 140 keV to 3 MeV could be localized. To be imaged, photons need to scatter in the detector first and then have to be absorbed, so that a low energy threshold is basically determined by the properties of germanium i.e. predominance of full-energy absorption of incoming photon at energies below 140 keV. Field of view of a Compton imager is 4π. Scientific plot of basic operator window shows, the intersection of Compton cones on the globe, so the operator could reveal presence of the source behind gamma-ray imager.

In case low-energetic full-energy peaks are identified, localization of radioactive source could be done by using pinhole mode of operation and new measurement needs to be performed. GeGI was equipped with two removable 25 mm thick blocks made from lead with 1 mm and 5 mm pinholes having 60° opening cone.

For imaging geometries of extended sources, the pinhole mode of operation is considered as a default and more contrast images can be obtained with a 1mm pinhole compared to the images obtained with a 5mm pinhole. In this mode apart from basic gamma-ray image, energy spectrum and 3D-diagram of events deposition across field of view are available. The main window of the graphical user interface is shown in Figure 6 below.

At the workshop two identical systems were used, one operating basically in Compton mode and the second one in pinhole mode.

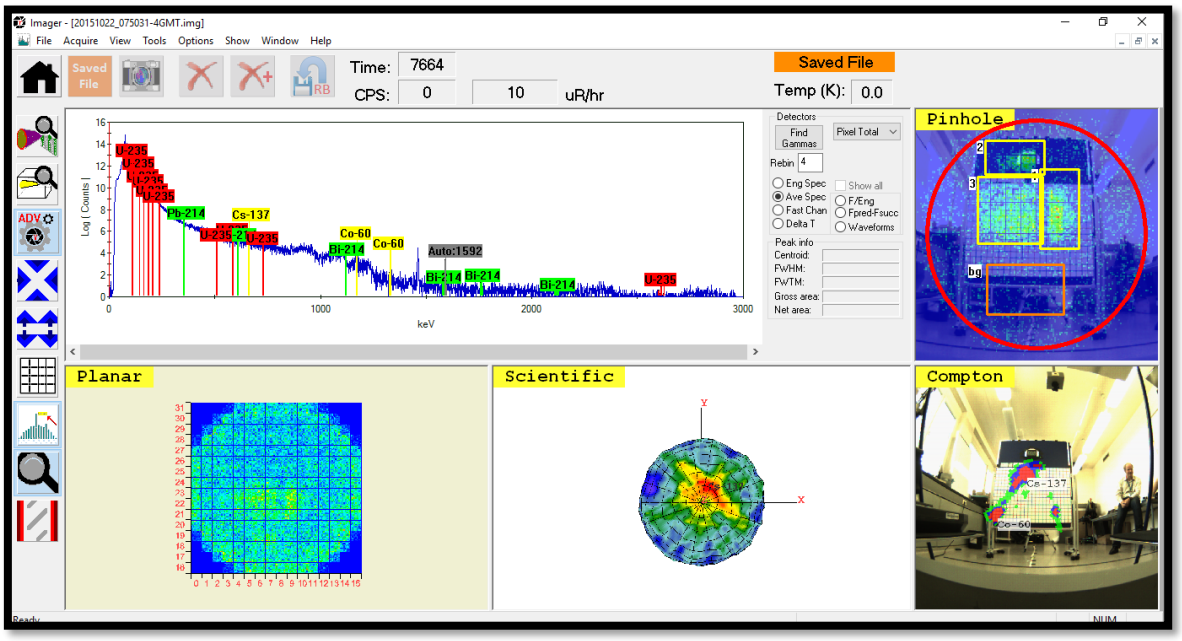

Figure 6. GeGI operator window, advanced mode.

Summary of technologies utilized in GeGI:

- Electrical cooling of HPGe detector with little compromise on energy resolution
- Reliable vacuum support system
- Amorphous Ge contacts with high level of segmentation
- 3D position sensitive HPGe detector
- Compton imaging
- Pinhole imaging

4.2 HEMI

HEMI is a prototype hand-portable gamma-ray imaging system. It consists of 96 individual 1 cm^3 CZT crystals, each with a coplanar grid electrode configuration and low-power ASIC readout. The detector elements are arranged in a two-plane active-mask configuration with the front plane half populated (32 elements) and the back-plane fully populated (64 elements).

Imaging results for HEMI and analysis of the imaging results in the course of this report were provided by the developers, as well as information below with description of the imager operating principles and hardware.

The active mask configuration was selected to allow both coded aperture and Compton imaging modalities, principally providing gamma-ray imaging capabilities for energies ranging from below 100 keV to several MeV. HEMI has a modular design that enables it to be packaged with different sensors and in different deployment modes, such as hand-held or unmanned aerial platforms.

When fully assembled in the hand-held configuration, HEMI, including an on-board battery and all auxiliary sensors, weigh less than 4.5 kg. The battery is sufficient to operate continuously for about four hours. As is, HEMI is capable of traditional 2D directional gamma-ray imaging, without any additional sensors. Currently, only the Compton modality has been implemented in real-time. The coded-aperture capability, while demonstrated conceptually, is an area of active research.

HEMI leverages a new ability to integrate gamma-ray and contextual information in 3D in real-time. This is accomplished by combining the system with a visual sensor, that is used to track the location and orientation (or pose) of the detector, while also creating a 3D map of the scene via a technique known as simultaneous localization and mapping. The 3D model and tracking information are then combined with the gamma-ray data to localize gamma-ray sources within the reconstructed scene in all three spatial dimensions. The 3D model, not only provides context for the gamma-ray image (analogous to overlaying a 2D gamma-ray image onto an RGB image), but can also be incorporated in the gamma-ray image reconstruction. Simple data fusion techniques have been shown to improve the tractability of the imaging problem; improving localization capability and reducing image noise, while greatly reducing the computation time. The visual sensor used in this case is a Microsoft Kinect, which provides, both RGB images and dense point cloud models in the field of view at up to 30 Hz frame rate.

The most obvious advantage of the volumetric imaging approach, is the ability to reconstruct the spatial distribution of radiation sources in all three spatial dimensions.

Having a real-time mobile imaging platform confers other advantages as well. For example, the 3D measurements require runs on the order of one minute (30-90 seconds long). A limiting component in measuring gamma-rays is the inverse r-squared geometric factor that greatly reduces counts and is an inherent limitation for the static mode. Moving the detector throughout the scene can reduce the distance to objects, which helps to overcome the geometric factor thus reducing localization time or increasing sensitivity to weaker or shielded sources.

Summary of technologies utilized in HEMI:

- Two large volume room temperature CZT detector arrays
- Volumetric Compton Imager
- Active coded-mask (under research and development)

4.3 HiSpect

HiSpect is based on array of 4 room temperature CZT detectors. Dimensions of each detector are 20x20x5mm. Each detector has 64 pixels, energy resolution for Co-57 obtained with detectors array is about 2.5%. The software has a simple graphical user interface, which allows the operator to control measurements, see alarms, identification and localization flags, get gamma-ray images along with spectrum, as well as get image from particular ROI or dynamic range image based on the ratio of ROIs.

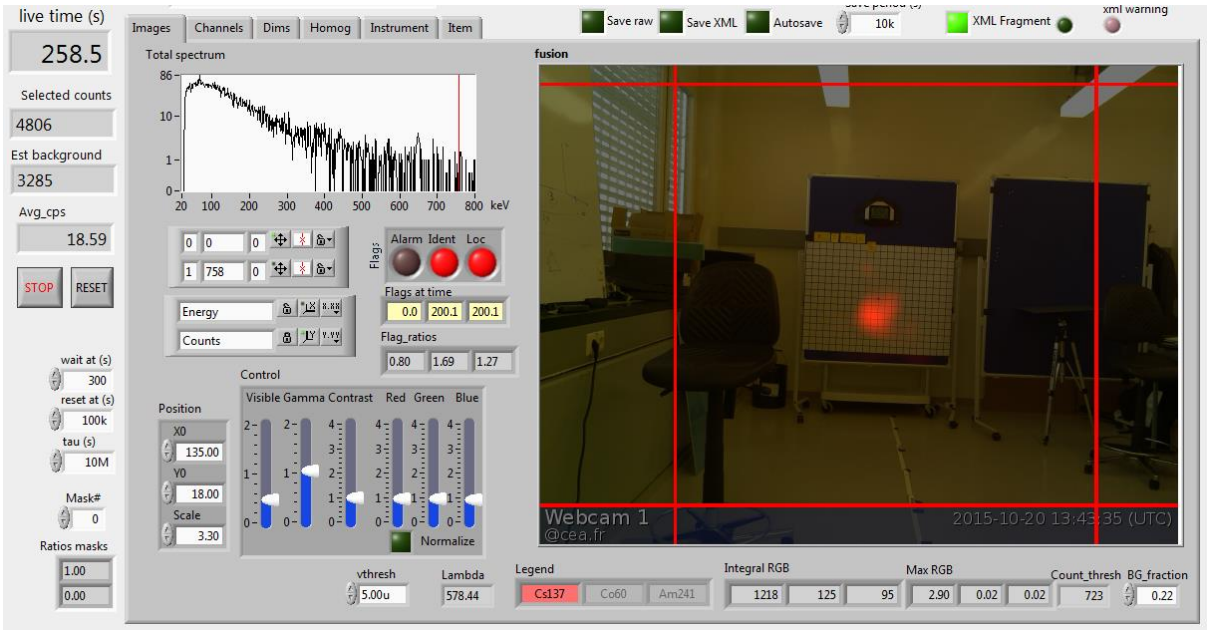

Figure 7. HiSpect main user interface window

Software is written in LabView and the main user interface tab shows:

- Blended image of optical and gamma ray views. Each color channel (red, green, blue) is attributed to a certain isotope.
- Total spectrum acquired by the detector (human readable export format)
- Control slides allowing to control relative intensities and contrast of the 3 gamma channel, and of the optical image
- Flags at time to alarm, time to identify and time to localize

Summary of technologies utilized in HiSpect:

- Coded-aperture imaging with HURA mask
- 3D position sensitive semiconductor radiation detector

4.4 iPIX

iPIX is a coded-aperture imager based on a room temperature CdTe detector that is 2D position sensitive and highly pixilated. While spectrometric information from room temperature of the CdTe detector could be obtained, the iPIX imager demonstrated at workshop does not have any spectrometric capabilities. There are three basic reasons, why the imager is not spectrometric:

a) Operation at room temperature does not fully explore spectrometric capabilities of CdTe detector
b) Thickness of the detector is 1mm, which limits full-energy peak efficiency even at relatively low energies (about 10% of intrinsic photoelectric efficiency at energy 200 keV and about 1% at energy 500 keV)
c) Spectrometry is not a requirement for coded-mask imaging method.

iPIX is based on a Timepix photon counting chip, hybridized with 14x14x1mm CdTe substrate. The active area is divided into 256x256 pixels (55μm side) working in single photon counting mode. Each pixel is divided into an analog and a digital part and can be considered as an individual counter. The hybridization of Timepix with a semiconductor enables a direct conversion from gamma-ray into electrical signal, which removes multiple conversion steps occurring in scintillation detectors [28].

The masks used, are machined from a tungsten alloy and identified by their rank and thickness. Three different masks (R7e4, R7e8 and R13e2) are currently available for this platform, providing two different mask ranks and three different thicknesses. The benefit to the higher mask rank is that it is more precise with angular resolution, albeit with a decrease in efficiency (due to less open area). Increasing the mask thickness, provides more gamma filtering in order to enhance the signal-to-noise ratio, albeit with an increase of weight and a decrease the off-axis response due to the local photon collimation.

The iPIX mask design is based on the MURA (Modified Uniformly Redundant Array) pattern, which can be inverted by a 90° rotation to perform “anti-mask” measurements. By using such masks with a stream of incident photons (from a remote radioactive source within the system field-of-view), the detected events of interest can be discriminated, without the use of additional shielding as a shadow of the part of the mask pattern illuminated by the radioactive source is directly cast onto the Timepix sensor.

Summary of technologies utilized in iPIX:

- 2D position sensitive CdTe detector with high level of segmentation
- Coded-mask imaging
- Mask/anti-mask imaging approach with the R7e4 and R7e8 masks

4.5 N-Visage

This instrument is based on proximity gamma-ray imaging. It utilizes room temperature and a spectrometric CZT detector for measurements of gamma-radiation and 3D laser-based system for reconstruction of imaging scene. Sensitive volume of CZT detector is 0.5 cm^3. In order to obtain 3D volumetric a gamma-ray image, the instrument needs to be moved in the space along all 3-dimensional coordinates. The instrument is at a prototyping stage and proof of imaging concept needs to be performed.

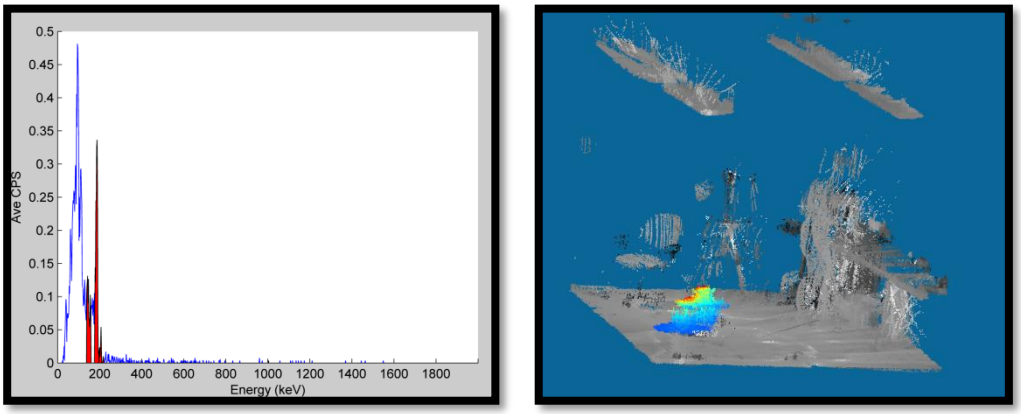

Figure 8. N-Visage proximity gamma-ray imaging of U source. Spectrum (left), offline reconstruction of imaging scene along with gamma-ray image (right)

4.6 ORNL HPGe Imager

In terms of hardware, ORNL HPGe Imager is similar to a GeGI completed by a coded-mask with 50% open area, thus improving the imaging efficiency of pinhole imaging method.

ORNL HPGe Imager uses mask / anti-mask data-acquisition strategy. MURA mask with 90° anti-mask is positioned on a software controlled mask positioning and rotating system, so distance between detector and mask could change and a higher field of view or better angular resolution of an image could be achieved, as well as the mask could be rotated by 90° to perform mask/anti-mask measuring cycles. Mask is 3 mm thick and is composed from Tantalum. Spectrum of each imaged pixel is available for operator.

The first figure below shows the setup window for point source alarms (upper window). There is a global alarm for all energy bands and three separate alarms, which can be user-defined. Each user-defined alarms, allow up-to three spectral regions of interest. In addition, a text identifier for the alarm and the threshold level can be set for each alarm. The alarms are displayed on the upper right of the acquisition display window (bottom left), and can be activated from that window via a check box. The indicator turns red when an alarm occurs. The acquisition display window includes a false-color picture of the gamma-ray image. To the right and below that image are one-dimensional histograms showing lineouts of the counts in the pixels in a row and column with the x and y for those histograms selected by clicking the mouse cursor. Each acquisition window can have up to four spectral windows associated with it. In the figure below, two spectral windows are open, the upper one showing the total

spectrum seen by the detector from a Cs-137 source, while the lower one shows the spectrum from the hot pixel in image.

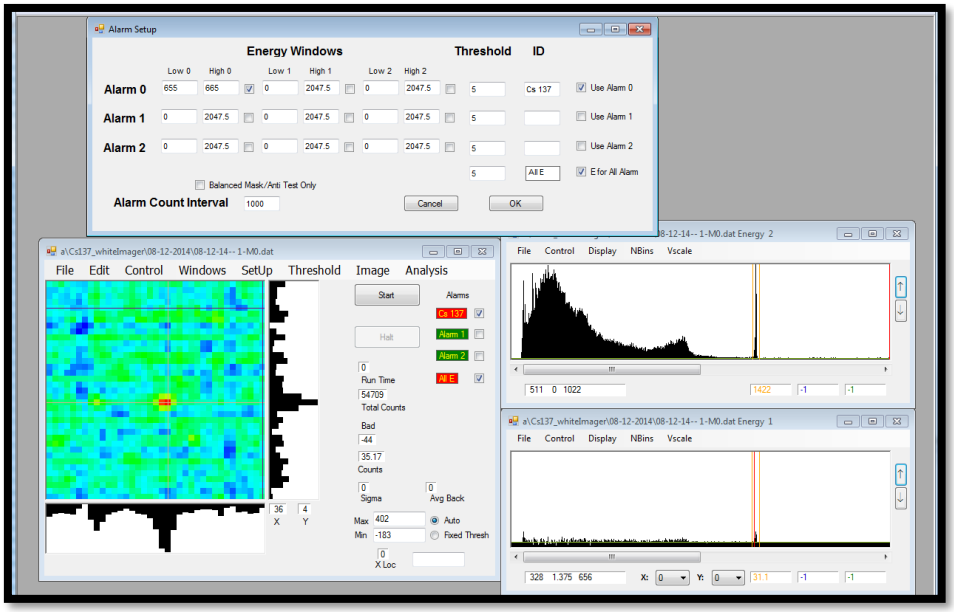

Figure 9. ORNL HPGe Imager basic operator setup windows.

The next figure below shows two setup windows, one for the acquisition time, and the other for the source distance and focal length (zoom). The acquisition window on the left shows the image obtained from several Pu blocks.

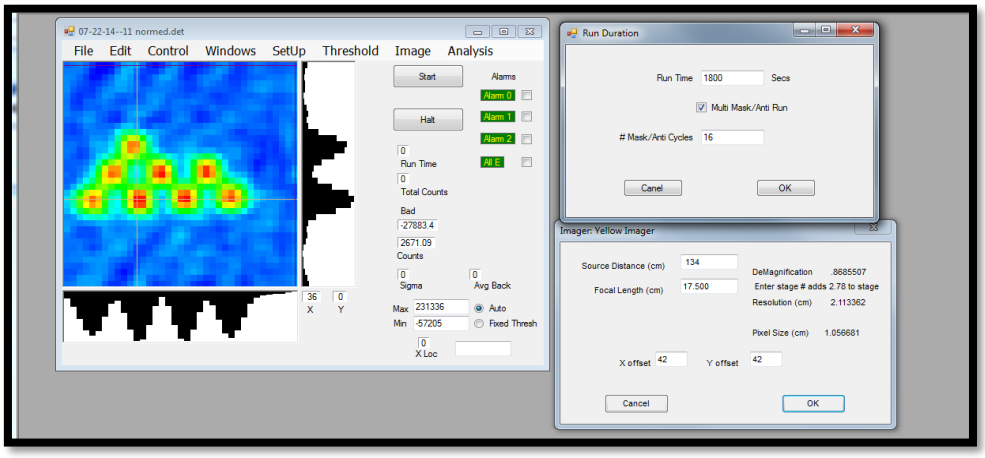

Figure 10. ORNL HPGe Imager additional operator setup windows.

The following figure shows some of the on-line analysis capabilities of the code. The data are stored as full hyperspectral data cubes and spectra can be viewed from regions selected in the image with the cursor (the lower spectrum is based on the pixels that are turned on in the false-color image). The image displayed can also be based on up-to three spectral regions of interest. A user selectable threshold allows one to turn pixels with low significance transparent to show where the hot spots fall on a scaled, visible-light image obtained with a stereo camera aligned with the system. The point cloud

data from the stereo imager can be used to map the gamma-ray data onto higher resolution point cloud data such as might be obtained with a laser scanner.

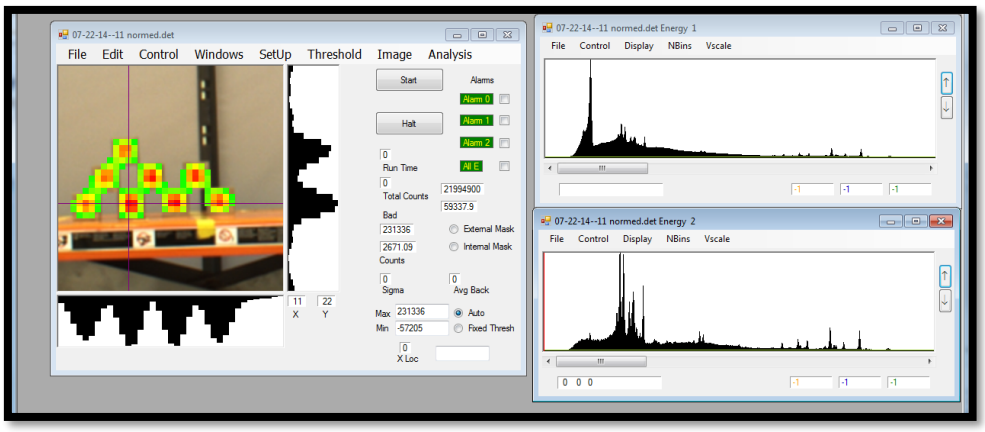

Figure 11. ORNL HPGe Imager online analysis capabilities.

The processing software used by the instrument is developed in the Microsoft Visual Studio.Net environment. It will easily handle kilohertz data rates, generating on-line gamma-ray images as the data are collected. Data acquisition is fully automated and uses a balanced mask / anti-mask acquisition cycle. This approach overcomes any issues with non-uniform radiation fields at the detector and makes the imaging very robust. The modified uniformly redundant array mask patterns used are antisymmetric on a 90° rotation. Such rotations are automatically performed by the software. The images are best with balanced mask / anti-mask sets, the system is generally operated by breaking long integration intervals into shorter individual mask / anti-mask sets. The rotations are handled by the software and this approach minimizes any artifacts that may occur due to the local radiation environment as the image is collected.

Overall, the software includes a full GUI that is part of the custom software. The GUI allows the user to enter the parameters for a given data acquisition (distance to the source, dwell time per mask configuration, the number of mask/anti-mask cycles, etc.), start and stop an acquisition, replay data files, and perform on- and off-line analysis. The code interfaces to the detector by sending commands via a memory pipe to the manufacturer's control software that runs in parallel with the code. Data are obtained via a separate memory pipe. The code will save list-mode data files that can be used to replay the data with corrected or updated parameters. In addition, the full hyperspectral data cubes can be saved in a compressed format so that the data can be explored in a simplified data viewer that does not include all of the instrument control functionality. Spectra and images can also be exported in text mode.

Summary of technologies utilized in ORNL HPGe Imager:

- 3D position sensitive semiconductor detector
- Coded-mask imaging
- MURA mask with 90° anti-mask
- Spectra on a pixel-by-pixel basis
- Variable focal length (variable field of view and angular resolution)

4.7 Polaris-H

Polaris-H integrates a 3D-position-sensitive pixilated CZT detector (20x20x15mm), associated readout electronics, an embedded computer, a 5h battery, and an optical camera in a portable water-proof enclosure. The total mass of the instrument is about four kilograms, and the system start up time is two minutes. Additionally, it has a connection for a tablet, which displays a gamma-ray spectrum and isotope-specific images of the gamma-ray distribution in all directions in real time. List-mode data is saved to an external USB memory stick. Based on pixilated depth-sensing technology, spectroscopy is routinely better than 1.1% FWHM at 662keV, and imaging efficiency at 662 keV varies less than a factor of two for all directions, except through the battery.

In the Polaris-H system, electron clouds produced by gamma-ray interactions in a CZT crystal drift in an applied electric field, inducing a signal on the planar cathode and on one of the 1.72-mm-pitch pixels on the anode surface (part of an array of 11-by-11pixels). The lateral position of the interaction is determined by the anode pixel that sees the signal. The interaction depth is determined by drift time of the electron cloud and/or the ratio of the cathode to the anode signal amplitude. As long as interactions occur under different pixels, multiple interaction positions – and the energy deposited at each – can be recorded simultaneously. This 3D position sensitivity allows calibration on a voxel-by-voxel basis (producing energy resolution often below 1% FWHM at 662keV) [23] and localization of gamma-ray interactions in the crystal permitting Compton imaging.

Low-energy Compton imaging threshold is about 250 keV please see Figure 12, however coded-mask imaging method is under development, which will allow to make imaging based on low-energy photon emissions such as 185.7 keV (U-235) and 208 keV (HBPu).

The instrument has a fully developed graphical user interface for recording spectra and creation of gamma-ray images online as well as useful post processing tool which allows operator to:

- reconstruct gamma-ray images based on the saved spectra
- save spectra in human readable format
- automatically identify radionuclides
- create images for particular full-energy peaks or sum of peaks
- generate files with 3D diagrams of gamma-ray imaging data
- reconstruct images for selected time interval

Basic window of software tool is shown on the Figure 13.

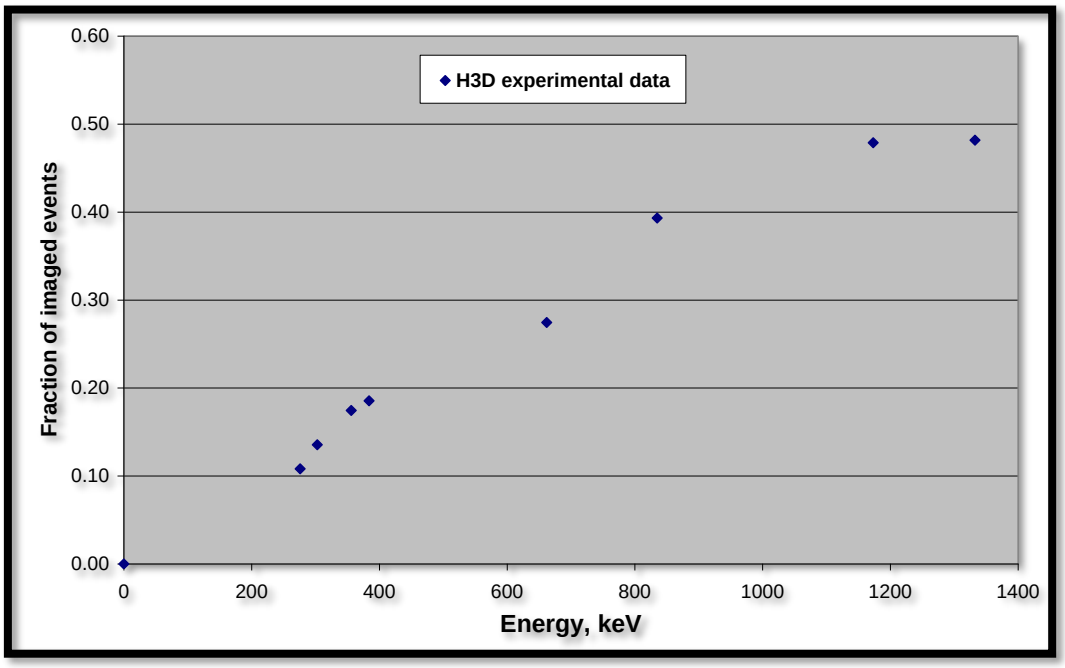

Figure 12. Polaris-H fraction of useful imaging events vs. energy of photo peak

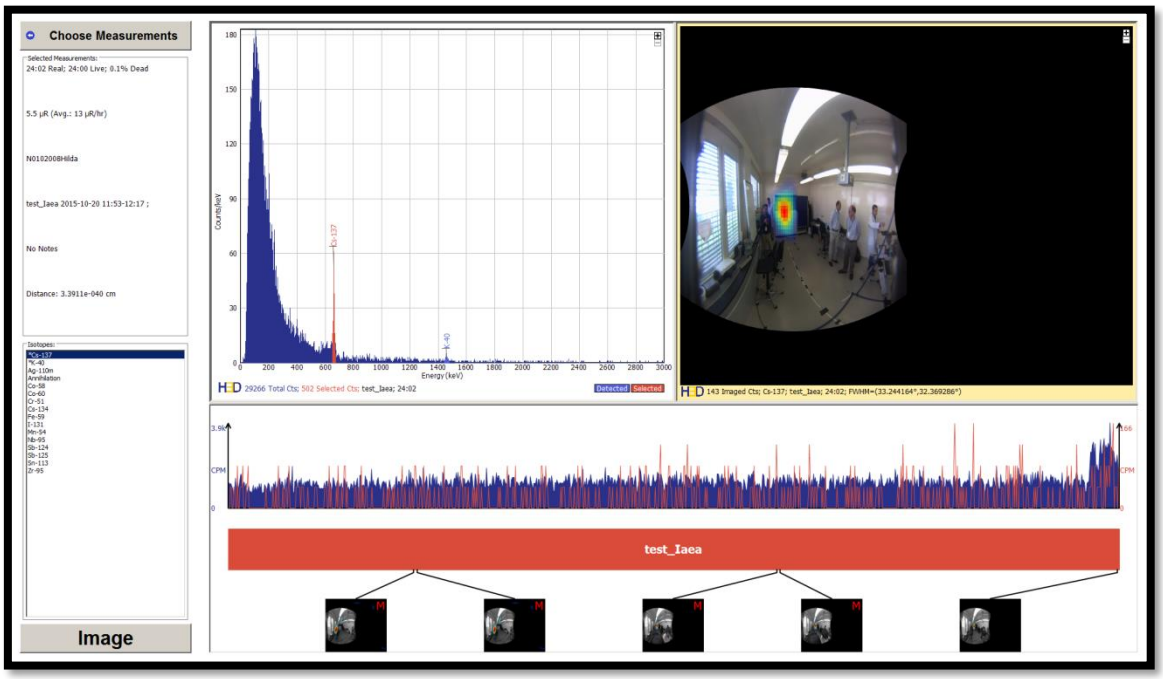

Figure 13. Polaris-H main window of software tool

Summary of technologies utilized in Polaris-H:

- Compton imaging
- Large volume single crystal CZT detector

- 3D position sensitive semiconductor radiation detector
- Excellent energy resolution for room temperature CZT detector
- Excellent full-energy peak events to imaging events ratio for Cs-137 and Co-60
- High-level of segmentation of CZT detector

4.8 RadSearch

RadSearch is a 2D scanner based on a collimated single crystal scintillation detector. Gamma-ray image is obtained by comparison of amplitudes of radiation signal between individual scan elements of inspection area. In order to achieve good contrast of the image, the detector must be well collimated, shall have limited field of view and multiple measurements needs to be performed.

The instrument combines in one detector head collimated, one by one inch $LaBr_3$ scintillation detector with an optical (video) camera with controllable zoom and focus and a laser range finder. The detector head is mounted on a pan/tile mechanism with a range of motion of 360 degrees (pan) and ±90 degrees (tilt). The detector head with pan/tilt is normally mounted on a tripod, but can also be mounted on vehicles or a mobile robot for access to high dose-rate areas.

The detector is housed in a tungsten shield, which provides a shielding ratio of 50:1 in the forward direction and 10:1 on the sides and to the rear for incident 1500 keV gamma-rays. The detector is collimated in two configurations. With the stainless steel and tungsten detachable barrel fitted, the detector has a 4-degree field of view (FOV). With the barrel detached the detector FOV is 18 degrees [10].

Using the pan and tilt mechanism, RadSearch operates by scanning an object or surface in a rectangular grid pattern. The scan pitch is user adjustable; however, better results are obtained with a degree of over-scanning. In practice a scan pitch of 3.5 degrees (barrel fitted) and of 15 degrees (barrel detached) work effectively.

Each individual component of the scanned area is called a Scan Element, and corresponds to the detector field of view. A rectangular array or grid of Scan Elements comprises the Scan Area. As part of the measurement process, the camera zoom feature allows close-up images to be recorded of individual Scan Elements.

When a measurement is completed, RadSearch provides a video image of the object or surface being measured divided up into the rectangular grid of Scan Elements each with a colored overlay showing the intensity of radioactivity detected in the Scan Element. 8K-channels gamma-ray spectrum is obtained for each Scan Element. From each measured spectrum, a number of different radionuclides can be identified. A different overlay can be produced for each radionuclide that has been identified.

Software allows both automatic and manual operation and an operator can specify coordinates to search a specific position or area or a search can be conducted automatically in 4π steradians, using the full capabilities of the pan/tilt mechanism. The unit reports the intensity (cps) and activity (μCi) for a variety of pre-selected radionuclides at different positions in relation to a video image.

Based on the measured dose-rate at the detector position, the operator could make a decision about number of scan elements and measurement time. In case, if insufficient contrast of the image is

obtained, then a new measurement cycle with higher zoom and higher measurement time needs to be performed.

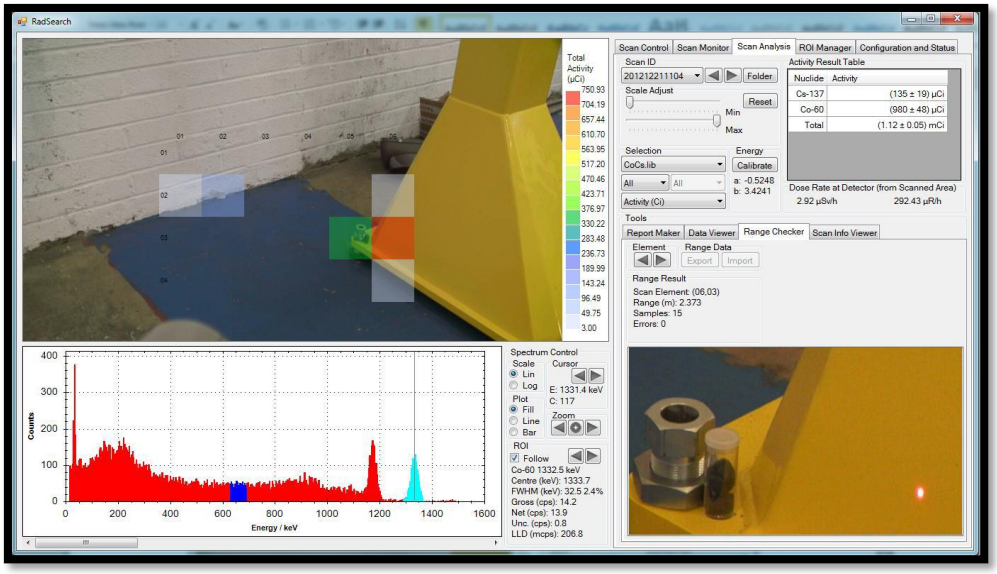

Figure 14. RadSearch basic operator window, resulting image and spectrum of green scan element (05, 03) are shown.

5 Experiments

All systems were set in far-field condition. The gamma-ray source have been placed behind target screen, not to disclose details of measurement setup to participants. The distance between the gamma-ray imagers and target screen was in range between 2.5 and 5 meters depending on the experiment. Systems were positioned on a shared rack equidistantly to the target sources and pointed towards them or on dedicated tripods.

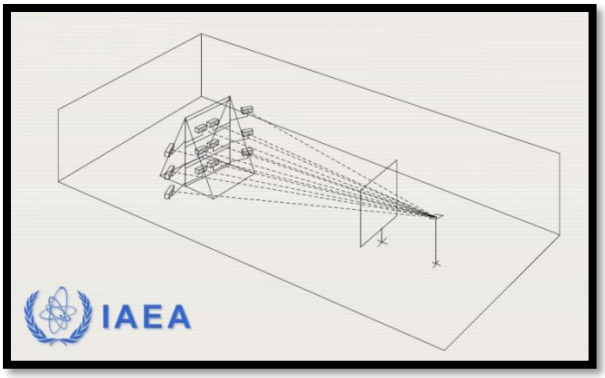

Figure 15. Illustration of experimental setup; from left to the right: gamma-ray imagers on the rack – target screen – radioactive source

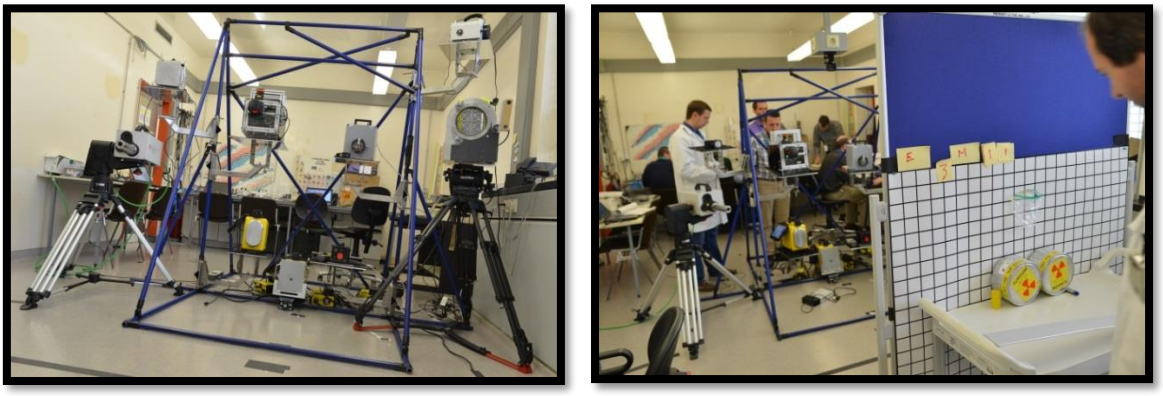

Figure 16. Gamma-ray imagers positioned on the rack and tripods and the target screen with sources behind screen.

Table 6. Description of sources used for measurements.

Source	Most prominent gamma-ray energies, keV	Activity or Mass
Am-241	59.5	24.5 GBq
Cs-137	661.6 (Ba-133m)	18.3 MBq
Co-60	1173.2 1332.5	65 MBq
LBPu CBNM Pu93 CBNM Pu84	59.5 (Am-241) 332.8 (Pu-239) 375 (Pu-239) 413.7 (Pu-239)	6.6 g
HBPu CBNM Pu70 CBNM Pu61	59.5 (Am-241) 160.3 (Pu-240) 164.6 (U-237) 208 (U-237) 332.4 (U-237)	6.6 g
LEU	185.7 (U-235) 1001 (Pa-234m)	Total U: 847 g (U-235: 169 g)
HEU (MTR plate)	185.7 (U-235)	Total U: 218 g (U-235: 193 g) (in one plate; up to 12 plates were used in single measurement)

The following eight experiments were conducted during the course of the workshop:

- Experiment 1 – Measurements of sensitivity in wide energy range of imager operation
- Experiment 2 – Overnight localization and identification of weak source in the presence of masking source
- Experiment 3 – Measurements of sensitivity to nuclear materials, time to detect, identify and localize nuclear materials
- Experiment 4 – Angular resolution
- Experiment 5 – Field of view
- Experiment 6 – Localization performance for extended sources
- Experiment 7 (a) – False alarm rate
- Experiment 7 (b) – High-background masking scenario
- Experiment 8 (a) – Angular resolution for extended sources
- Experiment 8 (b) – Glove box scenarios

The results in the reports have been anonymised, actual names of the systems being replaced by a System# (where # is a number).

5.1 Experiment 1: Sensitivity

In Experiment 1 the total sensitivity and detection efficiency in full-energy peaks, has been measured. Am-241, Cs-137 and Co-60 sources were used to cover wide energy range of imager operation. Basic spectrometric and imaging characteristics were studied. Sources were placed in the center and behind a target screen.

5.1.1 Comparison of spectra and images measured

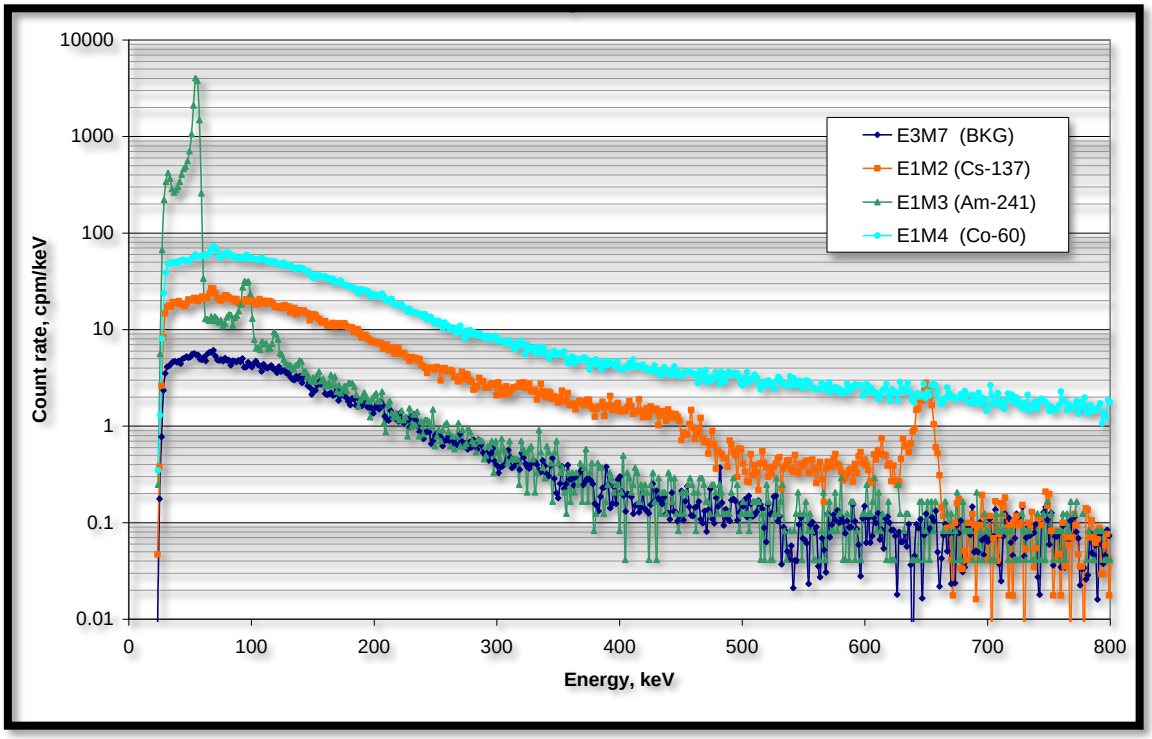

Figure 17. System3 spectra measured in Experiment 1

Currently multichannel analyzer with 1024 channels readout is integrated in System3, what limits ability to extend spectrometric energy range up to 1.4 MeV, so full-energy peaks of Co-60 will be visible.

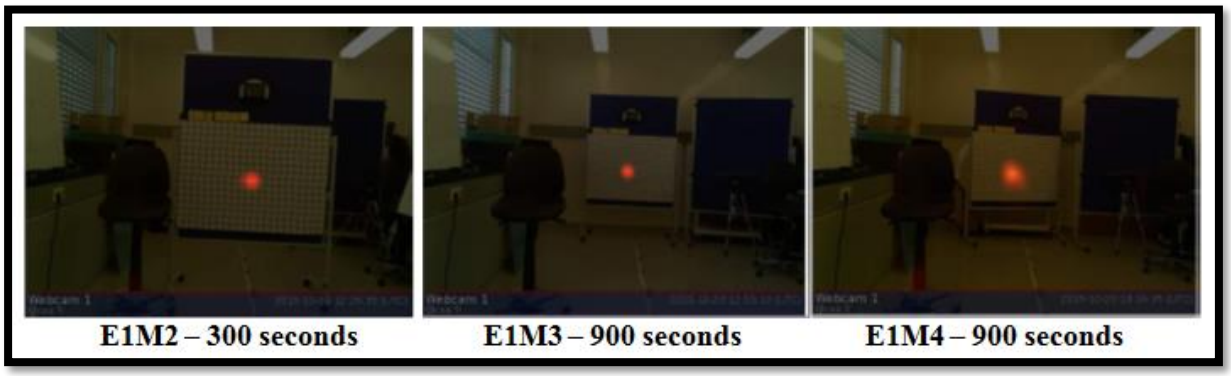

Figure 18. System3 imaging results for Experiment 1

With increase of energies of incoming photons coded-mask becomes more and more transparent. Co-60 source requires more time to be imaged compared to Cs-137 source. Also quality of image suffers.

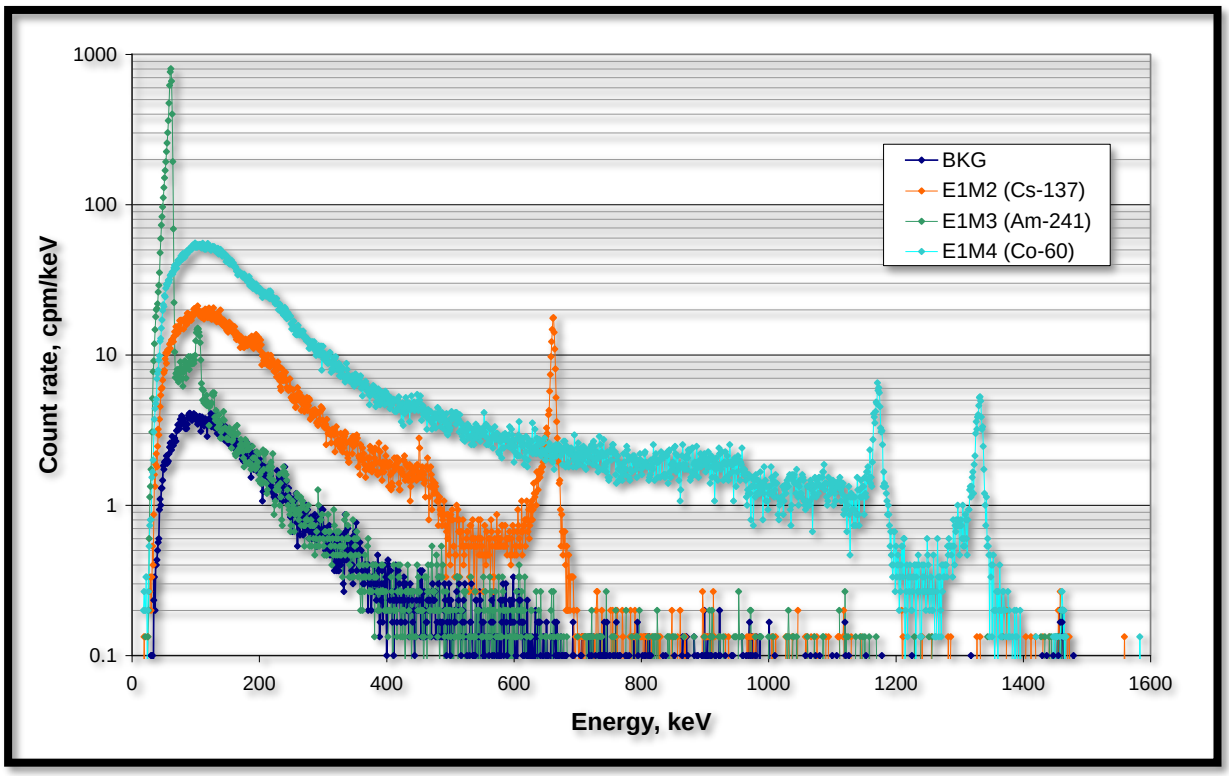

Figure 19. System1 spectra measured in Experiment 1

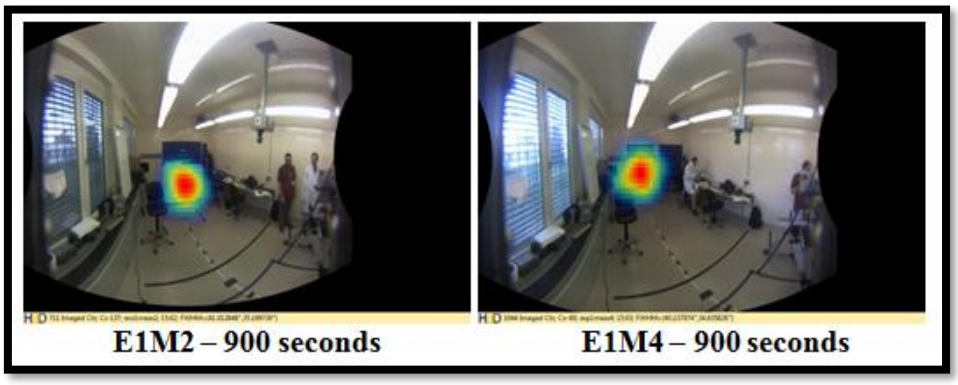

Figure 20. System1 imaging results for Experiment 1

Am-241 source cannot be imaged. Low energy thresholds for System1 is about 250 keV, below this energy threshold full-energy absorption of incoming photons is predominant process. Energy resolution in full energy peaks is of importance. For a Compton imager it is an indicator of imaging quality due to necessity in measurement of energies of Compton events in the detector with good precision.

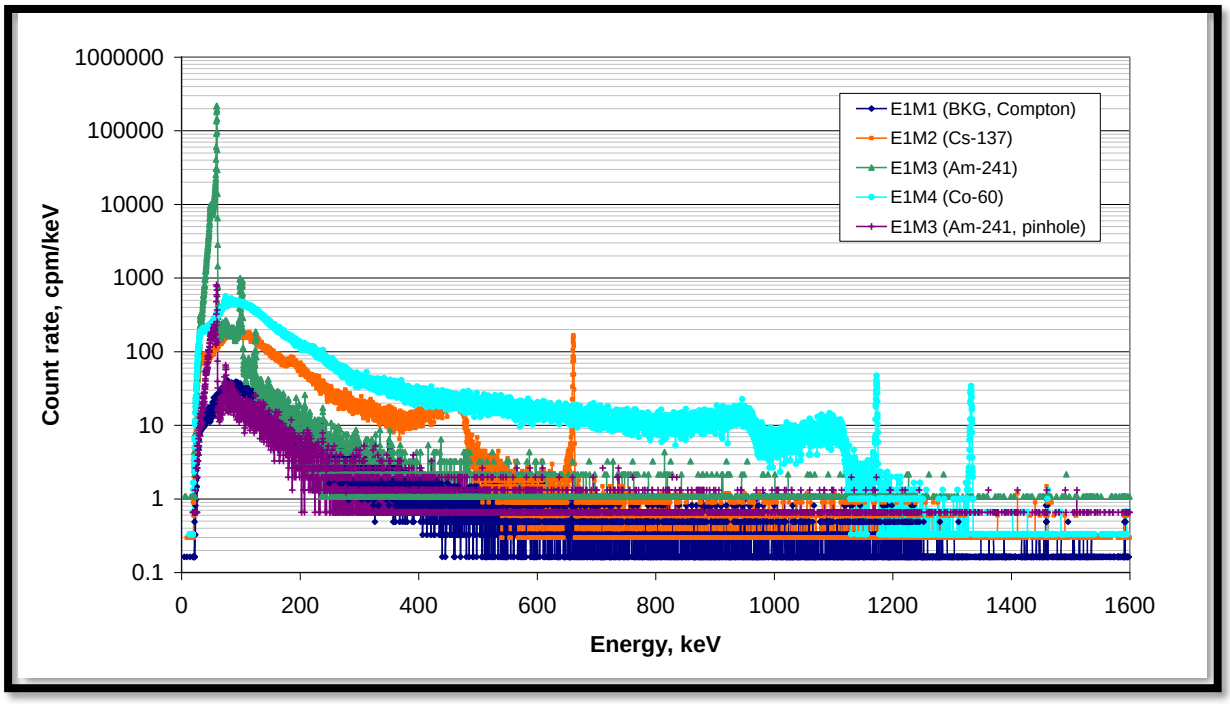

Figure 21. System4 spectra measured in Experiment 1.

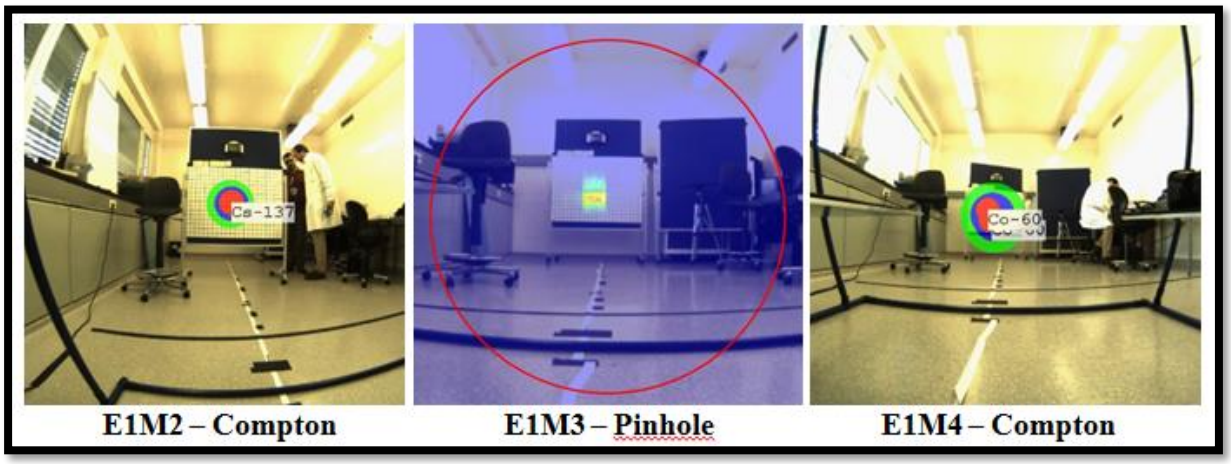

Figure 22. System4 imaging results for Experiment 1

Cs-137 and Co-60 are imaged in Compton mode of operation based on full-energy peak events. Two signs of Co-60 on the right picture correspond to 1773 keV and 1333 keV full-energy peak events. Am-241 is imaged in pinhole mode of operation. Red circle indicates field of view.

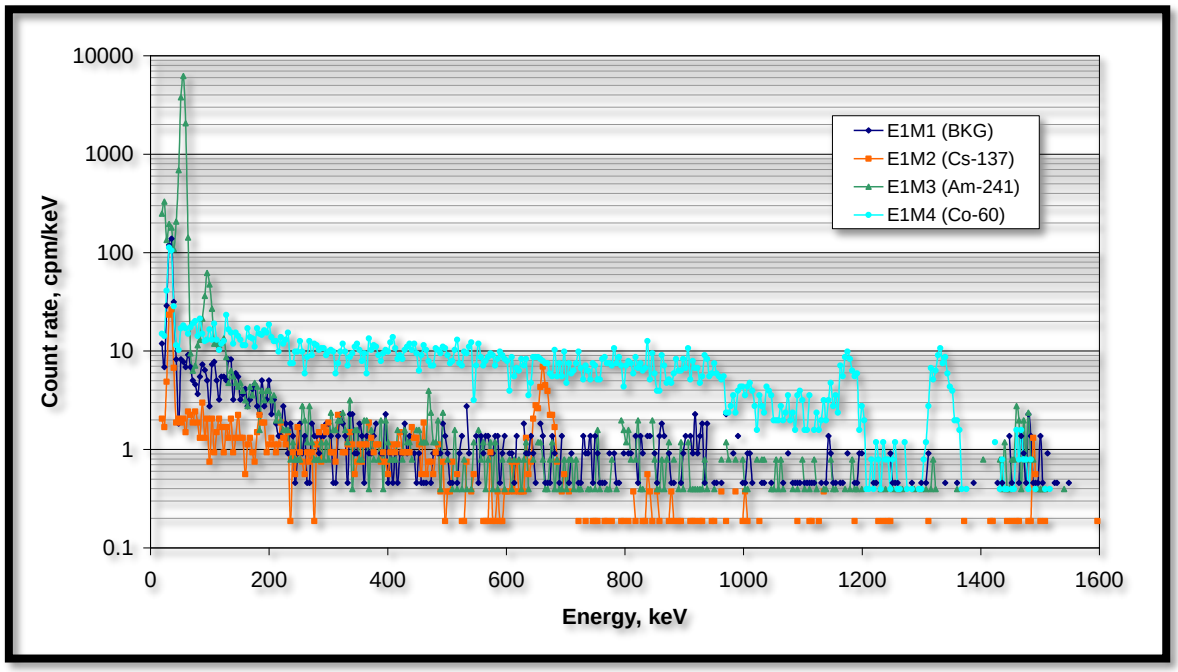

Figure 23. System8 spectra measured in Experiment 1.

Spectra are shown for detector focused on the source (red scan element on the images below).

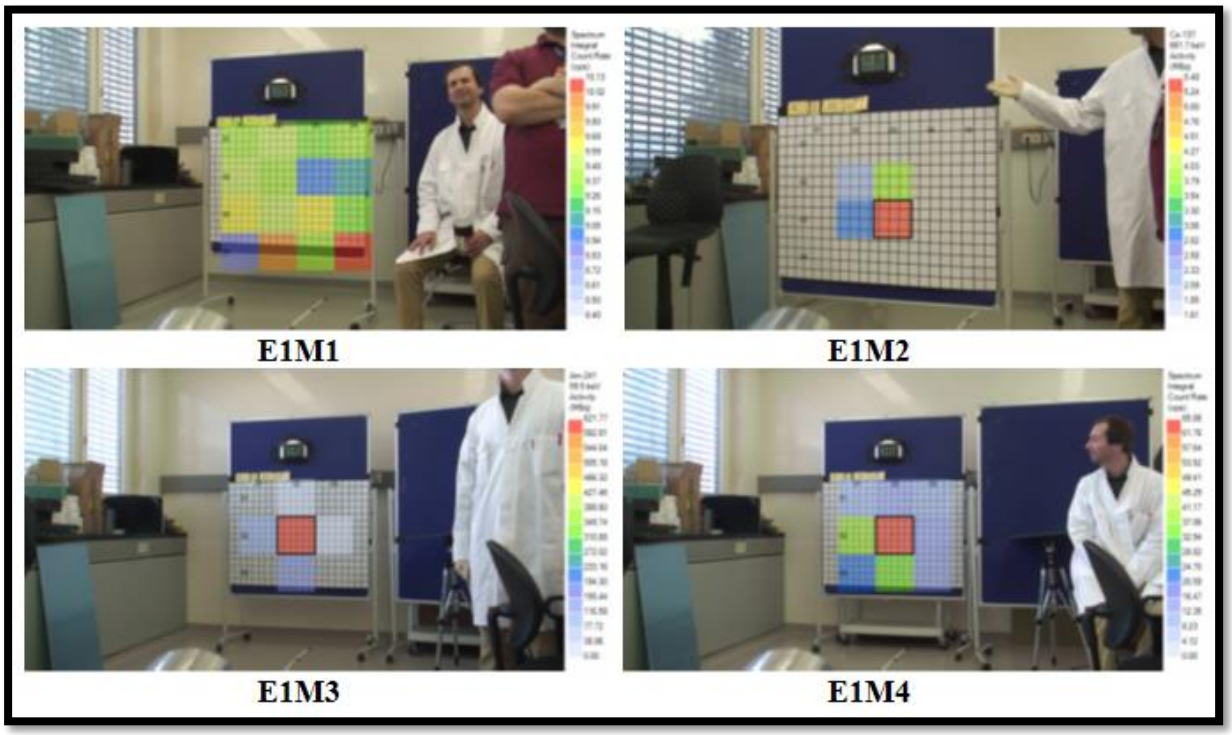

Figure 24. System8 imaging results for Experiment 1

5.1.1.1 Static measurements

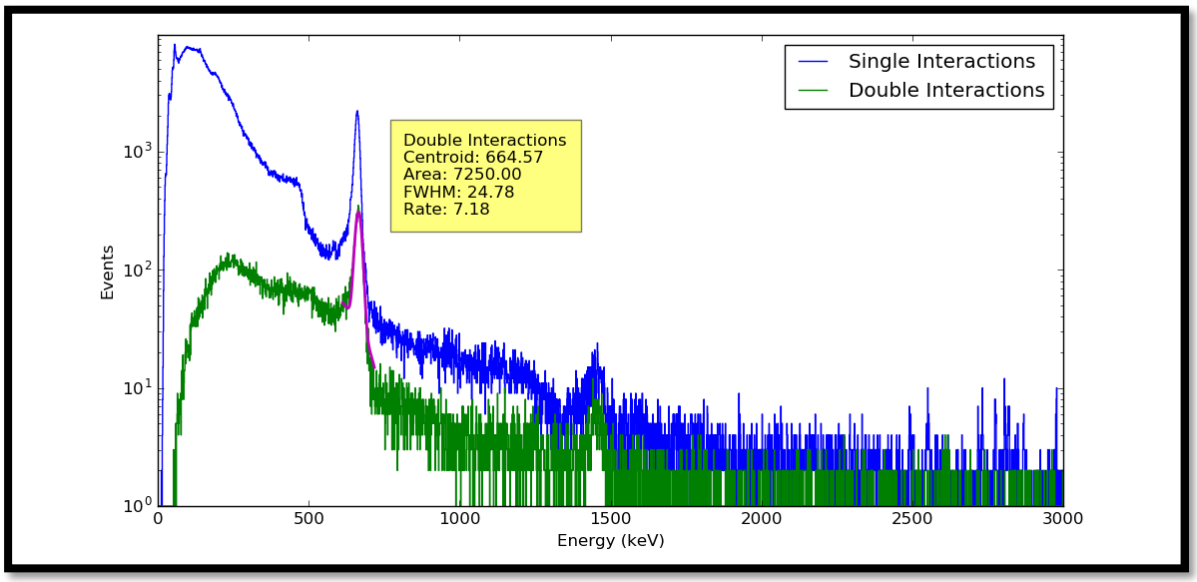

Figure 25. System5 comparison of 1000 seconds spectrum of total interaction events with spectrum of double interaction events under experiment E1M2 (Cs-137)

Compton imaging is based on the registration of energies and positions of double interaction events (scattering event followed by absorption event). Scattering must occur in one CZT detector array and

absorption in another one. Figure below shows improvement of angular resolution with measurement time, after 300 seconds angular resolution of 9.5 degrees was measured.

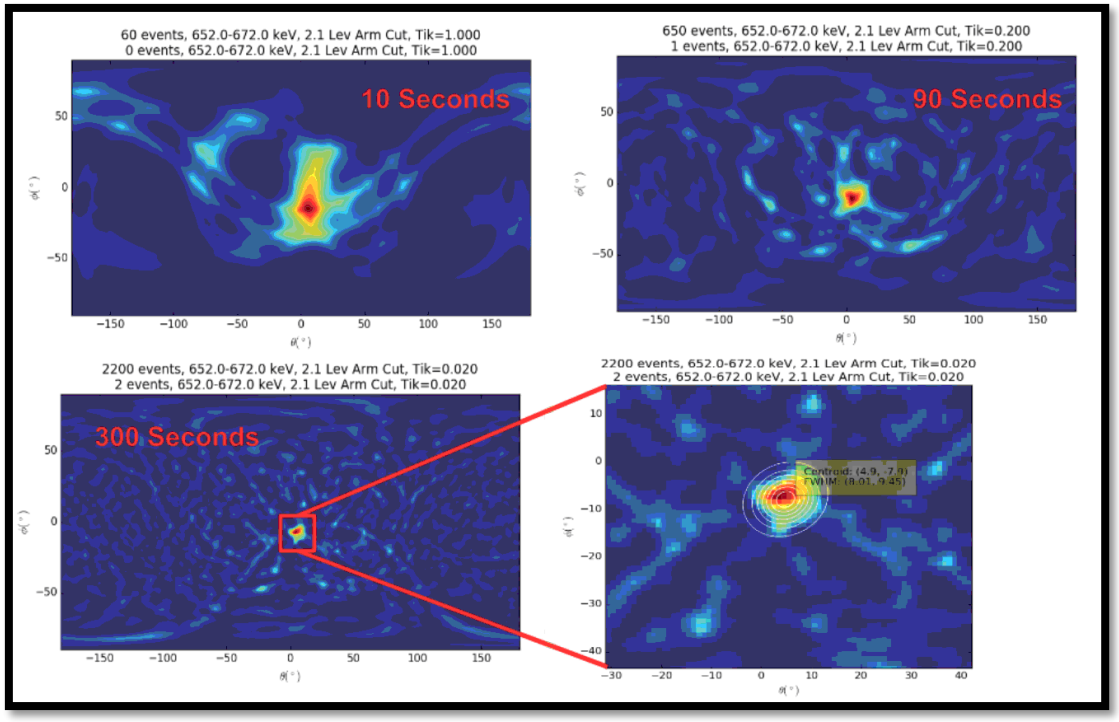

Figure 26. System5 angular resolution for Cs-137 source (E1M2)

5.1.1.2 Dynamic measurements

Cs-137, low activity

In this measurement, a weak Cs-137 source was hidden in one of the several boxes. The operator was asked to inspect a potentially contaminated area. The left image (Figure 27) shows the reconstruction scene by the operator during the real time acquisition. This image was acquired by taking a picture of the tablet. The result on the right is from the same data rerun through the code with a different color map and a grayscale version of the scene model. These images are shown side-by-side to emphasize the real-time nature of the volumetric results. The measurement time was 74 seconds, and 78 cones within the Cs-137 ROI were collected.

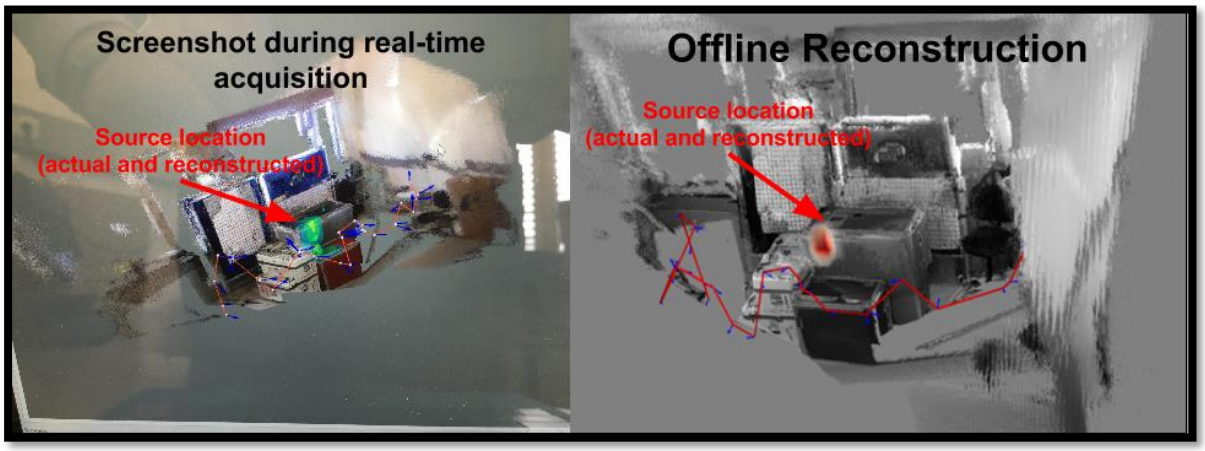

Figure 27. System5 real-time volumetric Compton imaging with a weak Cs-137 source

Co-60, high activity

In this measurement, a strong Co-60 source (65 MBq) was placed in the centre of the room (same source was used in static measurements E1M4). During a 50 seconds measurement, System5 was walked along a roughly linear path past the source and 1260 cones were acquired in the ROI about 1173 keV. The image reconstruction (Figure 37) is given by the red color map. This result demonstrates volumetric capability for scenarios with high energy and highly active sources.

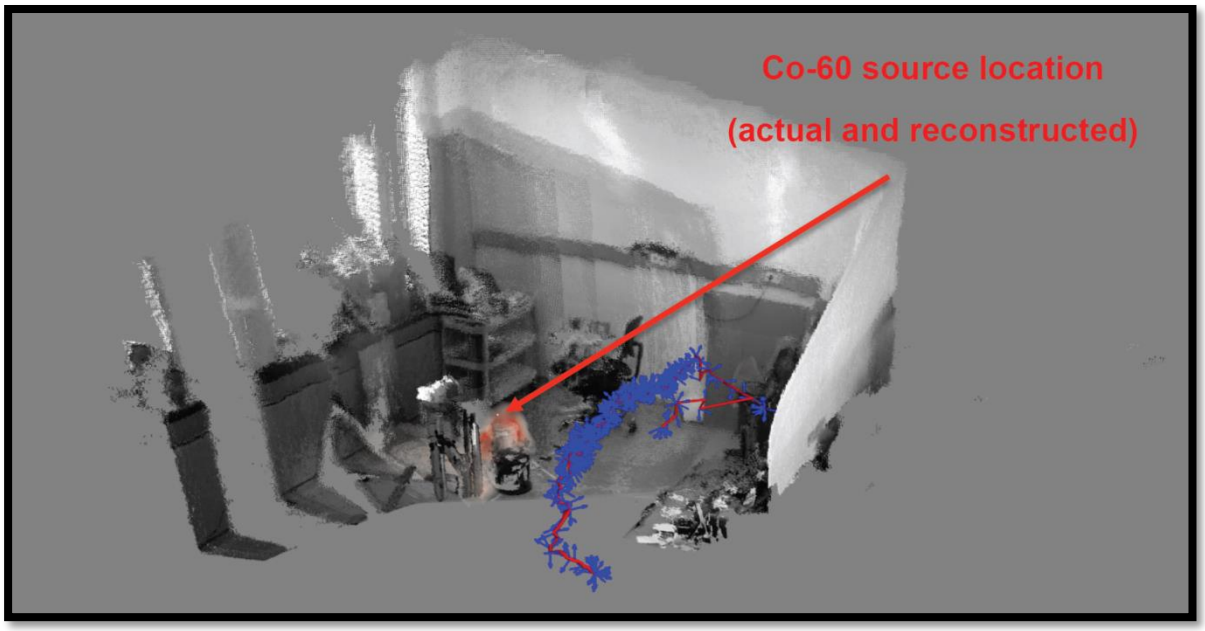

Figure 28. System5 real-time volumetric Compton imaging with a strong Co-60 source

5.1.2 Summary of the results

Due to different principles of operation of coded-aperture and Compton gamma-ray imagers, the value of total sensitivity (Table 7) could be used for estimation of imaging efficiency for coded-aperture imager or for cross-comparison of imaging efficiency between coded-aperture and Compton modes of imager operation when compared with sensitivity in full-energy peak (Table 8).

Total sensitivity (*TS*) is expressed by the following equation

$$TS = \frac{TCR - BCR}{DR}, [cpm / nSv \cdot h^{-1}]$$

where

TCR – total count rate in the whole energy range [*cpm*]
BCR – background count rate in the whole energy range [*cpm*]
DR – dose rate at detector position [$nSv \cdot h^{-1}$]

Table 7. Experiment 1: Summary of the results of total sensitivity measurements

Experiment	Source	Source dose rate, $nSv \cdot h^{-1}$	Total sensitivity, $cpm/nSv \cdot h^{-1}$							
			System3	System1	System4	System8	System5	System6	System7	System2
E1M2	Cs-137	175	16.0	17.2	135.8	5.4	ND	NP	NP	0.1
E1M3	Am-241	315	95.0	21.4	1433.5 (3.2)	66.9	ND	NP	NP	42.3
E1M4	Co-60	805	13.2	12.7	68.4	4.2	ND	NP	NP	0.1

Dose-rates were measured with Thermo FH 40GL10 dose-rate meter positioned on the shelf in the middle of the rack populated with instruments. Measured background dose-rate was 65 nSv/h. Source dose-rate is obtained by subtracting the background dose-rate.

System6 and 7 were not able to participated (NP) in the first day of measurement campaign due to their late arrival to Seibersdorf

No data (ND) with regard to total sensitivity were provided for System5 but sensitivity is clearly high since total sensitive volume of two CZT detector arrays is approximately 96 cm^3.

System7 total sensitivity for Am-241 is about half of System4 since it has similar detector and 3 mm thick tantalum mask is used with 50% of the mask is open area.

Table 8. Experiment 1: Summary of the results of sensitivity in full-energy peaks

Experiment	Description	Source dose rate, $nSv \cdot h^{-1}$	Sensitivity in full-energy peak, $cpm/nSv \cdot h^{-1}$							
			System 3	System 1	System 4	System 8	System 5	System 6	System 7	System 2
E1M2	Cs-137 (662 keV)	175	0.2	0.9	6.4	1.3	ND	NP	NP	ND
E1M4	Co-60 (1173+1333 keV)	805	NA	0.2	1.3	0.2	ND	NP	NP	ND

NP – not participated
ND – no data
NA – not available

Table 9. Experiment 1: Comparison of detection and imaging sensitivity of Compton imagers

System1		**Total events, cps**	**NET total events, cps**	**Full-energy peak events*, cps**	**Imaged events, cps**	**Full-energy peak/NET total**	**Imaged/Full-energy peak**
E1M1	BKG	11.7					
E1M2	Cs-137	61.8	50.1	2.5	0.8	0.049	0.32
E1M4	Co-60	181.2	169.6	2.7	1.2	0.016	0.43
System4		**Total events, cps**	**NET total events, cps**	**Full-energy peak events, cps**	**Imaged events, cps**	**Full-energy peak/NET total**	**Imaged/Full-energy peak**
E1M1	BKG	72.4					
E1M2	Cs-137	450.8	378.4	18.8	1.9	0.050	0.10
E1M4	Co-60	1199.4	1127.0	17.8	1.6	0.016	0.09

** Cs-137 – events in 662 keV peak, Co-60 events in 1173 and 1333 keV peaks*

Table 10. Experiment 1: Comparison of imaging efficiency of Compton imagers

E1M2 (Cs-137)	**Imaged events rate, cps**
System1	0.8
System4	1.9
System5	7.2

5.2 Experiment 2: Overnight Localization

The goal of experiment E2M6 was to evaluate the capability of gamma-ray imagers to detect, identify and localize:

a) relatively weak point gamma-ray sources of same radionuclide composition; and

b) Co-57 source masked by Compton continuum induced by Cs-137 sources.

The grid attached to the target screen, was used as a coordinate map. Each cell on the grid is 5 x 5 cm. The notation [**X, Y**] was used for pointing positions of sources. Negative **X** number corresponds to a shift to the left from [0, 0] coordinate with reference to gamma-ray imagers. Negative **Y** number corresponds to a shift below the central point. For some measurements with complex set of sources a photo is given; note that the photo is taken from behind the screen, so source location is mirrored from the gamma cameras' point of view.

Coordinates with reference to gamma-ray imagers (E2M6):

- Cs-137 point sources at (0, 0), (6, 0), (10, 0), (3, -4), (0, 4.5)
- Co-57 point source at (-5, -4) (position is marked by red circle)
- U_3O_8 point source at (-1.5, -3)

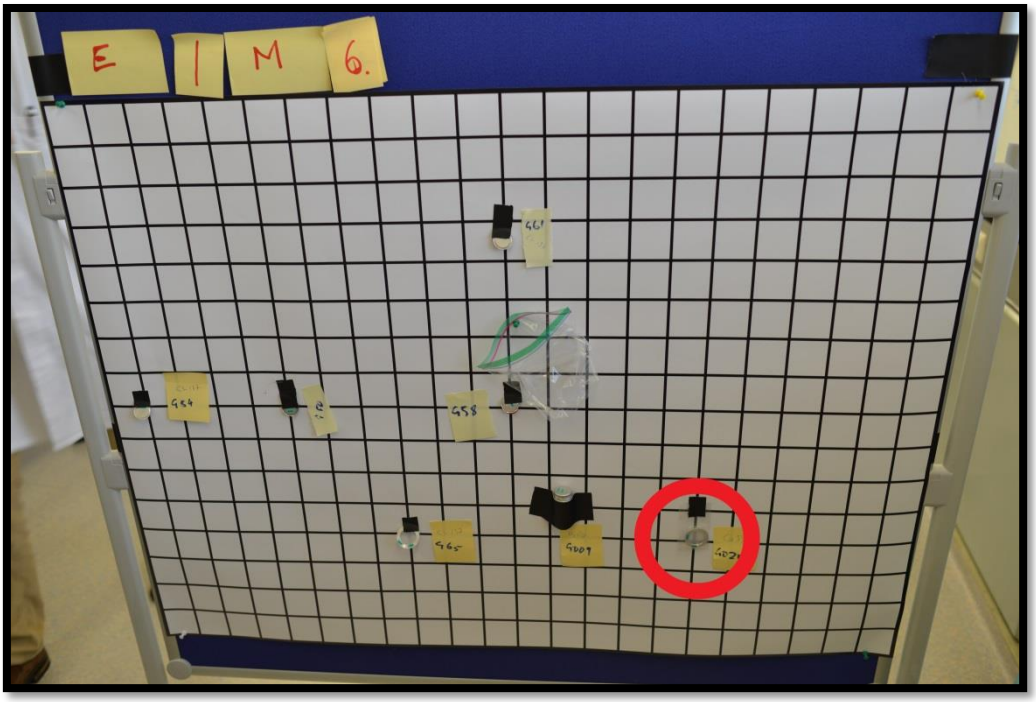

Figure 29. Experiment 2: Photograph of overnight measurement setup with multiple sources. Note the results from each camera will mirror the location of these sources.

5.2.1 Comparison of the results

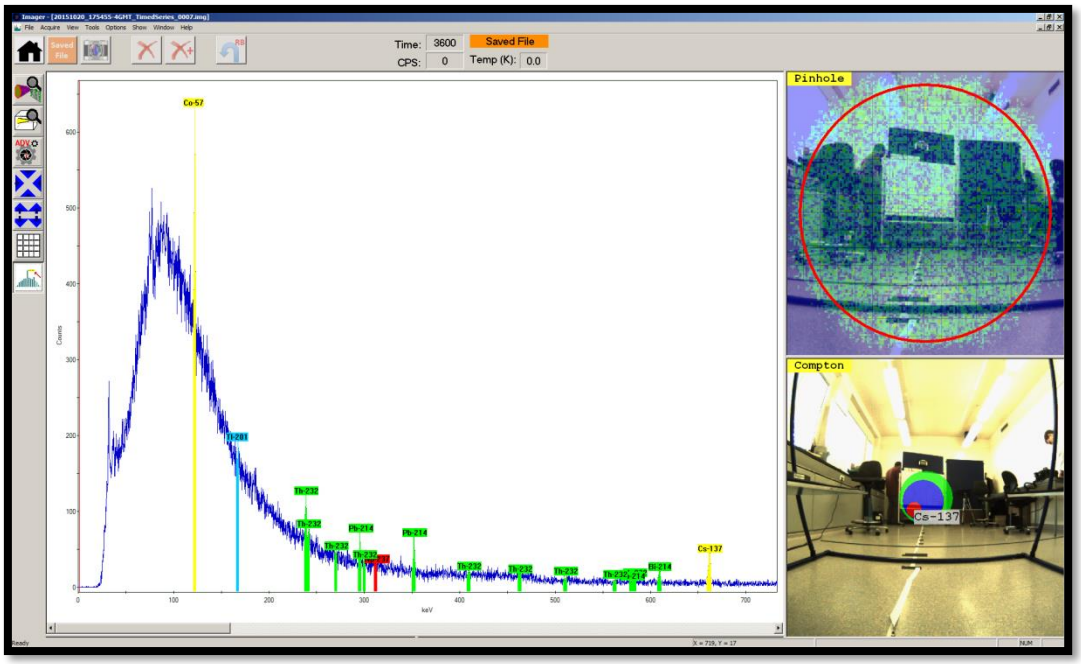

Figure 30. System4 (E2M6): 1 hour of measurements in Compton mode, Co-57 and Cs 137 are identified; Cs 137 is imaged.

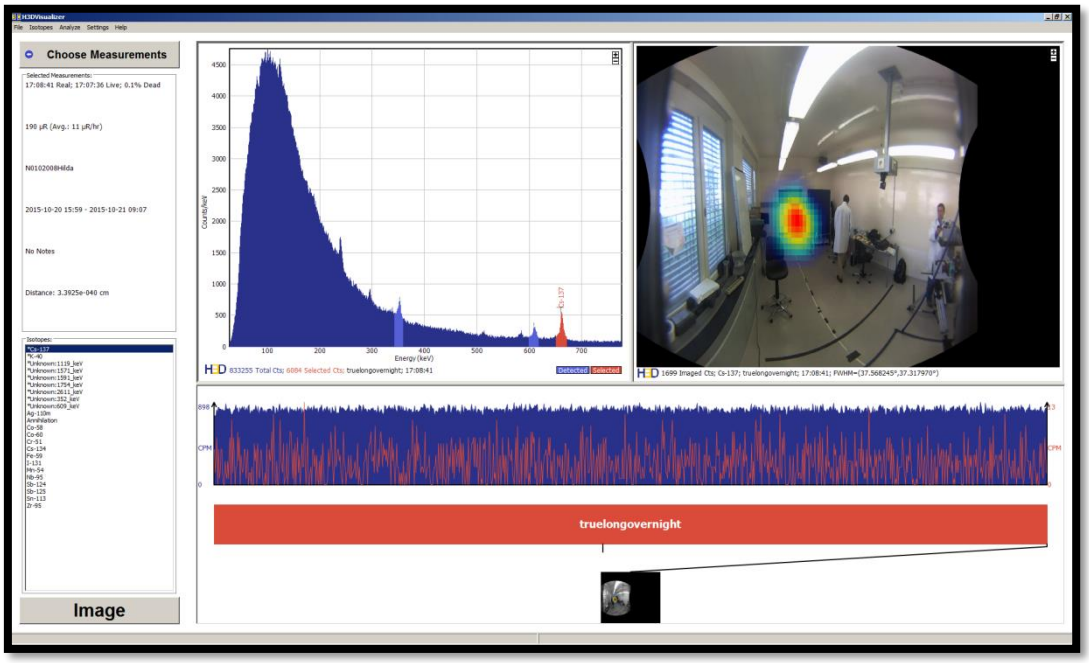

Figure 31. System1 (E2M6): 17 hours of measurement, Cs-137 is identified and imaged.

Co-57 peak is visible, but was not detected. Angular resolution does not allow separate Cs-137 sources which however have different activities.

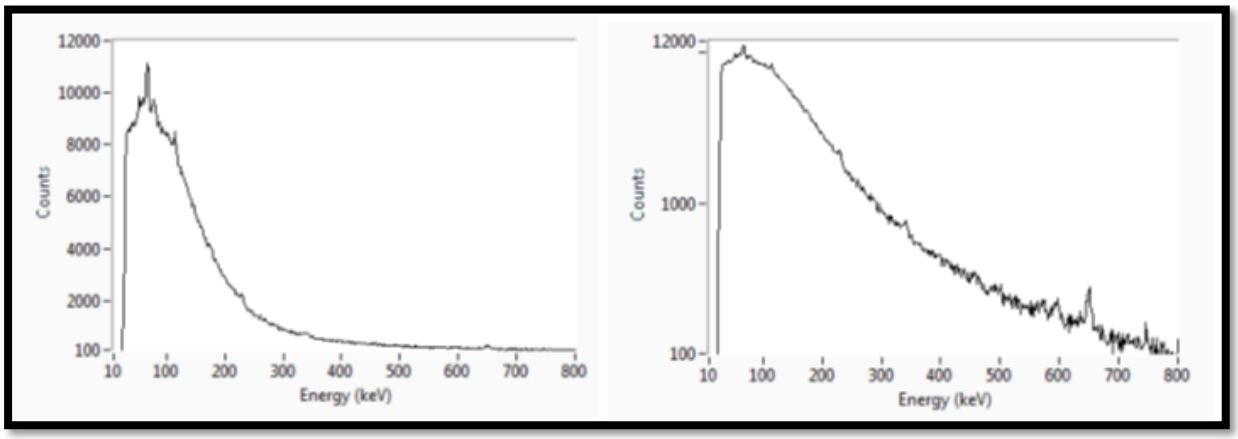

Figure 32. System3 (E2M6): 17 hours spectra in linear and logarithmic scale. Cs-137 is identified and peak in 120 – 130 keV ROI is detected.

Figure 33 System3 (E2M6): 17 hours gamma-ray images from left to right (whole energy window – high energy window 600-800 keV and low energy window from 90-130 keV).

Relatively thin CZT detector (5mm), but with relatively large area (40x40mm) has improved signal to background ratio at relatively low energies compared to thicker detector having same sensitive volume. Energy resolution does not allow make definite conclusion about identification of Co-57, however peak in 120 – 130 keV ROI is detected and low-energy source is imaged based on the low-energy window.

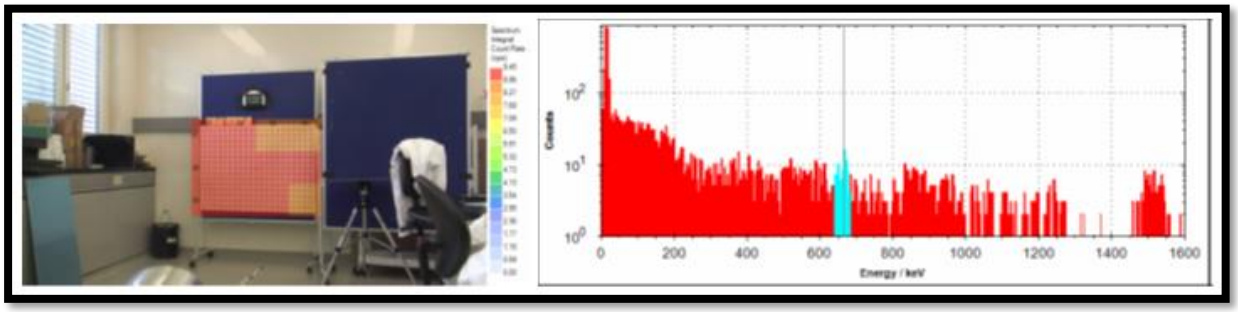

Figure 34. System8 (E2M6): 1 hour gamma-ray image and spectrum of scan element.

Image area was automatically divided into 12 scan elements. Each scan element was measured for 300 seconds. Total measurement time was 1 hour. 300 seconds spectrum of scan element (03, 02) is shown, Cs-137 is identified. Angular resolution does not allow separate Cs-137 sources which however have different activities.

5.2.2 Summary of results

Table 11. *Experiment 2: Summary of the results*

	Detected		Identified		Localized	
Imager	**Cs-137**	**Co-57**	**Cs-137**	**Co-57**	**Cs-137**	**Co-57**
System3	Yes	Yes	Yes	Yes**	Yes	Yes**
System1	Yes	No	Yes	No	Yes*	No
System4	Yes	Yes	Yes	Yes	Yes*	No
System8	Yes	No	Yes	No	Yes*	No
System5	ND	ND	ND	ND	ND	ND
System6	NP	NP	NP	NP	NP	NP
System7	NP	NP	NP	NP	NP	NP
System2	NP	NP	NP	NP	NP	NP

** Hotspot is localized but sources are not separated*
*** Peak is identified in 120-130 keV region of interest and is localized not in 1 hour but in 17 hours of acquisition*

NP – not participated due to the late arrival to Seibersdorf
NA – not applicable for proximity imaging as dynamic measurements shall be done
ND – no data

5.3 Experiment 3: Sensitivity to Nuclear Materials

In Experiment 3, total sensitivity has been measured for HEU, LEU, HBPu and LBPu. Such basic spectrometric/detection characteristics such as: time to detect and time to identify as well as basic imaging characteristics such as time-to-alarm and time-to-localize under the same measurement conditions have been evaluated.

5.3.1 Plutonium measurements

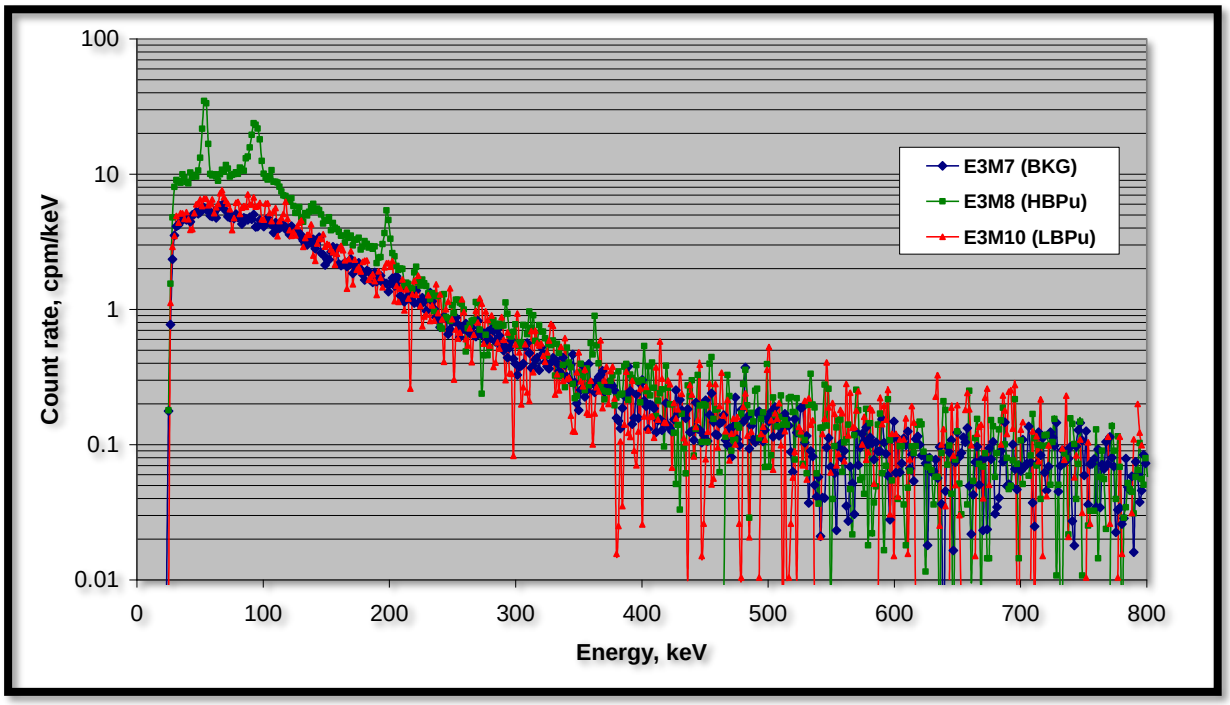

Figure 35. System3 Pu spectra measured in Experiment 3.

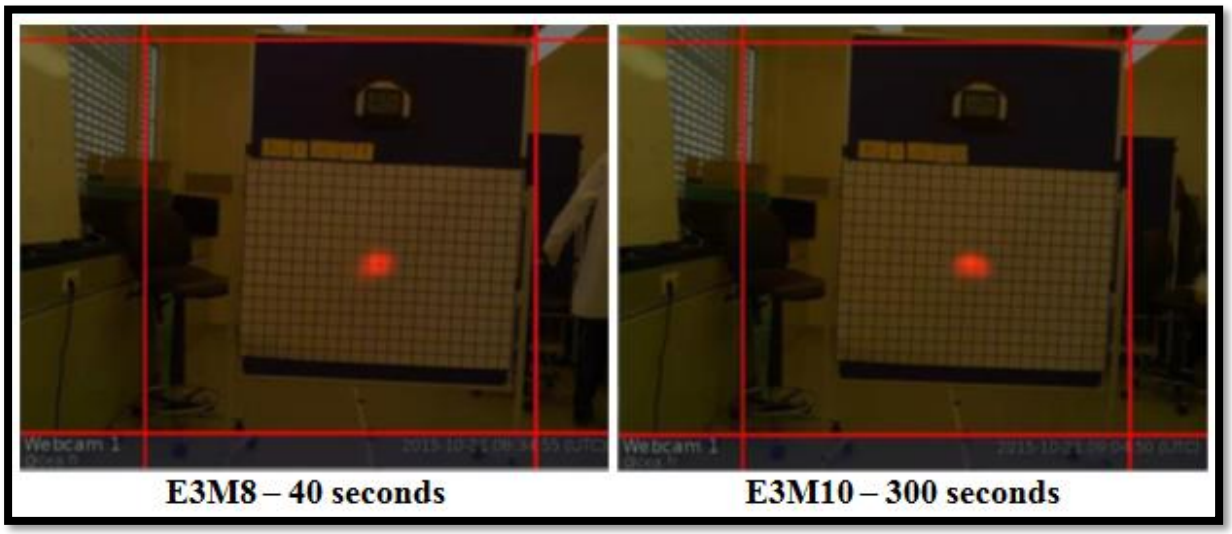

Figure 36. System3 imaging results for Experiment 3 (plutonium)

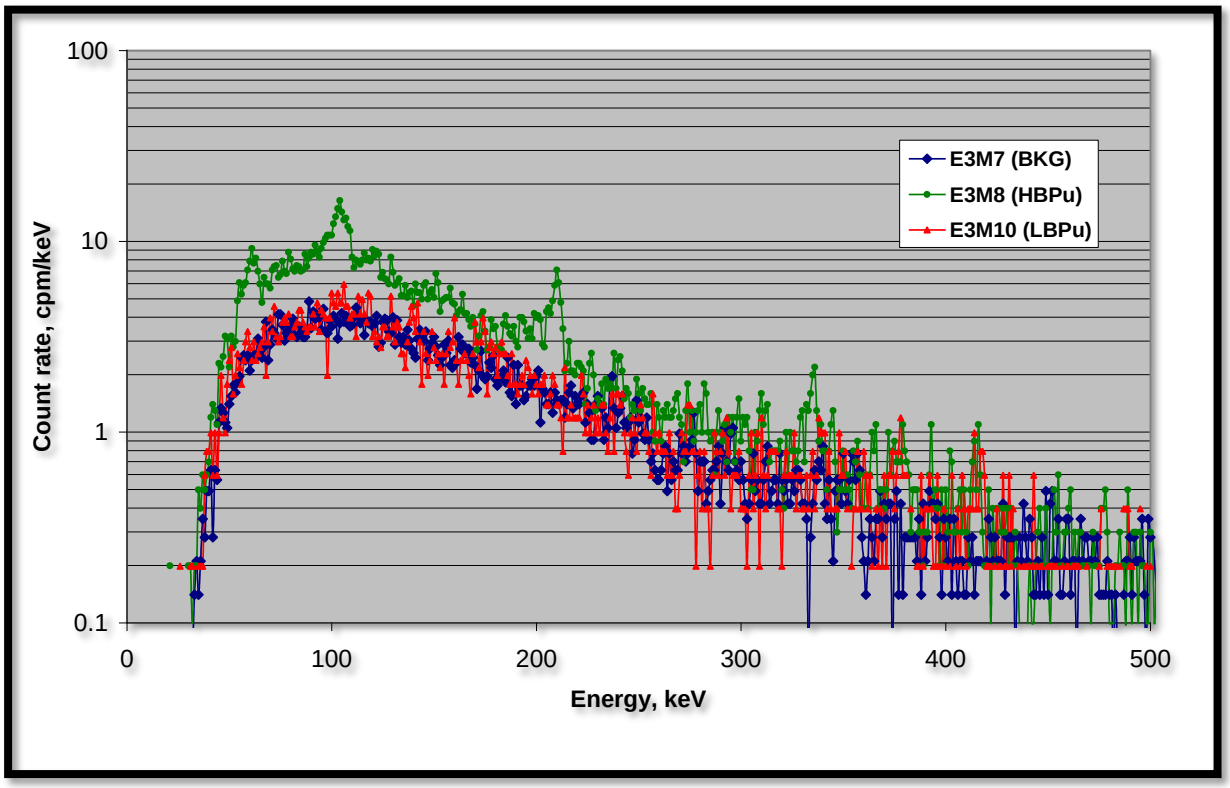

Figure 37. System1 comparison of Pu spectra measured in Experiment 3.

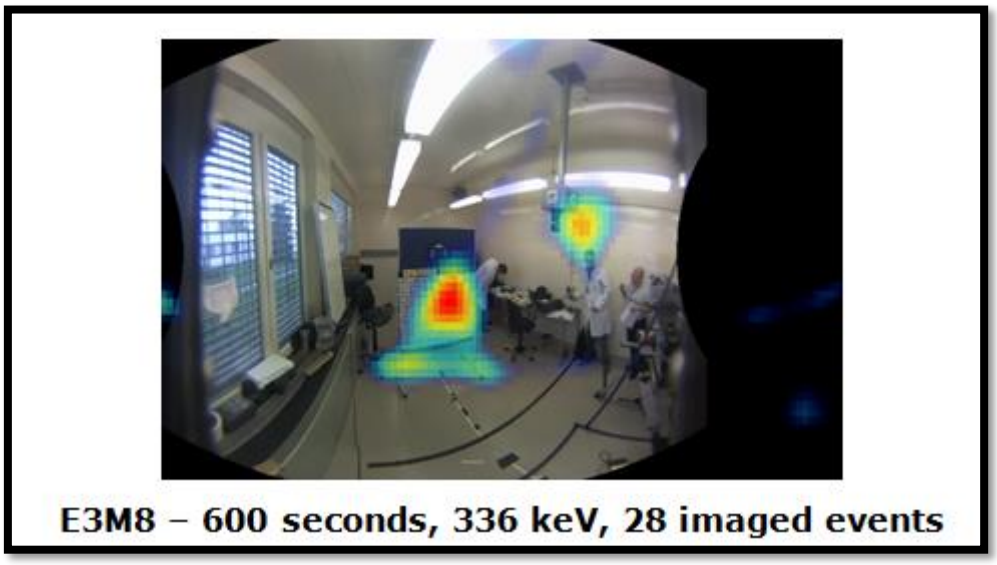

Figure 38. System1 imaging results for Experiment 3 (plutonium).

Based on the 208 keV peak, the image cannot be created by System1 due to properties of CdZnTe detector material (relatively high density and atomic number of CZT crystal and therefore predominance of full-energy absorption of photons with 208 keV energies). Plutonium source could be imaged using 336 keV peak. For imaging purposes a fraction of events in full-energy peak is useful (about 1/6).

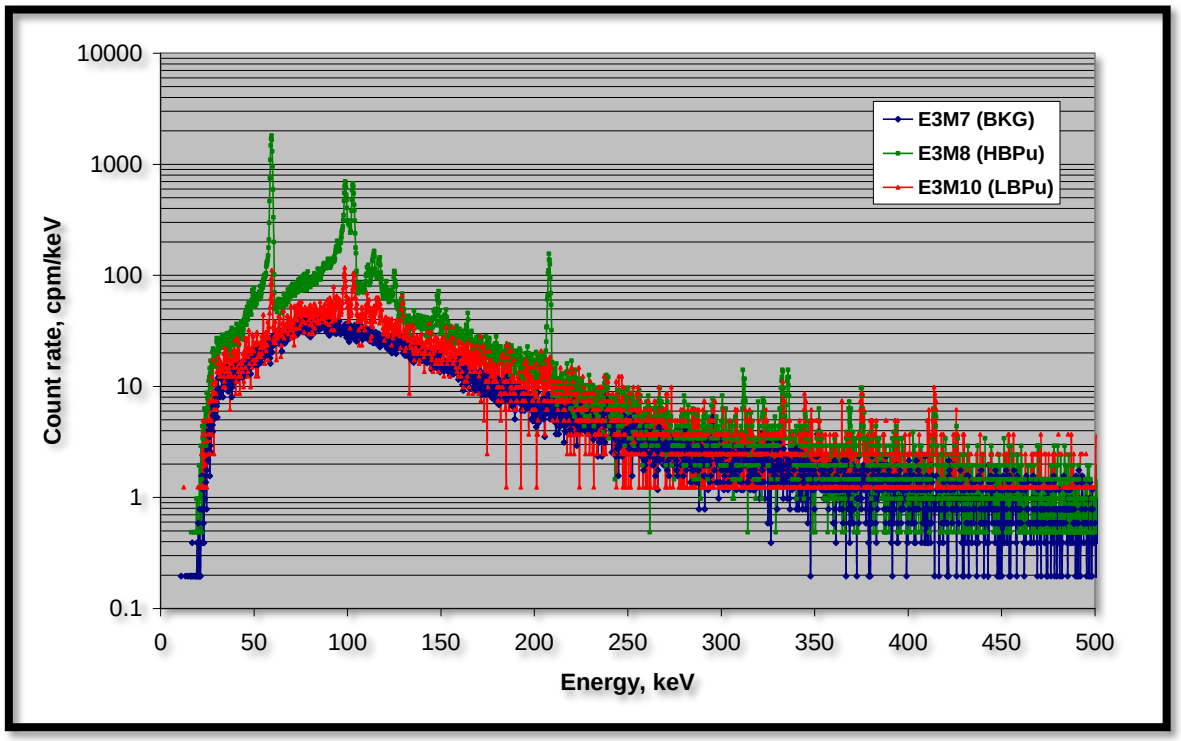

Figure 39. System4 comparison of Pu spectra measured in Experiment 3.

Basic energy peaks of interest for imaging purposes are 208 keV (HBPu) and 414 keV (Pu-239). Image can be created by System4 imager running in Compton mode. A fraction of events in 208 keV full-energy peak can be imaged (about 1/10).

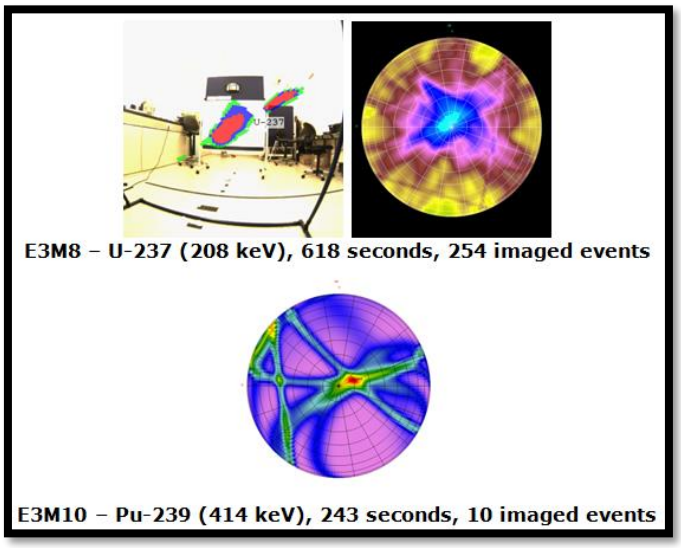

Figure 40. System4 imaging results for Experiment 3 (plutonium).

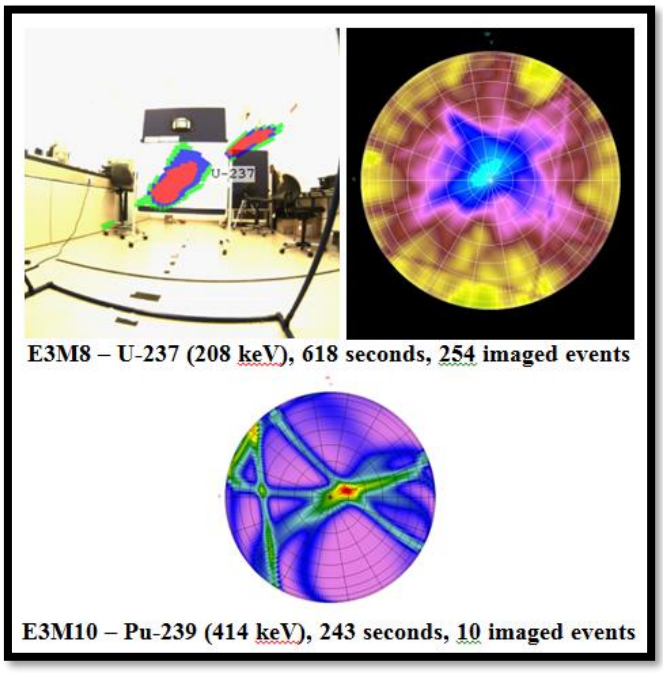

Figure 41. System4 imaging results for Experiment 3 (plutonium).

In measurement E3M8, the total balanced mask / anti-mask data for this run included two mask cycles of 200 s duration, for a total of 400 s of data. This resulted in the false-color images shown in Figure 42. The histograms below and to the right of the image are the counts in the pixels under the horizontal and vertical cursor lines, respectively. These together with the false color allow one to judge the signal-to-noise ratio (SNR) in the image.

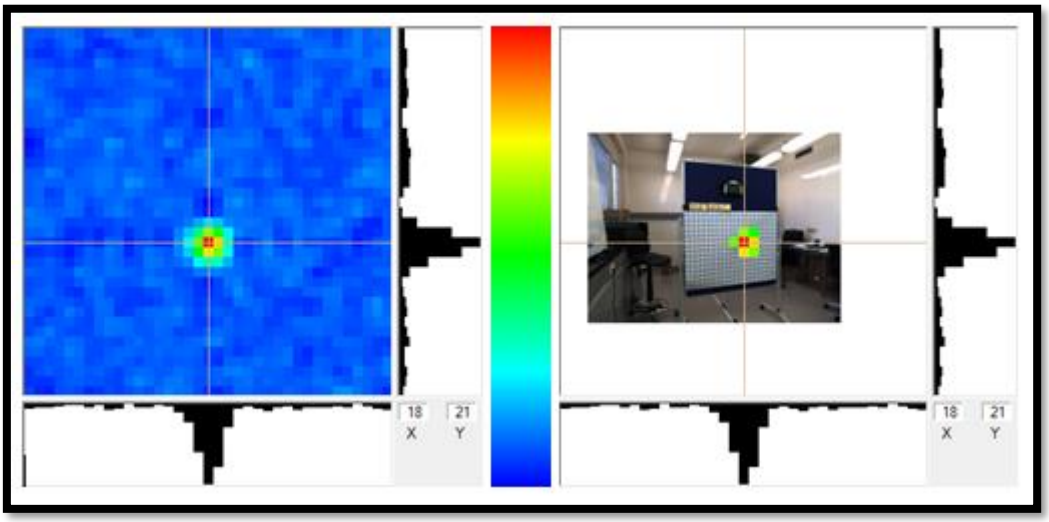

Figure 42. System7 false-color gamma-ray image from run E3M8.

In the image on the right all gamma-ray image pixels below 50% of the maximum are set clear to allow one to see the overlay of the gamma-ray on the video data. This data was collected with the widest field of view, which is considerably larger than the field of view of the video camera.

The total spectrum for the run is shown in Figure 43. As can be seen the spectrum is commensurate with HBPu. This is evidenced by the weak 60-kev line from ^{241}Am, prominent U K_α lines (around 100 keV) and the strong 208-keV line.

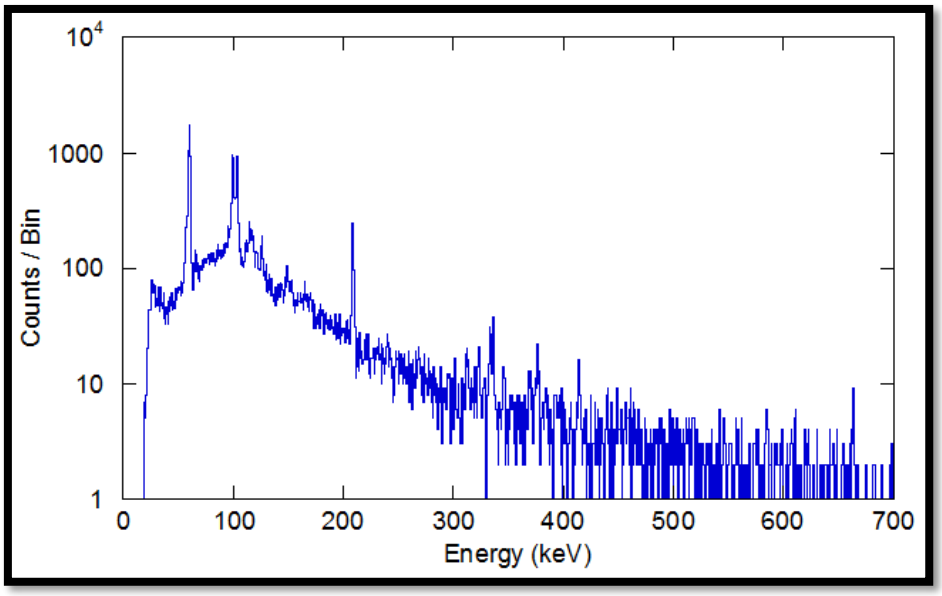

Figure 43. System7 total spectrum from run E3M8.

The system can also generate spectra from selected regions of the image and these are inherently background subtracted (Figure 44).

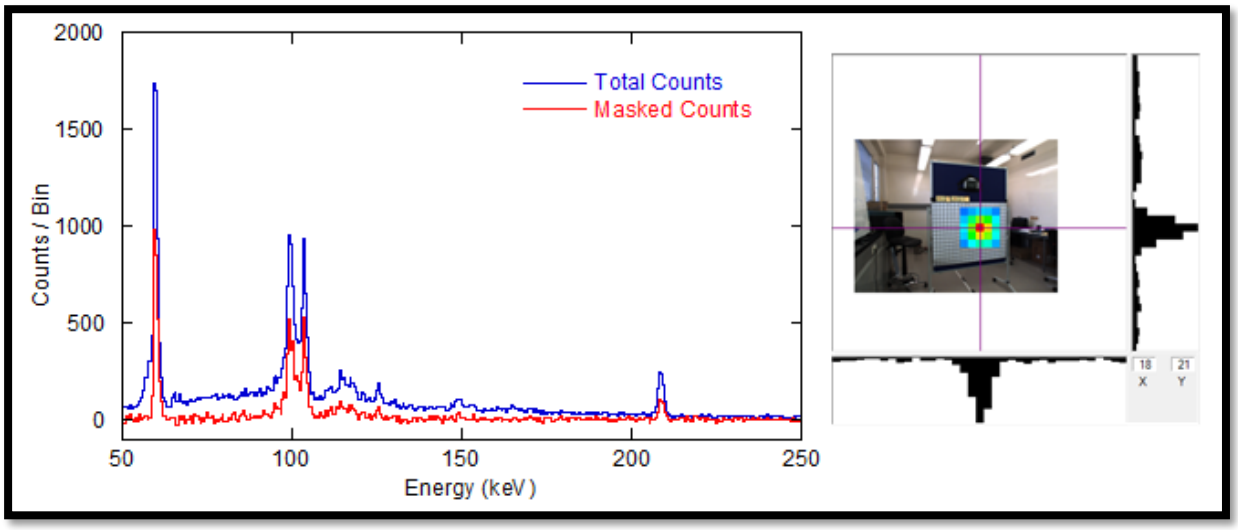

Figure 44. System7 spectrum from the source region indicated by the false color overlay in the image on the right. The whole-detector spectrum is shown in Figure 43 and is also plotted (blue).

The time to achieve a 50% alarm rate was just 3.5 s, while the 90% alarm time was reached in 6 s.

Measurement run E3M10 was similar to the E3M8, but obviously used a weaker source. There are a total of 3 min. of balanced mask/anti-mask data. The log file from the run shows an alarm at 44 s. The γ-ray image and spectra, which are now commensurate with ^{239}Pu, are shown in Figure 53. The Pu ID is based on the presence of the 375 and 414-keV lines and the absence of the 208-keV line. The spectrum masked to the source shows only the K-shell lines and the 60 keV ^{241}Am peak, the others are lost in the noise.

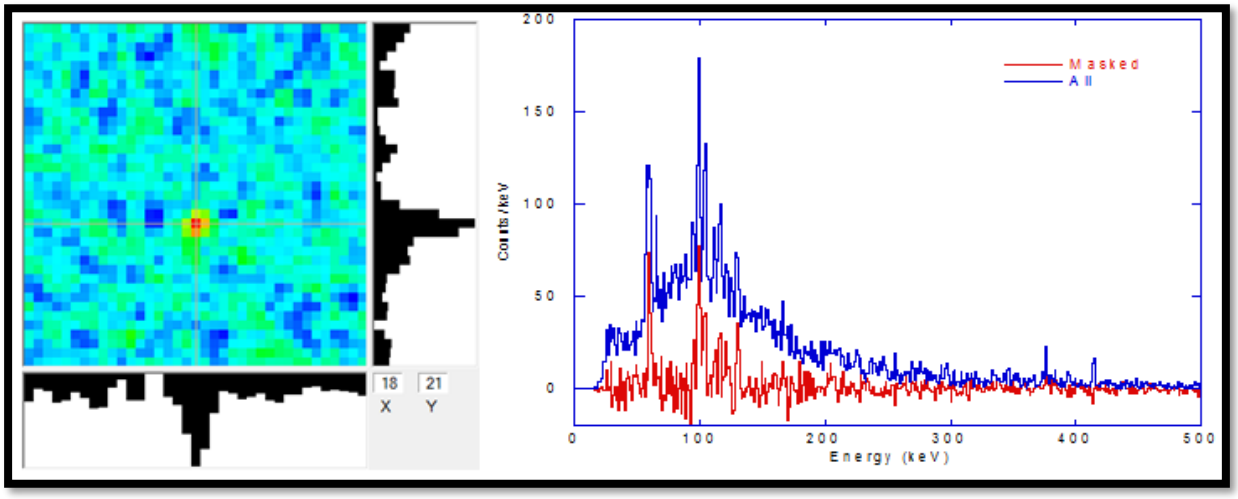

Figure 45. System7 source image (left) and spectra (right) for run E3M10.

The median detection time is 91 s (4,970 counts) while 90% detection occurs just at the 10,000 count limit for a time of 172 s.

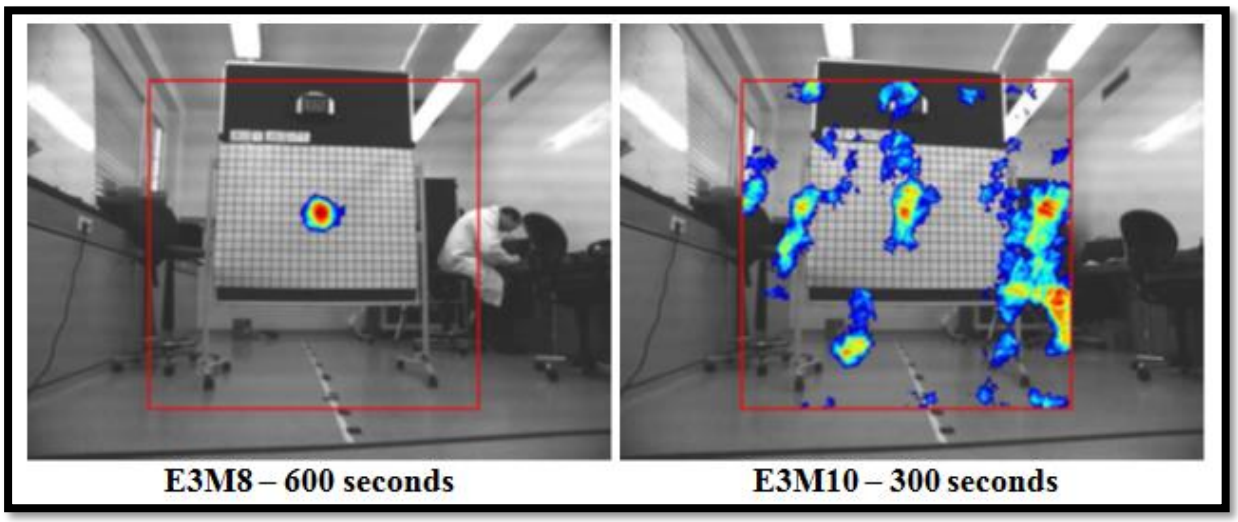

Figure 46. System6 imaging results for Experiment 3 (plutonium).

Source is localized in measurement E3M8, basically due to strong low-energy emissions from Am-241.

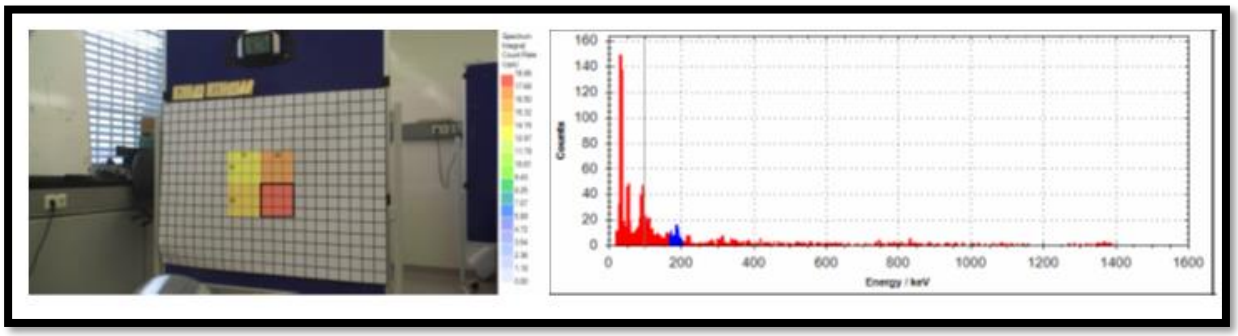

Figure 47. System8 imaging results for E3M9.

Measurement time of individual scan element was 50 seconds. Source is localized; Am-241 was identified; however U-235 instead of Pu was identified. In E3M9 run the same source was used as in E3M8 run.

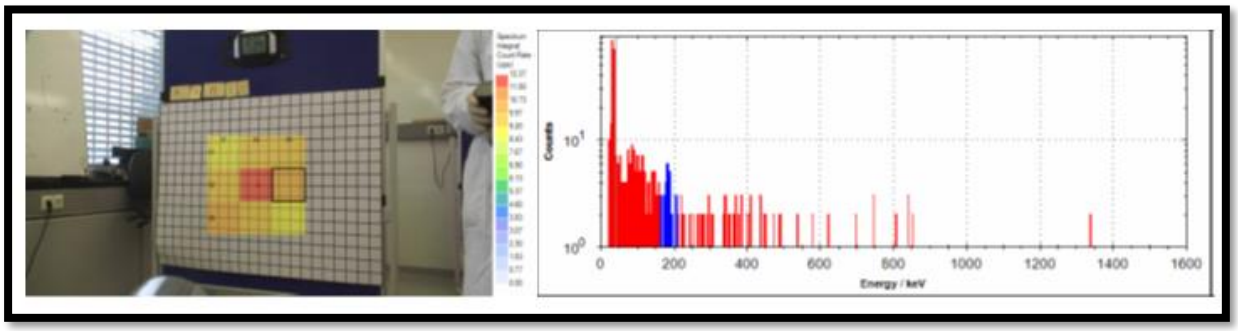

Figure 48. System8 imaging results for E3M10

In measurement E3M10, the measurement time of individual scan element was 30 seconds. Source is localized; however U-235 (186 keV) instead of Pu was identified.

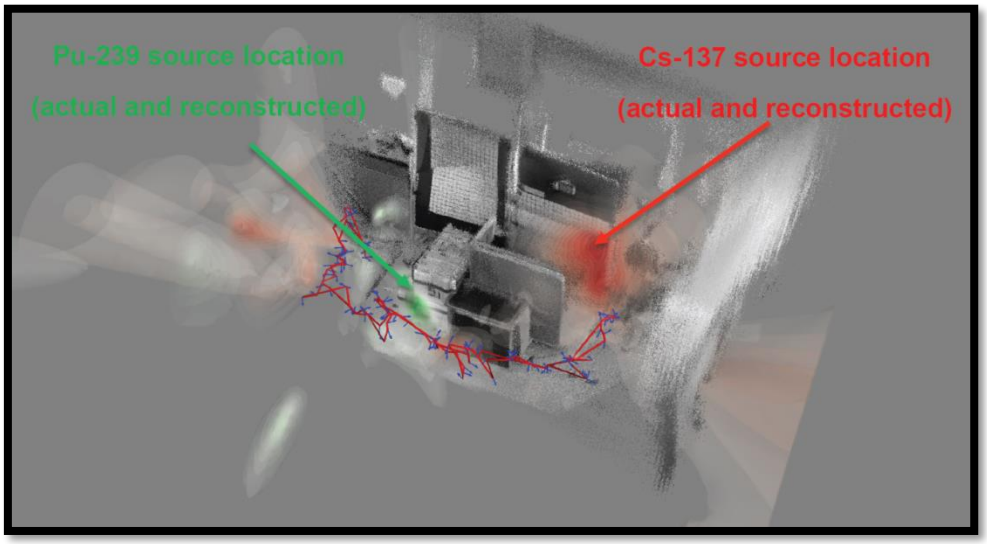

Figure 49. System5 3D volumetric Compton imaging of plutonium and Cs-137 sources, workshop dynamic experiment.

System5 is based on CZT detectors. Low-energy imaging threshold for Compton mode of operation is about 250 keV. This limits possibility of HEU and HBPu imaging. LEU and HEU sources could be imaged based on 1001 keV spectral line and LBPu and HBPu sources could be imaged based on spectral lines characteristic for Pu-239 (Figure 58). The green color map corresponds to the reconstruction about the ROI around 414 keV (Pu-239), while the red color map corresponds to the ROI around 662 keV (Cs-137).

5.3.2 Uranium measurements

The goal of measurement was to study capabilities of gamma-ray imagers to image non-complex geometries of U sources. Experimental setup is illustrated on Figure 58. Such characteristics as time to alarm and time to localize have been evaluated.

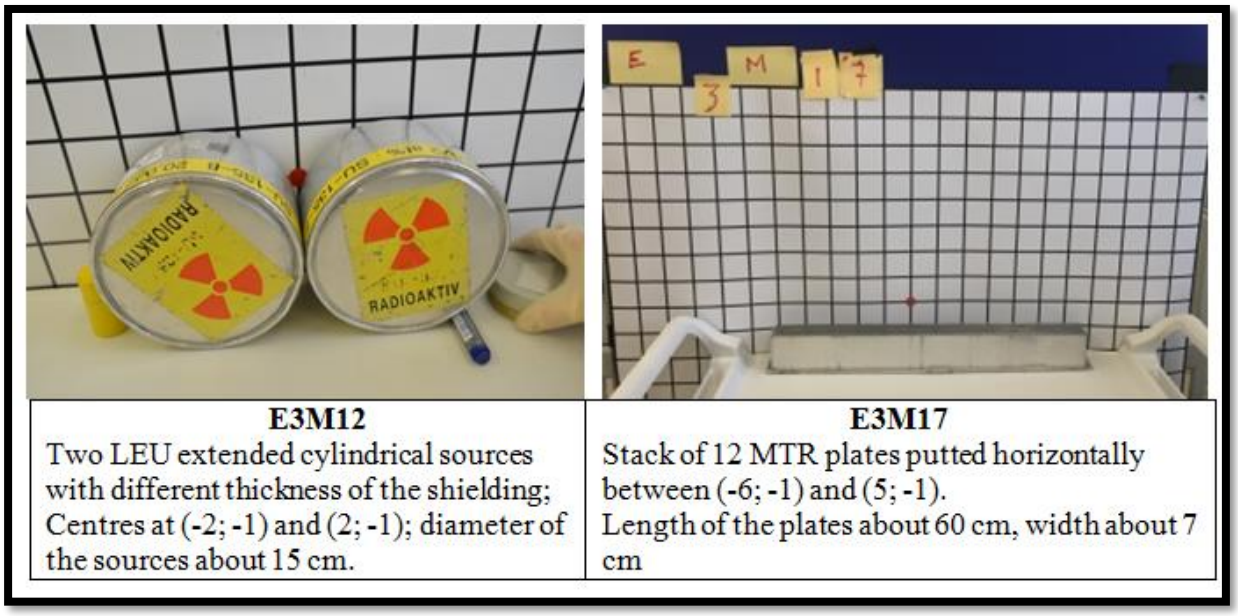

E3M12	E3M17
Two LEU extended cylindrical sources with different thickness of the shielding; Centres at (-2; -1) and (2; -1); diameter of the sources about 15 cm.	Stack of 12 MTR plates putted horizontally between (-6; -1) and (5; -1). Length of the plates about 60 cm, width about 7 cm

Figure 50. Experiment 3: Illustration of geometry of experimental setup for U measurements E3M12 (left) and E3M17 (right)

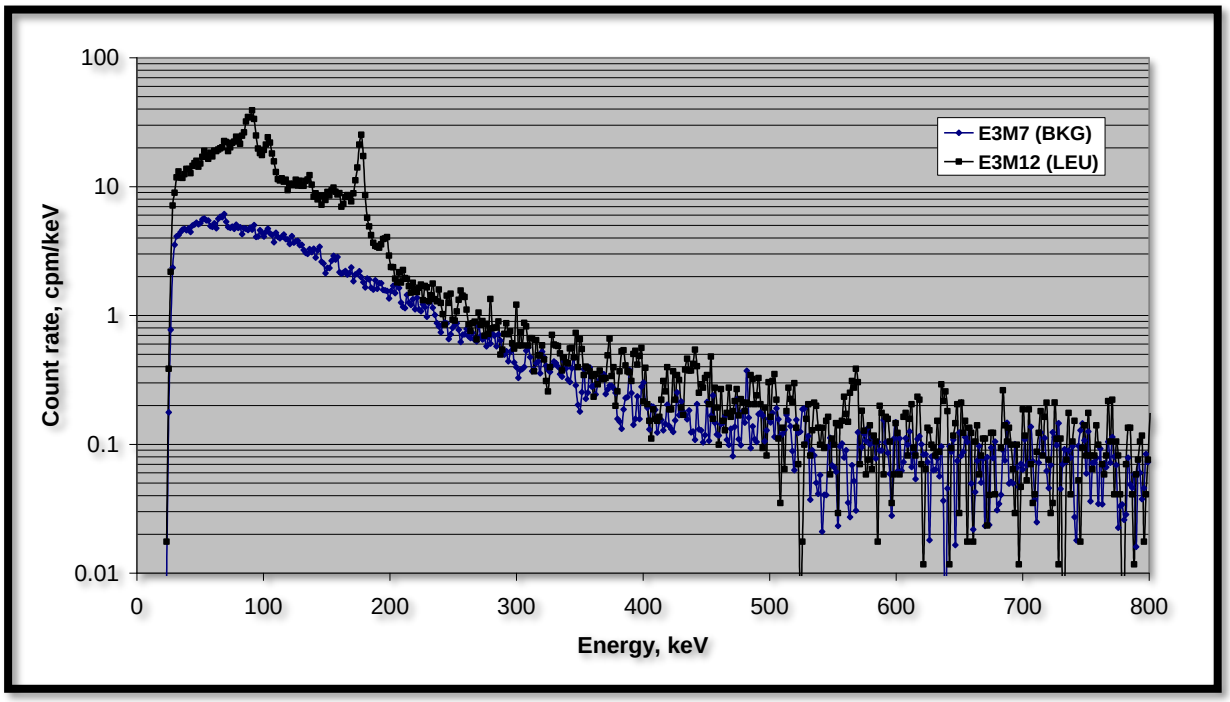

Figure 51. System3 comparison of U spectrum (E3M12) vs. background spectrum.

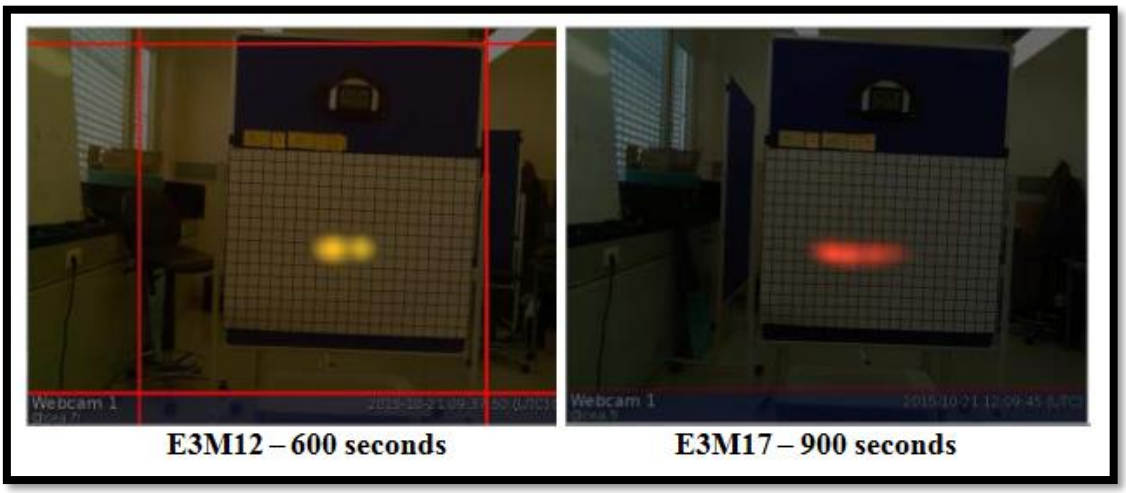

Figure 52. System3 imaging results for Experiment 3 (uranium).

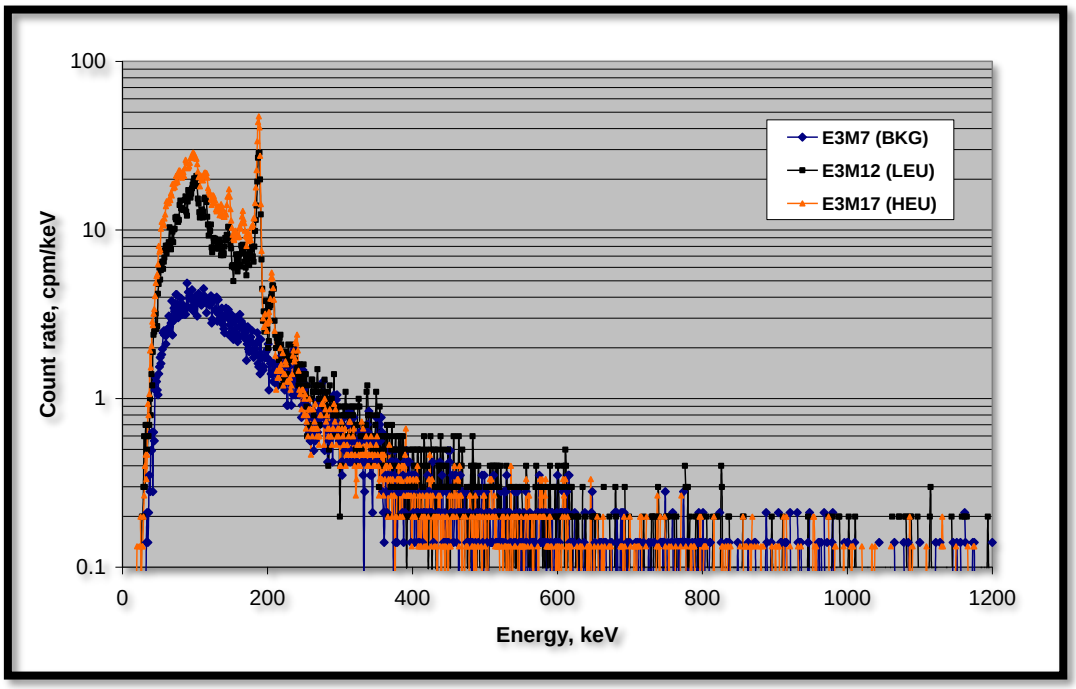

Figure 53. System1 comparison of U spectra measured in Experiment 3.

Based on 186 keV, the full-energy peak image can't be created. 1001 keV peak (Pa-234m) cannot be identified; measurement time was limited to 300 seconds, more long measurement needs to be conducted.

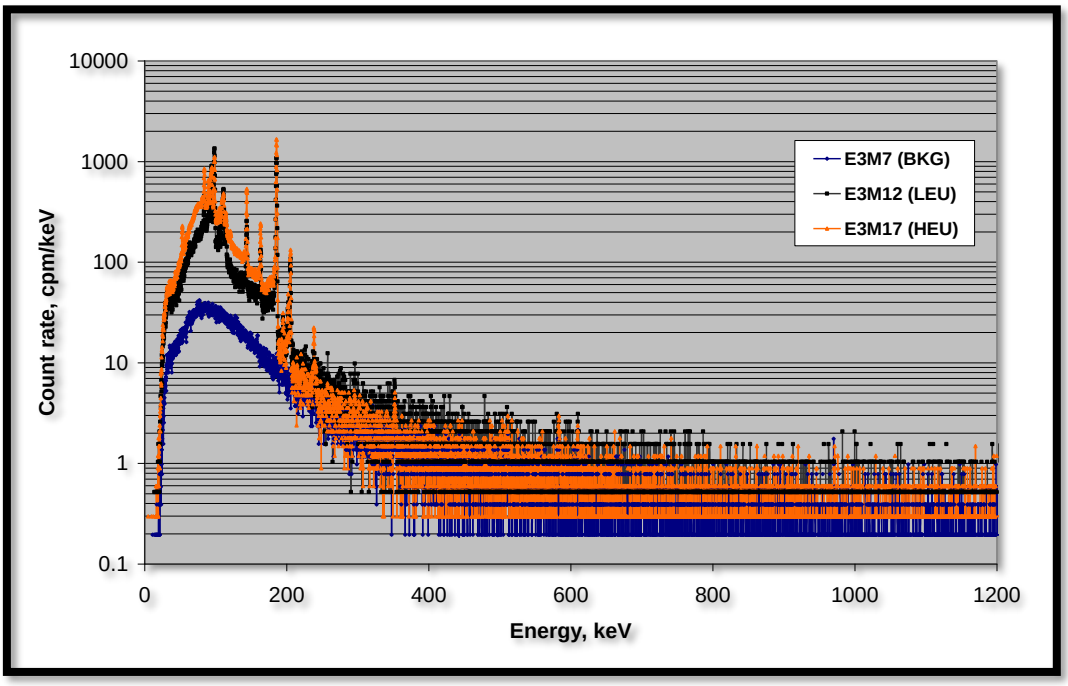

Figure 54. System4 comparison of U spectra measured in Experiment 3.

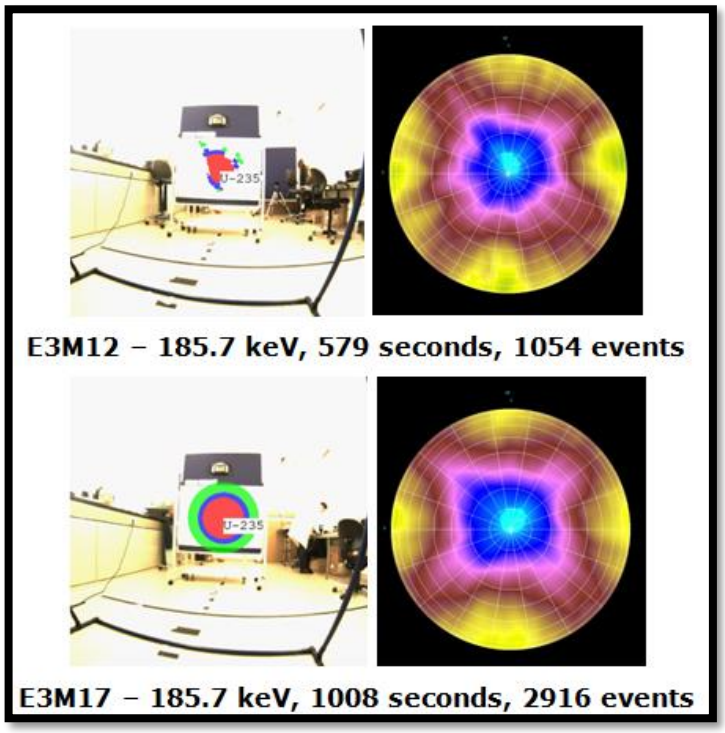

Figure 55. System4 imaging results in Compton mode for Experiment 3 (uranium).

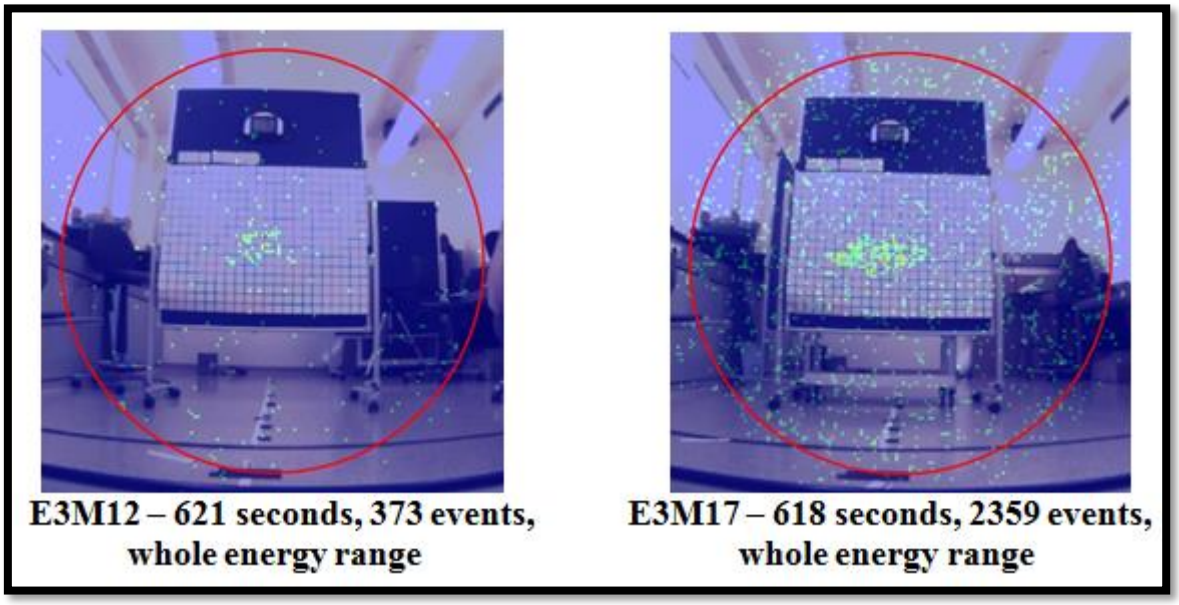

Figure 56. System4 imaging results in pinhole mode for Experiment 3 (uranium).

Basic energy peak of interest for imaging purposes is 186 keV (U-235). Image can be created by System4 in Compton mode. A fraction of full-energy peak events can be imaged (about 1/20).

1001 keV peak (Pa-234m) can be identified and as soon as certain N*sigma value is achieved LEU could be categorized. 1001 keV peak in practice is not useful for imaging purposes unless 186keV and 204keV peaks are suppressed by a shield.

Imaging of plutonium and uranium in Compton mode is limited to localization of a source; a source pattern cannot be correctly imaged.

During measurement E3 M12, the base distance is 260 cm and the information was provided that an extended source could be expected. Based on this, the focal length was set to 7 cm, providing a resolution of 7.46 cm with a pixel size of 3.73 cm. The image (Figure 65) shows an extended object that is stronger at either end. This is likely two side-by-side point sources separated by just more than the spatial resolution of the imager at this zoom.

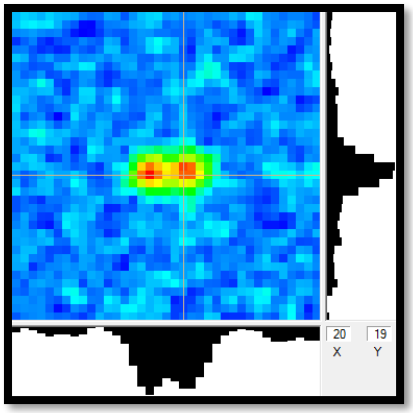

Figure 57. System7 gamma-ray image obtained for E3M12.

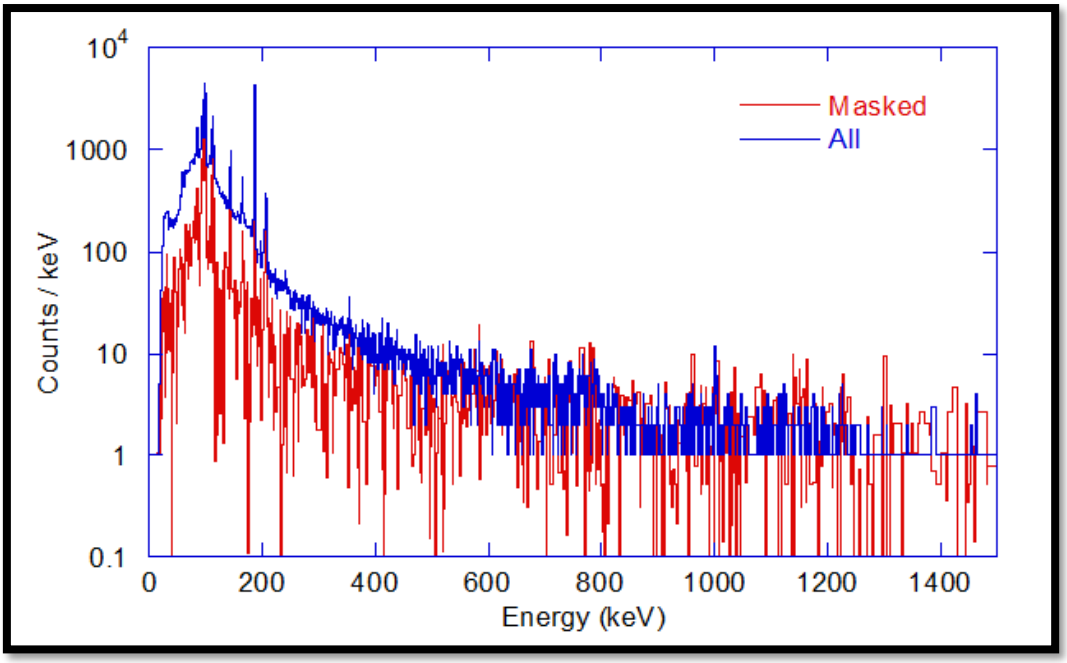

Figure 58. System7 total spectrum and masked spectrum for E3M12.

The total spectrum (Figure 58) indicates the presence of enriched uranium (EU) with both the 186-keV and 1-MeV lines visible. The masked spectrum has too few counts in the MeV line to generate reliable enrichment information. Spectra obtained by masking the individual sources (Figure 59) shows that they are both EU and of comparable magnitudes.

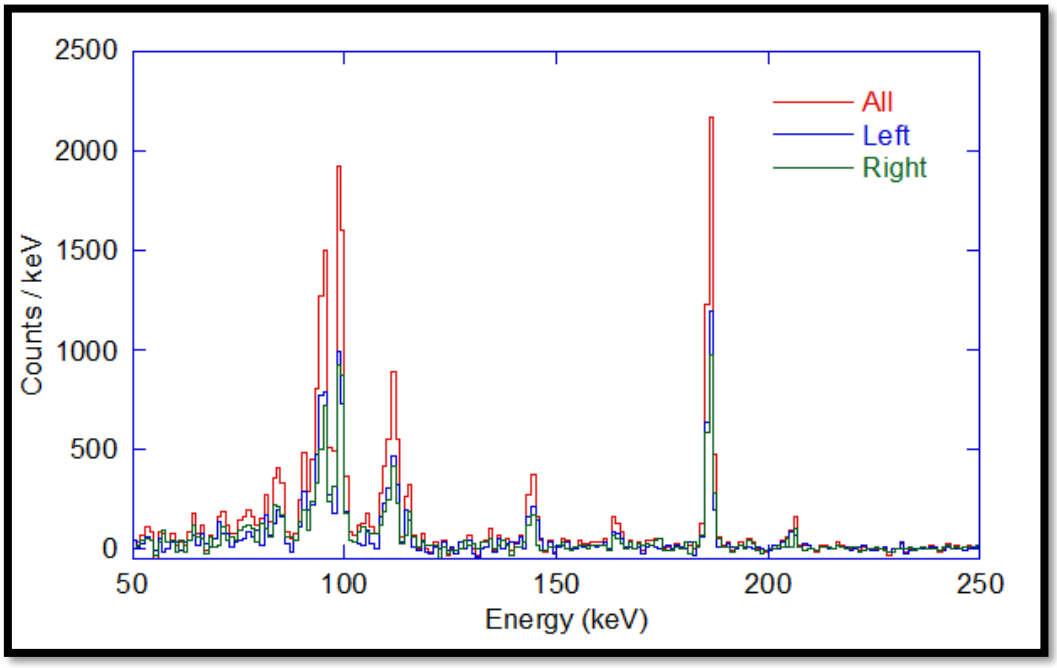

Figure 59. System7 masked spectra from the left and right sources compared to the entire source region for E3M12.

To determine the distance between the two point sources, a 2D Gaussian fit with the bounding box between the two sources is used. This is not as good as having a function that fits 2 point sources simultaneously. The net result is that the fit gives the centre of the right source at (20.48, 18.62) and the left source at (16.18, 18.77) for an x-spacing of 4.3 pixels or 16.0 cm. Note that the result changes linearly with the true distance to the image plane so any error in this number directly impacts the results.

The 90% alarm event count is at 10,926 counts or 49 s. A look at the alarm location shows a wide spread in x as one might expect given the distribution of the source. The x vs y plot shows 2 outliers that are flagged as false alarms. Due to the extended source, valid alarm pixels cover a wide area.

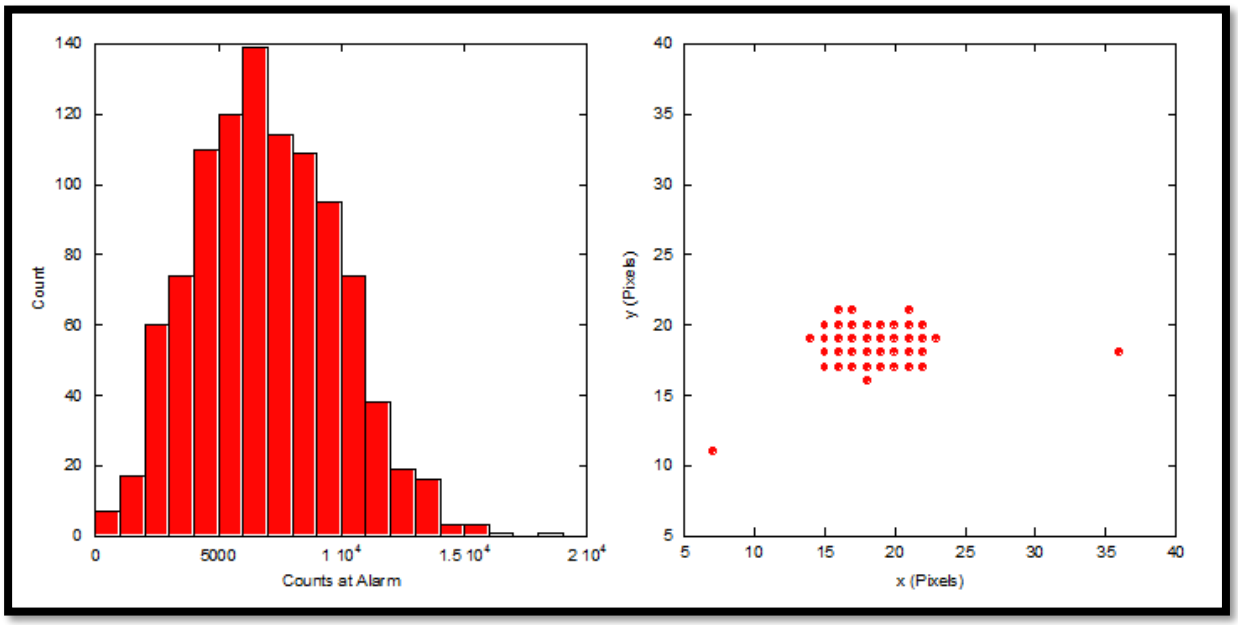

Figure 60. System7 bootstrap results for E3M12.

Measurement E3M17 was at a source distance of 240 cm and used a 7-cm focal length for a spatial resolution of 6.9 cm and a pixel size of 3.45 cm. There were some issues with starting the system, but it still managed to record a total of 4 mask cycles of 200 s per cycle, for a total of 800 s of data. The images (Figure 69) show a horizontal extended source. Note that with the imager offset from the experimental centreline (estimated at 1 m) the almost 23° view angle will add some distortion and clearly means any length estimate must be adjusted. The fact the system is at an angle (~ 23°) with the centreline is clearly evident.

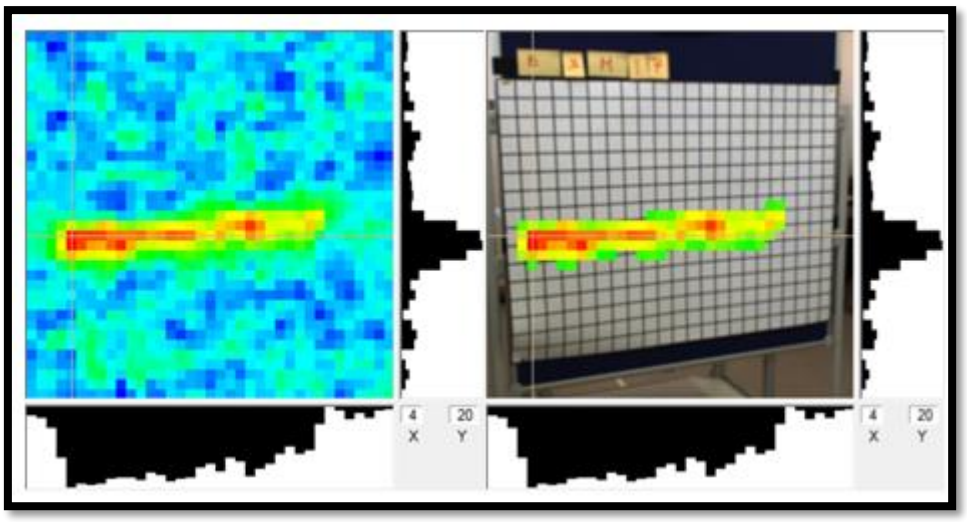

Figure 61. System7 images for measurement E3M17.

The spectra (Figure 70) are commensurate with EU. There is no evidence of the 1-MeV line, while there is some evidence for the Th K-shell fluorescence lines. Trying different energy cuts does not significantly enhance the image, but it does improve the calculated significance of some of the on-source pixels.

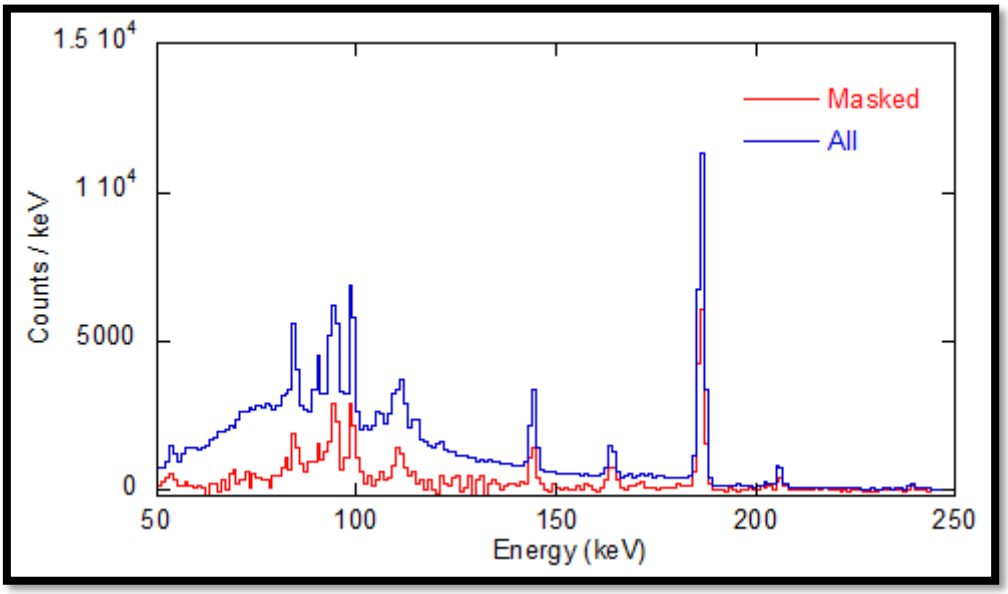

Figure 62. System7 spectra for run E3M17.

While the image appears to be “hotter” on the left side, this is presumably an artifact of how the image falls on the pixels, although the left side is also closer to the imager and there will be a small solid angle effect as well. The alarming algorithm in the software is currently poorly suited to detect a distributed source. It calculates an initial variance based on all of the pixels. Nevertheless, the system did alarm while the data were being collected at 361 s after the data collection started. Using the event rate for the run of 363 cps, the 50% alarm time was 268 s while the 90% alarm time was 551 s.

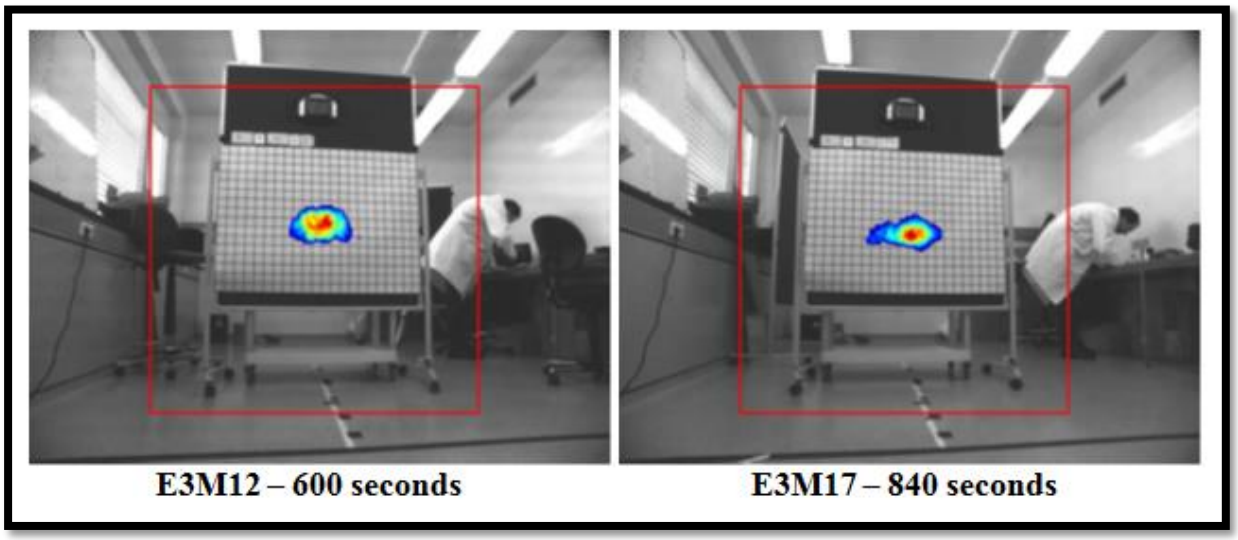

Figure 63. System3 imaging results for Experiment 3 (uranium).

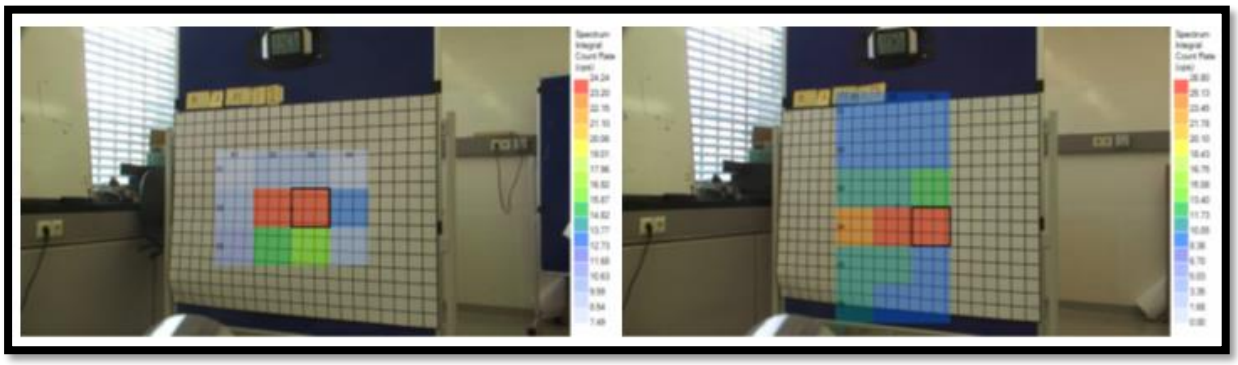

Figure 64. System8 imaging results for E3M12 (left) and E3M17 (right).

Sources are localized but not separated (E3M12). Pitch between scan elements is 3.5° and U-235 is identified. The extended source is localized (E3M17) and U-235 is identified.

5.3.3 Simultaneous U and Pu measurements

The goal of this experiment (E3M15) was to evaluate capabilities of gamma-ray imagers to localize U and Pu sources simultaneously. Ability of imagers to separate U and Pu sources was studied. Geometry of the measurements is described below and illustrated on Figure 65.

Geometry of measurements

- Two LEU extended cylindrical sources with different thickness of the shielding; centres at (-2; -1) and (2; -1); diameter of the sources is about 15 cm.
- Point HBU Pu source at (0; 3)
- Point LBU Pu source at (5; -2)
- Empty box with the centre at (-6; -1)

Figure 65. Photograph of the geometry of measurements (E3M15)

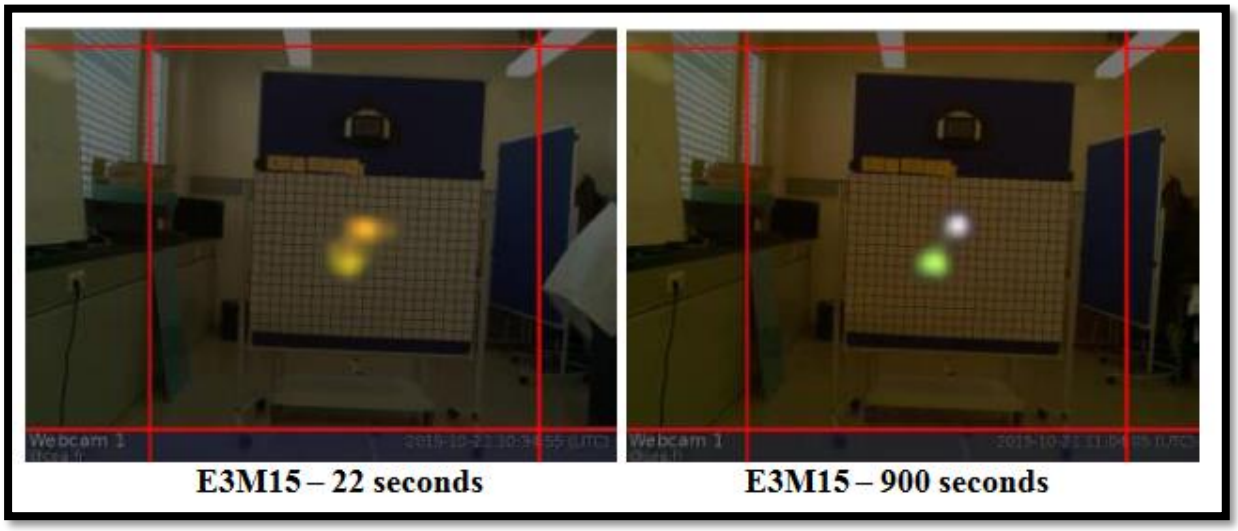

Figure 66. System3 imaging results (E3M15)

Sources are localized, separated and identified in 22 seconds (left). Resulting image with the U source in green and Pu source in white (right).

In System1 the 186 keV and 208 keV peals are identified, although it was not possible to get an image in Compton mode of operation.

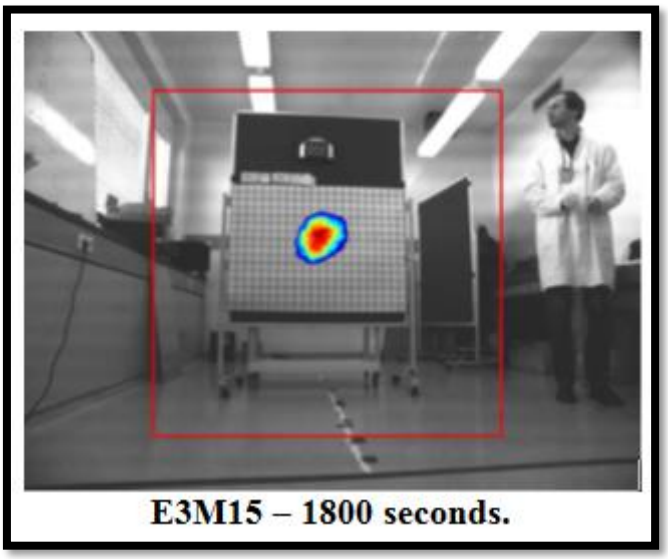

Figure 67. System6 imaging results (E3M15)

Two major sources are localized, but not separated (Figure 67). Availability of spectrometric information would be helpful in terms of sources separation based on ROIs.

Sources are localized (Figure 68) and separated based on the analysis of spectra (Figure 68 and Figure 69).

Figure 68. System8 imaging results (E3M15)

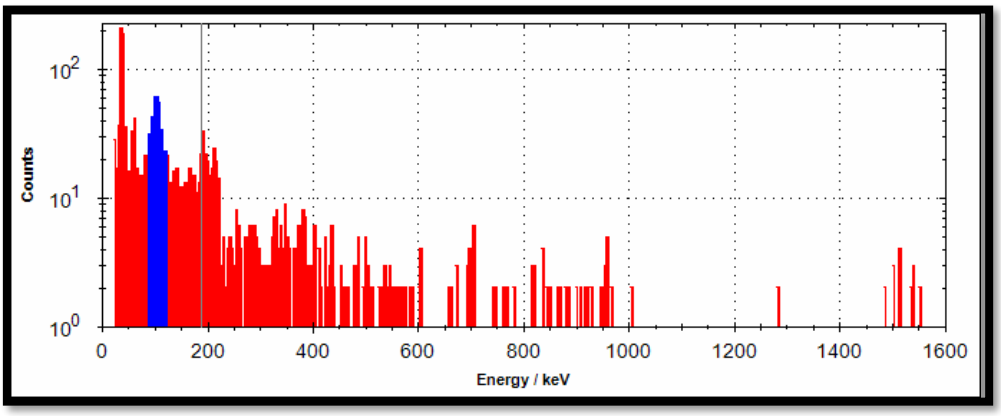

Figure 69. System8 spectrum of scan element (03, 02), measurement time 70 seconds; Pu-240 (104 keV) is identified.

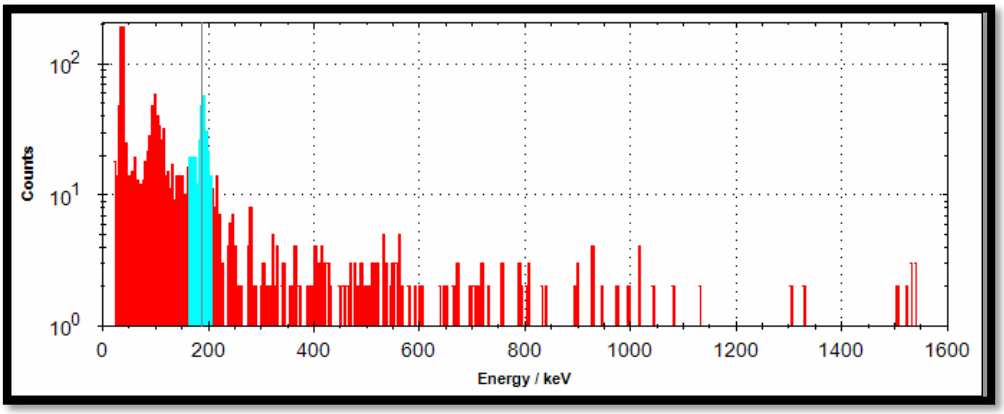

Figure 70. System8 spectrum of scan element (03, 03), measurement time 70 seconds; U-235 (186 keV) is identified.

Sources are localized and separated in pinhole mode based on the ROIs and are localized in Compton mode.

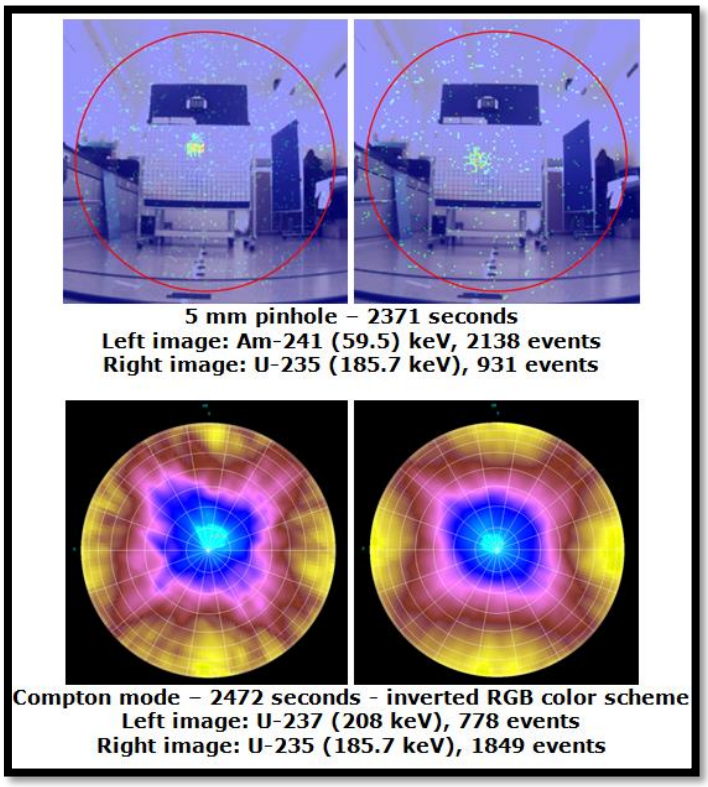

Figure 71. System4 imaging results (E3M15)

The results (Figure 72) clearly show two distinct sources, a point source near the top of the image with a HB Pu spectrum and an extended disc with an EU spectrum (Figure 73).

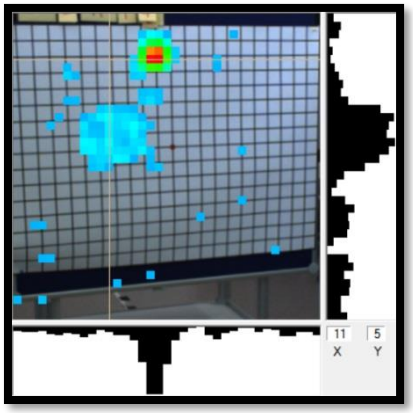

Figure 72. System7 Gamma-ray image for run E3M15. Measurement time 600 seconds.

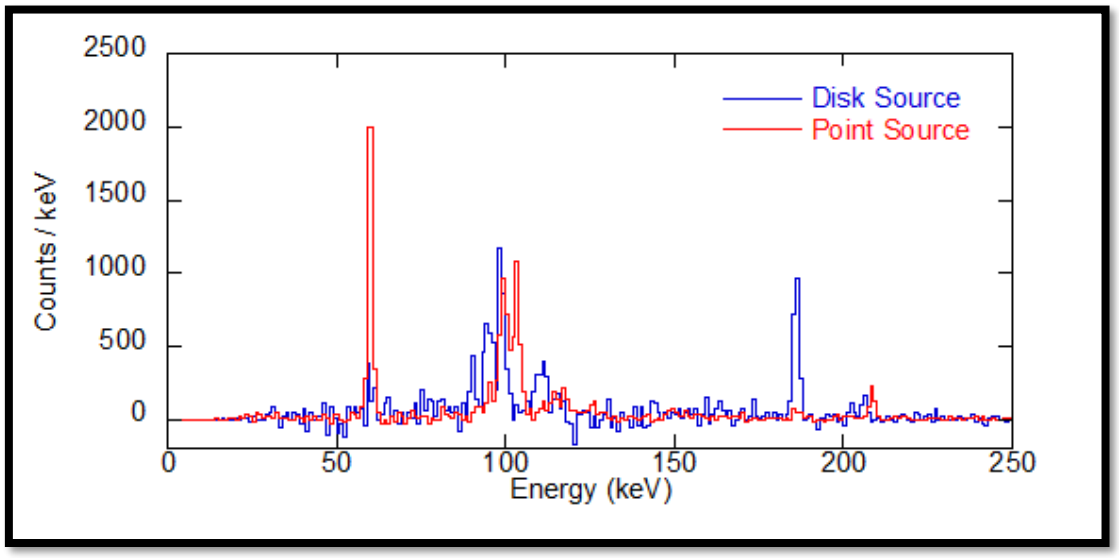

Figure 73. System7 Spectra from the two source regions in the image E3M15

Table 12. Experiment 3. Summary of the results: total sensitivity

Experiment	Source	Source dose rate, nSv·h^{-1}	Total sensitivity, cpm/nSv·h^{-1}							
			System1	System3	System4	System8	System6	System7	System5	System2
E3M8	HBPu	20	33.2	45.9	600.4	28.7	15.0	258.0	ND	0.21
E3M10	LBPu	10	4.2*	13.8	174	17.8	2.4	90.0	ND	0.06
E3M12	LEU	20	59.8	81.9	1001.9	44.8	ND	570.0	ND	0.81
E3M17	HEU	40	51.1	62.0	793.6	26.3	ND	480.0	ND	ND

** Data are representative only as imager was shielded by somebody standing in front.*
ND – no data

Table 13. Experiment 3. Summary of the results: sensitivity in full-energy peaks

Experiment	Source (peak energy)	Source dose rate, nSv·h^{-1}	Sensitivity in full-energy peak*, cpm/nSv·h^{-1}		
			System1	System3	System4
E3M8	HBPu (208 keV)	20	2.3	1.4	12.5
E3M12	LEU (186 keV)	20	15.5	9.6	87.8

** Sensitivity was calculated substracting background in the ROI corresponding to the full-energy peak. For CZT-based gamma-ray imagers width of ROIs was 20 keV, for HPGe-based gamma-ray imager width of ROIs was 5 keV.*

Table 14. Experiment 3. Summary of the results: time to alarm /identify /localize (in seconds)

	Measurement														
	E3M8			**E3M10**			**E3M12**			**E3M17**			**E3M15**		
	HBPu			**LBPu**			**2 x LEU**			**MTR plate**			**U+Pu**		
Imager	***TTA***	***TTI***	***TTL***	***TTA***	***TTI***	***TTL***	***TTA***	***TTI***	***TTL***	***TTA***	***TTI***	***TTL***	***TTA***	***TTI***	***TTL***
System3	12	54	60	300	300	300	7	7	30**	15	20	32**	8	8	22**
System1	252	252	600	NR	NR	NR	12	12	NR	18	18	NR	72	468	NR
System4	3	3	38	48	48	290	0.1	0.1	7	1	1	12	0.1	0.1	5
System8	200	200	200	270	270	270	540	540	540	810	810	810	1660	1660	1660
System5	ND	ND	ND	ND	ND	ND	ND	ND	ND	ND	ND	ND	ND	ND	ND
System6	ND	NA	100	ND	NA	NR	ND	NA	60*	ND	NA	70*	ND	NA	1800*
System7	6	6	6	86	86	86	47	47	47**	551	551	551**	200	200	200**

** Source geometry is visible*
*** Source geometry is clear*
NA – not applicable, no spectrum available
NR – not reached within measurement time
ND – no data
TTA – time to alarm
TTI – time to identify
TTL – time to localize

System3

Time to alarm is determined from gamma-ray image. As soon as signal value (in pre-defined energy range) in any imaged pixel exceeds mean signal value calculated from all imaging pixels for certain threshold, an alarm is generated. Time to identify, is determined from cross-comparison of amplitudes of radiation signal in pre-defined ROIs, which correspond to full-energy absorption peaks. In case, if the amplitude of signal in one of the ROIs is clearly higher than in the others, an identification flag is raised. Identification cannot be triggered in case, if alarm flag was not raised. Time to localize is determined from gamma-ray image. As soon as mean signal value (in pre-defined energy range) in the cluster of imaged pixels exceeds mean signal value calculated from all imaging pixels for certain threshold, a localization flag is raised.

System1

Time to identify is determined from spectrum. In case if the net full-energy absorption peak area exceeds background area under the peak for certain N-sigma value, identification is made. Time to localize was reached in E3M8 and was determined visually based on the contrast of gamma-ray image, which however had some artefacts. In E3M15 185.7 keV peak was identified in 72 seconds and 208 keV peak in 468 seconds.

System4

Time to identify is determined from spectrum. In case, if the net full-energy absorption peak area exceeds background area under the peak for 8-sigma identification is made. Time to localize was determined visually depending on the contrast of gamma-ray image. Background calculations are performed by averaging the counts in windows on the low side and high side of a peak. The average of these counts multiplied by number of peak channels is subtracted from total peak area in order to obtain the net peak value. N-sigma value could be adjusted by operator. Time to alarm is equal to time to identify and not linked to imaging data. Values are reported for Compton mode of imager operation. Extended sources geometries were not clear.

System8

Actual time required to scan area of interest is reported. From one side value could be improved making shorter scans; from the other side measurement time could be increased in case if better angular resolution is needed.

System6

Time to localize was determined visually depending on the contrast of gamma-ray image.

System7

Time to alarm is determined from gamma-ray image. As soon as signal value (in the whole energy range) in any imaged pixel exceeds mean signal value calculated from all imaging pixels for 5-sigma, an alarm is generated. Values reported in the table correspond to 0.9 probability of alarm at 0.95 confidence level. Extended sources geometry at alarm time in all cases was clear. To generate a gamma-ray image more energy windows could be defined by the operator and each could have up to 3

ROIs. Alarm comparisons could be made for each energy window and N-sigma value could be adjusted by the operator. As soon as a high-resolution spectrum of each imaged pixel is available, the time for the operator to identify is within TTL.

5.4 Experiment 4 and 5: Angular Resolution

5.4.1.1 Angular resolution – same radionuclides

The goal of this experiment was to measure angular resolution. 2 Am-Li sources having similar activity were used. Distance between sources for the measurements M19, M20, M21 and M22 was 50, 30, 20 and 10 cm correspondingly. Sources were placed symmetrically with reference to the centre of the screen and distance from the screen to the rack populated with gamma-ray imagers was 4 m. The geometry of measurements is illustrated on the Figure 74 and is defined in Figure 75. Sources had cylindrical shape.

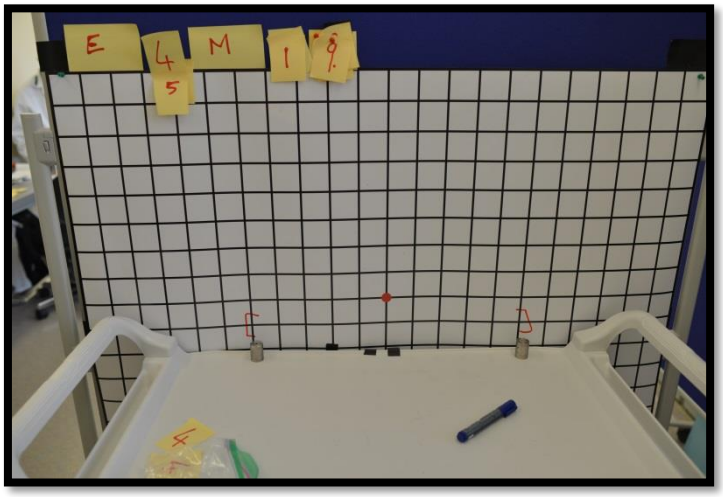

Figure 74. Illustration of the geometry of angular resolution measurements. Distance between two Am-Li sources is 50 cm.

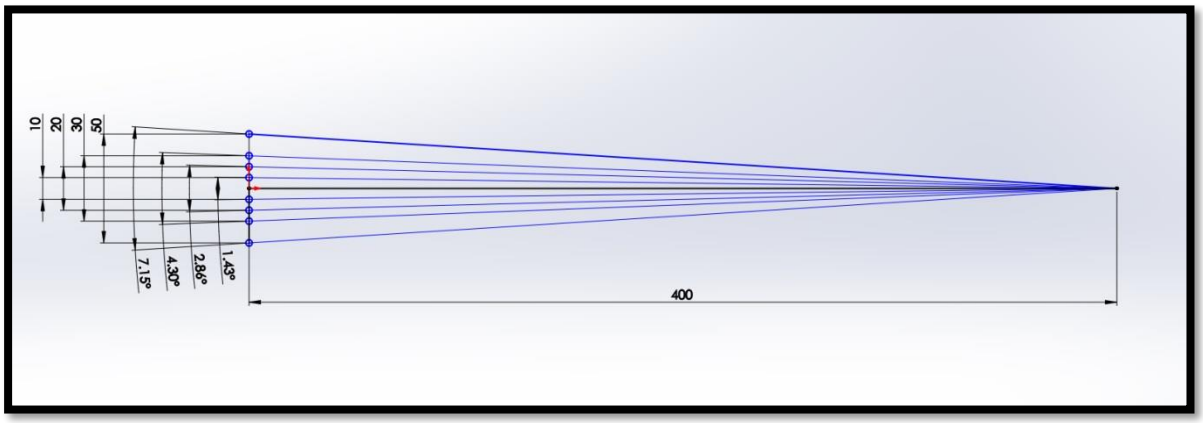

Figure 75. E4/5M19 – E4/5M22, geometry of measurements, dimensions are in centimetres.

For the measurements M23, M24 and M25 screen was moved to the side, so the centre of the screen was 1 meter away from the centre of the field of view of gamma-ray imagers. Distance between sources was 10, 20 and 30 cm correspondingly. Dependence of angular from the field of view was qualitatively studied.

Results of measurements of angular resolution under measurements E4/5M19–E4/5M22 are summarized in Table 15. Resulting images for measurements E4/5M19–E4/5M25 are shown on the

Figure 76-Figure 80. Results of comparison of sensitivity under measurements M22 and M23 for System3 and System7 are summarized in Table 16.

Table 15. Experiment 4 and 5: Angular resolution. Summary of the results

	Measured angular resolution, degrees
Imager	**E4/5M19 – E4/5M22 2 x Am-Li sources**
System3	2.9
System1	NA
System4	4.3
System8	4.3
System5	NA
System6	4.3
System7	1.4

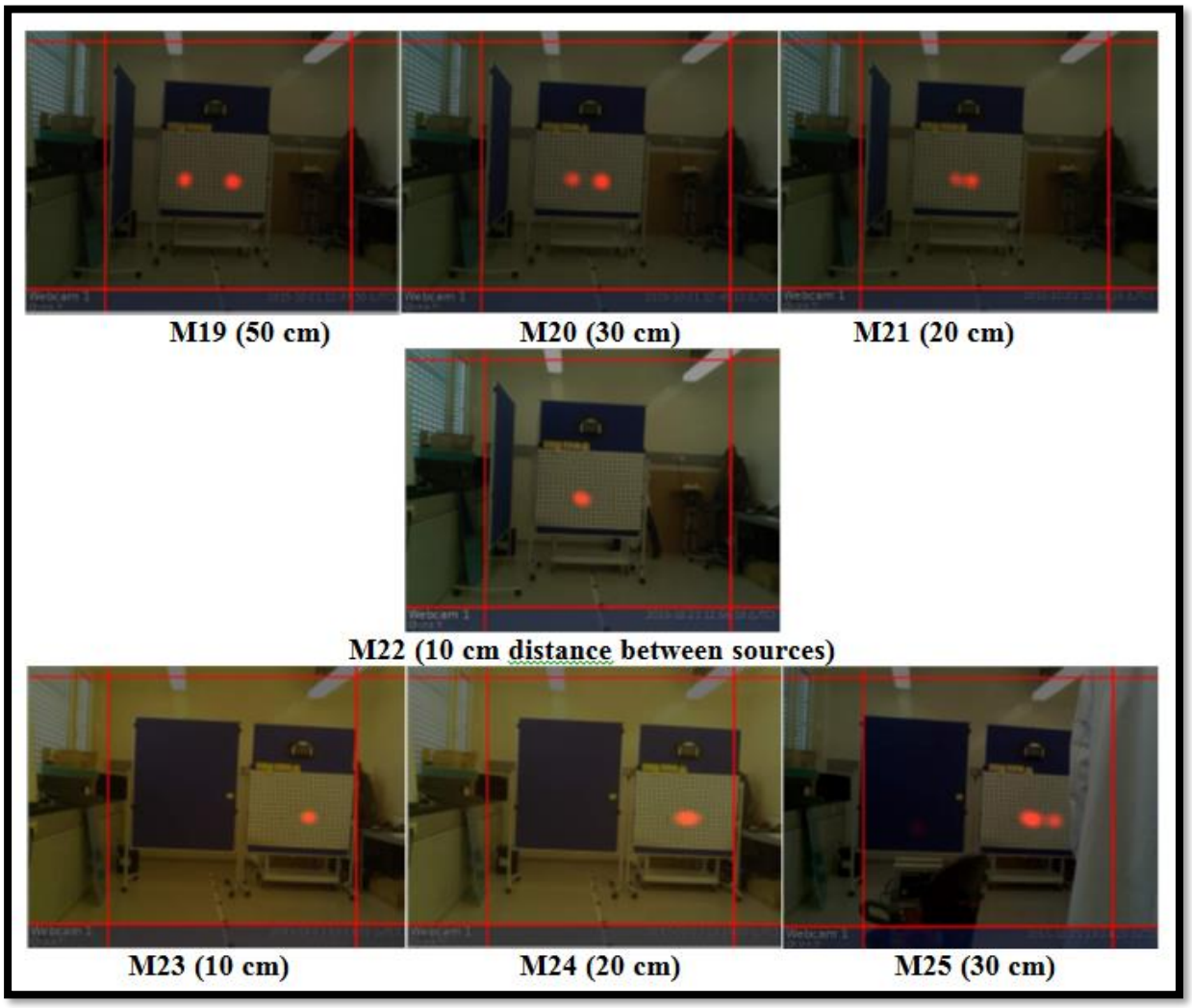

Figure 76. System3 imaging results (E4/5M19 – E4/5M25)

Angular resolution is 2.9 degrees (20 cm distance between sources) for the sources in the centre of the field of view and 4.3 degrees (30 cm distance between sources) for the sources moved for 1 meter out from the centre of the field of view.

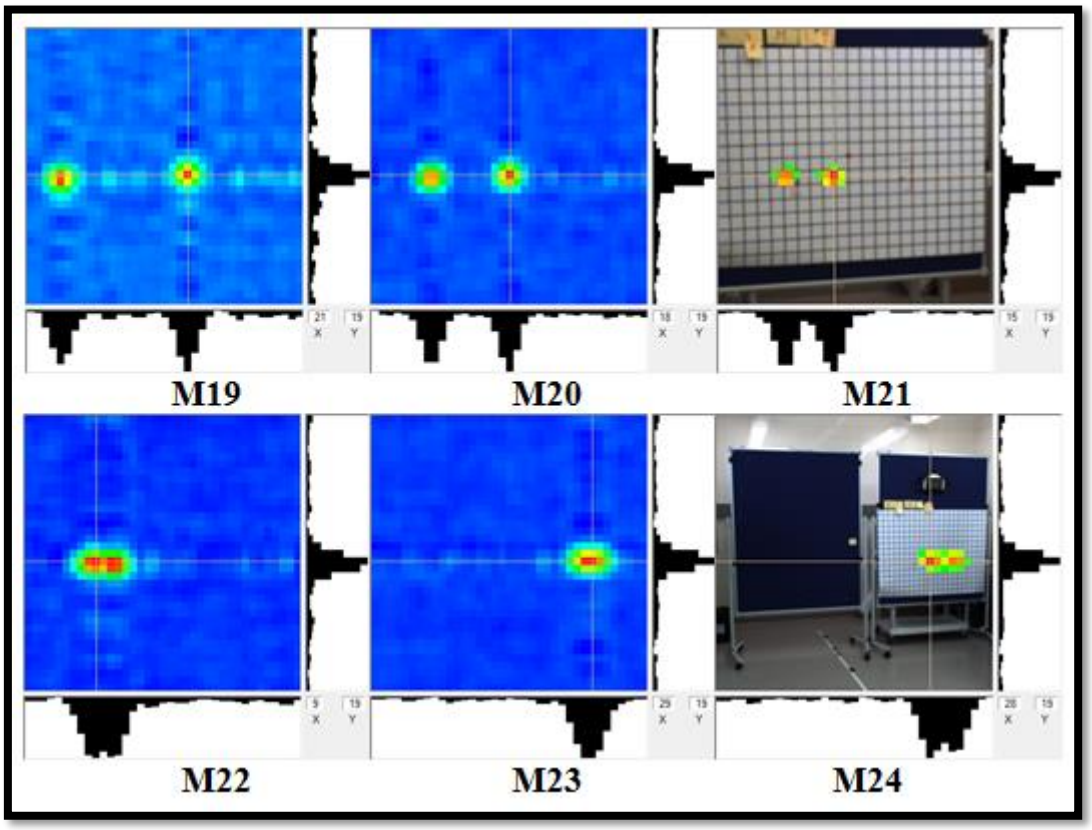

Figure 77. System7 imaging results (E4/5M19 – E4/5M24)

Angular resolution is 1.4 degrees (10 cm distance between sources) for the sources in the centre of the field of view and 2.9 degrees (20 cm distance between sources) for the sources moved for 1 meter away from the centre of the field of view.

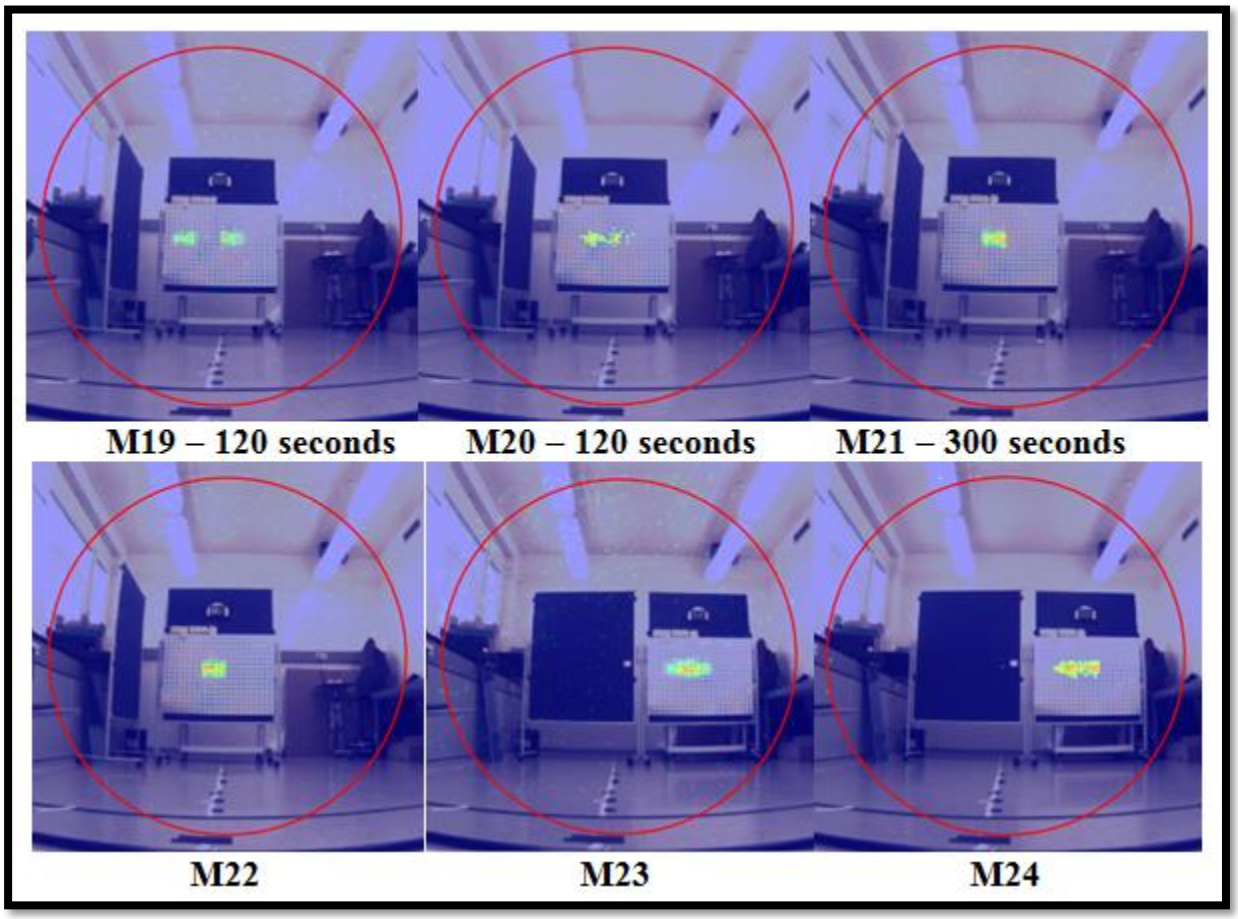

Figure 78. System4 imaging results (E4/5M19 – E4/5M24)

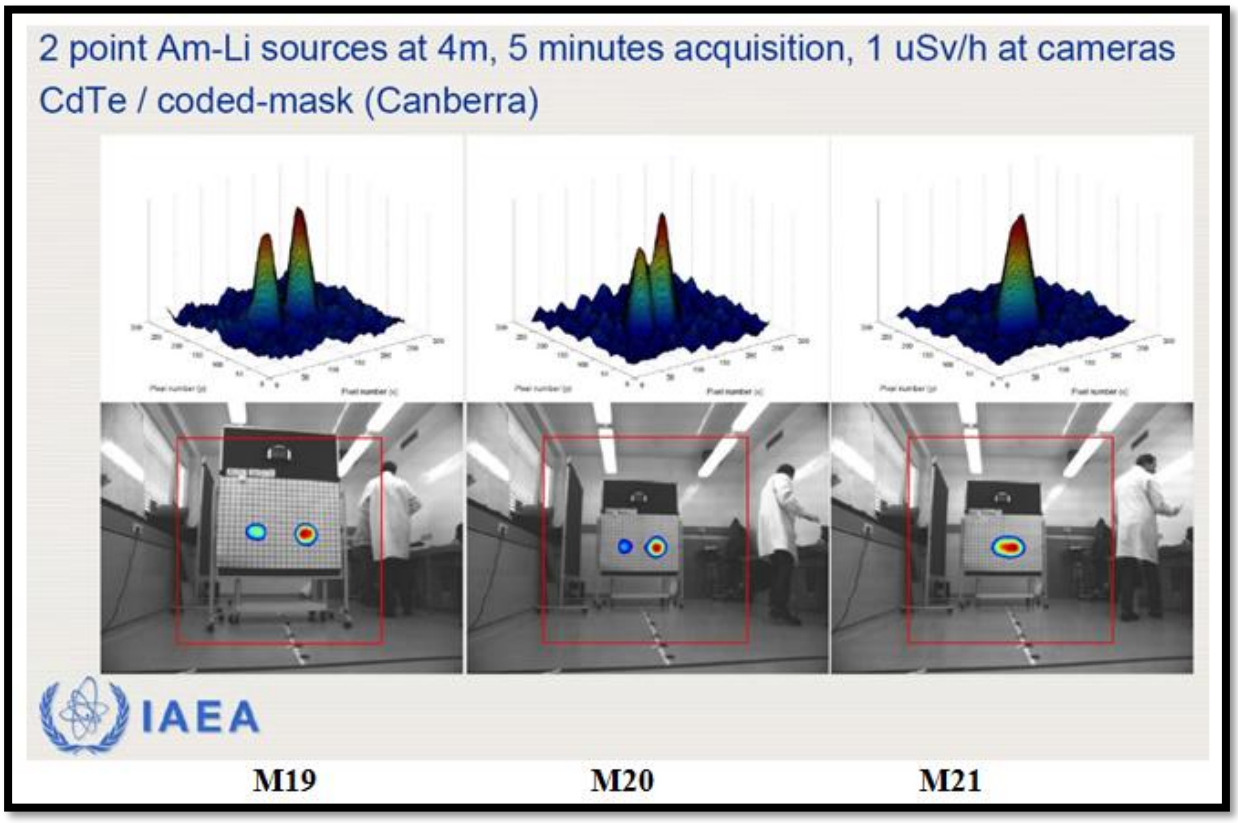

Figure 79. System6 imaging results (E4/5M19 – E4/5M21)

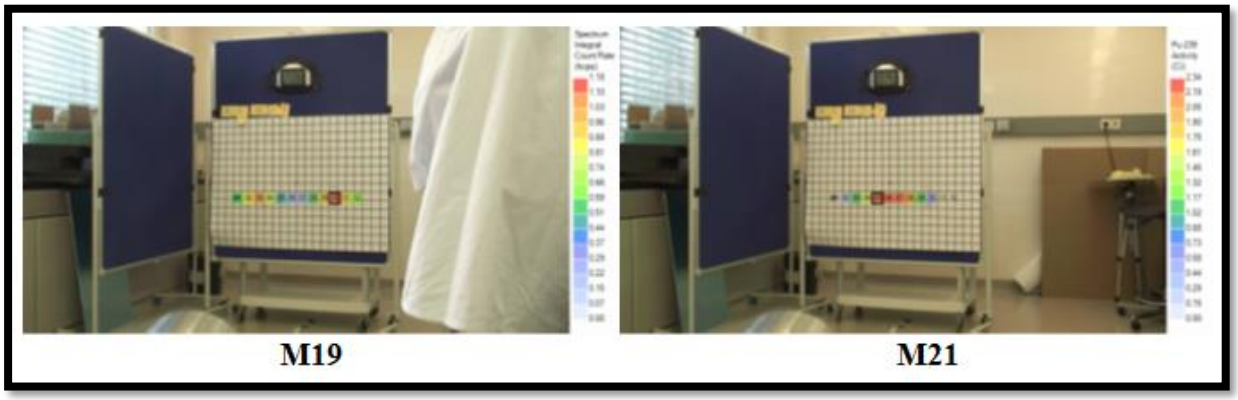

Figure 80. System6 imaging results (E4/5M19 and E4/5M21)

Table 16. Comparison of sensitivity for measurements M22 and M23

	Count rate, cps		**Ratio**
Imager	**M22**	**M23**	**M22/M23**
System3	499	278	**1.82**
System7	12727	8937	**1.42**

For System7, a 40% decrease in sensitivity was partly associated with an increase of distance to the sources as imager was positioned at an angle to the target screen and sources for measurement M23 were moved to the opposite corner.

For System3, an 80% decrease in sensitivity is related to the drop of sensitivity across field of view. In M22 measurement sources were in the centre of the field of view (FOV) and in M23 measurement sources were close to the edge of the FOV.

5.4.1.2 Angular separation – different radionuclides

In terms of angular resolution ability to separate different radionuclides, is an inherent property of Compton imagers as imaging is made based on full-energy peak events. For coded-aperture imagers ability to separate different radionuclides could be enhanced creating images based on the different ROIs characteristic for these radionuclides.

In measurements E4/5M26 - E4/5M28 unshielded Cs-137 and shielded Co-60 sources were used. Geometry of measurements is described in Table 17 and illustrated on Figure 81.

Table 17. Experiment on Angular separation, geometry of measurements

Measurement	Description of experimental setup	Distance between sources, cm
E4/5M26	Cs-137 point source at (-2; -1) Shielded Co-60 source at (2; -1)	20 (X-axis)
E4/5M27	Shielded Co-60 source at (-2; -1) Cs-137 point source at (4; -1)	30 (X-axis)
E4/5M28	Shielded Co-60 source at (0; -1) Cs-137 point source directly on it, at (0; 0)	5 (Y-axis)

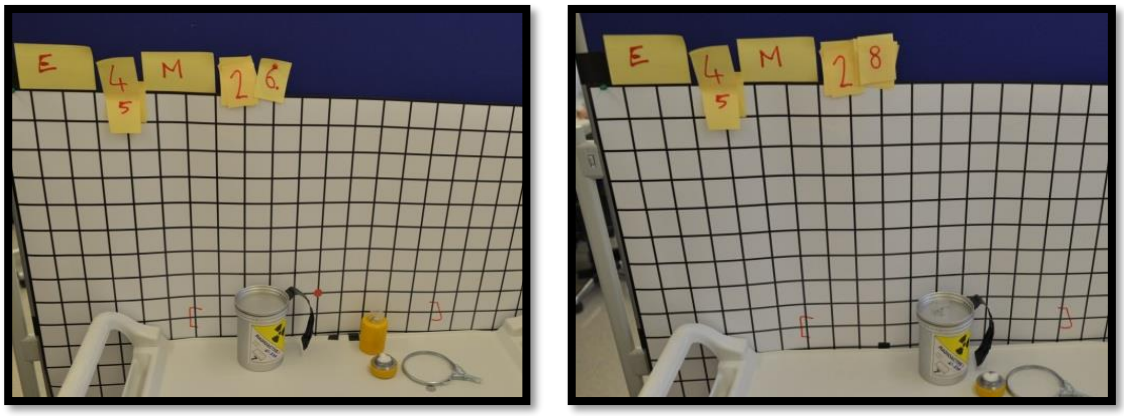

Figure 81. Angular separation, illustration of experimental setup.

Imaging results are shown in Figure 82- Figure 92.

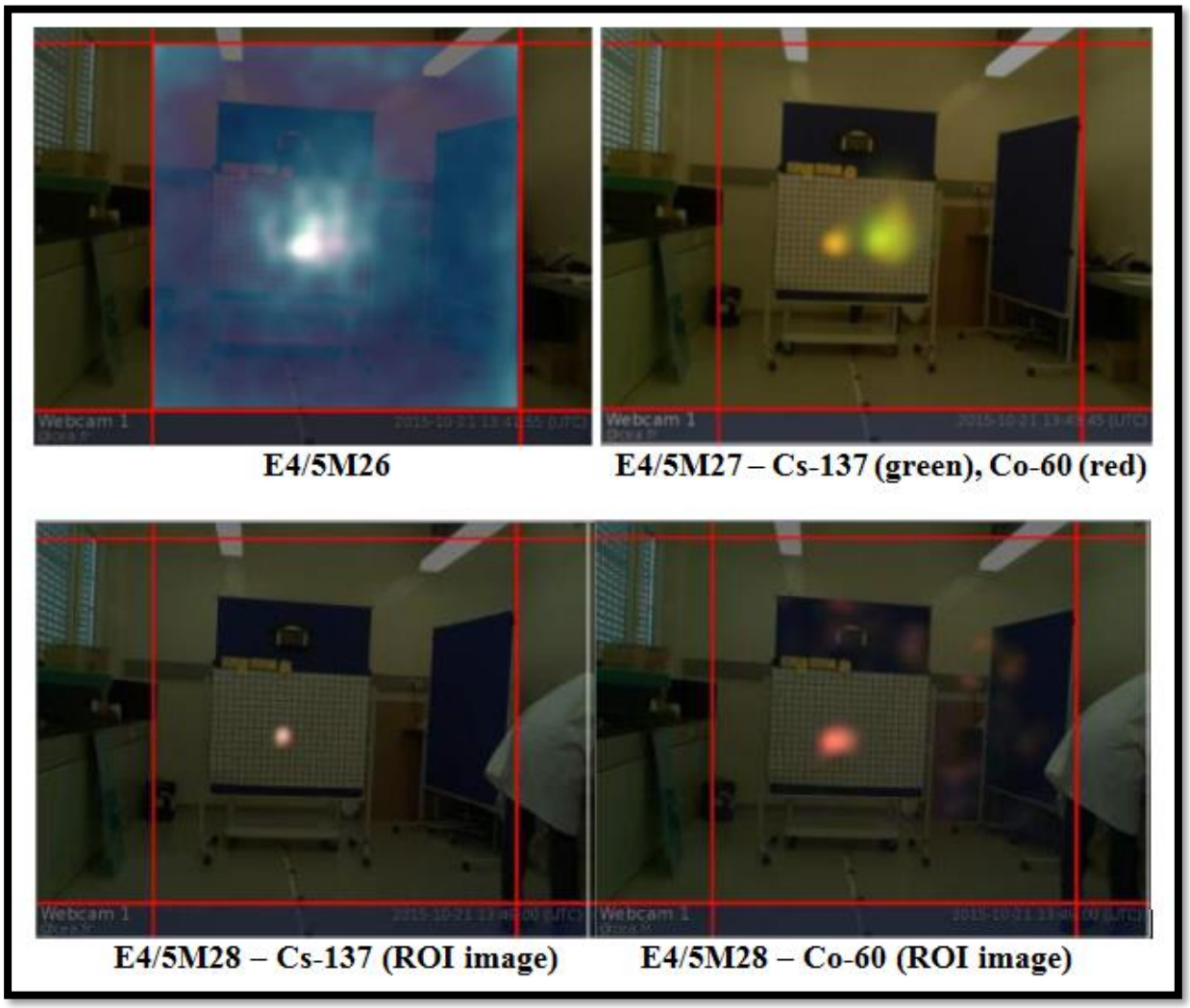

Figure 82. System3 imaging results for E4/5M26-E4/5M28.

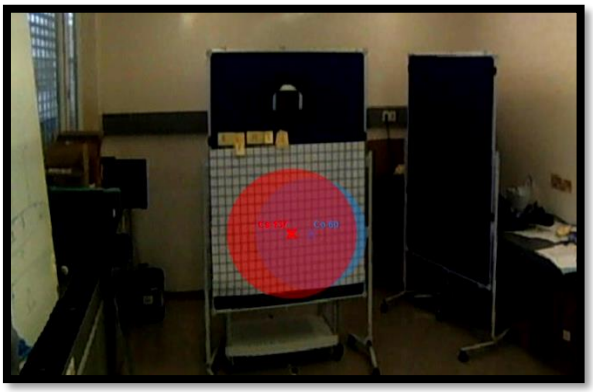

Figure 83. System1 imaging results for E4/5M26

On the Figure below 3D diagrams of intersections of Compton cones are shown for Cs-137 and Co-60. Localization of Co-60 is more precise since 3D peak is sharper (better FWHM). This could be attributed to better space separation of the events at higher energies.

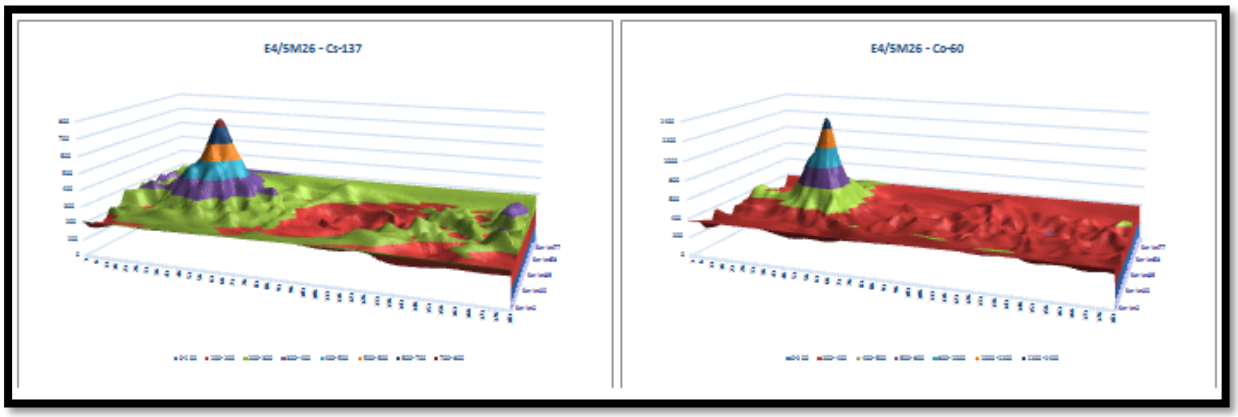

Figure 84. System1, 3D Diagrams of Compton cones intersections for E4/5M26; Cs-137 (left), Co-60 (right)

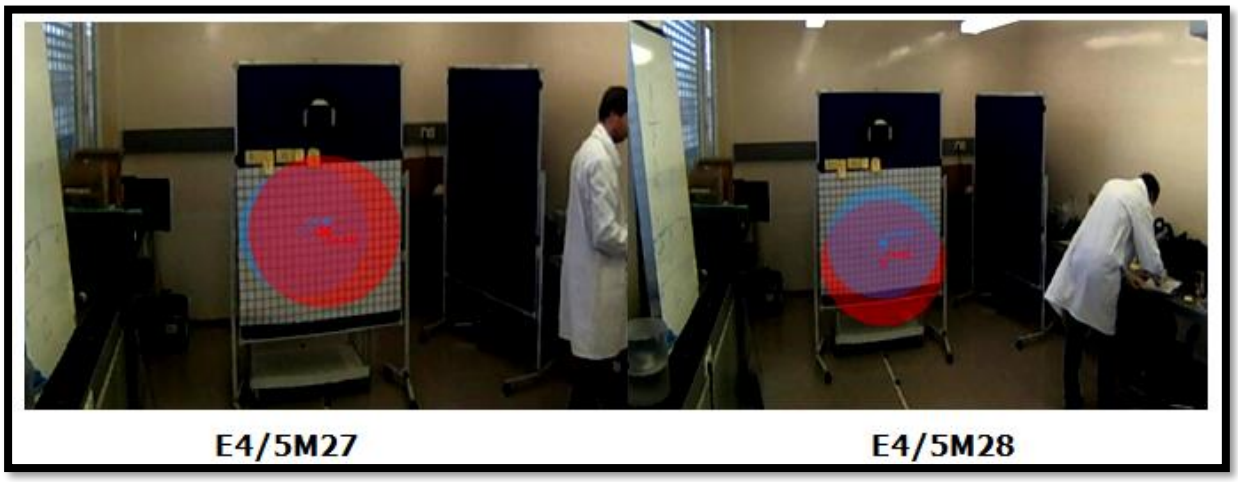

Figure 85. System1 imaging results for E4/5M27 and E4/5M28

Measurement run E4/5M26 used isotopes with emissions at or above the upper end of the imaging energy range for this instrument. The spectrum indicates the presence of ^{137}Cs and ^{60}Co and at the emission energies of these isotopes both the 1-cm-thick Ge and the 3-mm-thick Ta mask become relatively transparent. Nevertheless data were collected and reveal a source at (20.0, 18.1) (Figure 86). For this run the focal length was set to 12 cm giving a spatial resolution of 7.57 cm and a pixel size of 3.78 cm.

Cutting on the weak 662-keV line reveals a weak source with a 3.8 sigma significance. It is to the left of the other source and can be made somewhat more significant (5.5 sigma) by using all of the energy in the 662-keV peak plus the data from 100 keV up to the bottom of the 662-keV Compton edge at 486 keV (Figure 87).

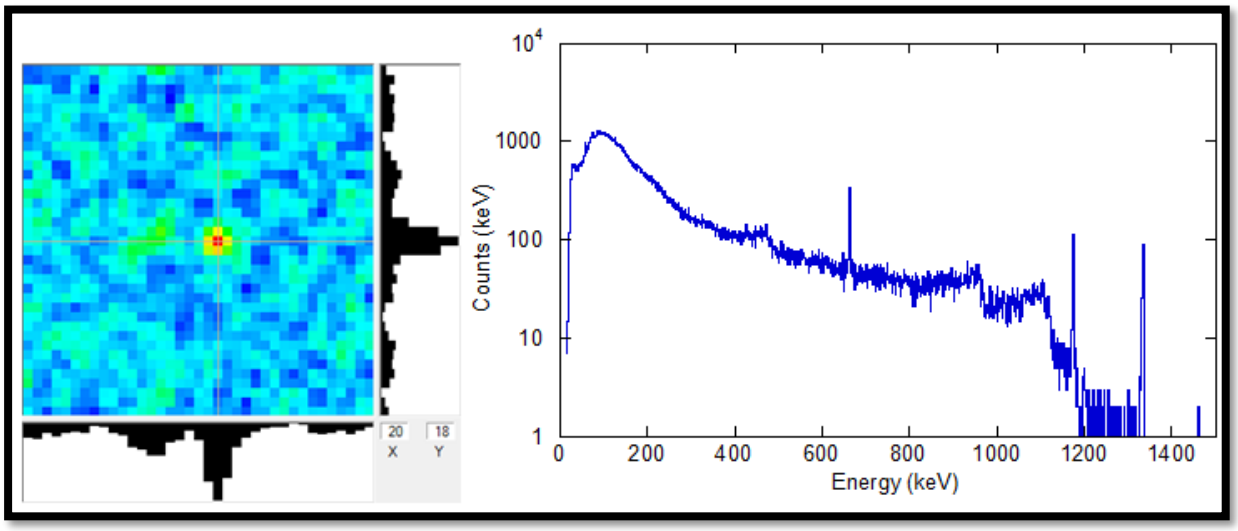

Figure 86. System7 gamma-ray image (left) made from the entire gamma-ray spectrum (right) from run E4/5M26.

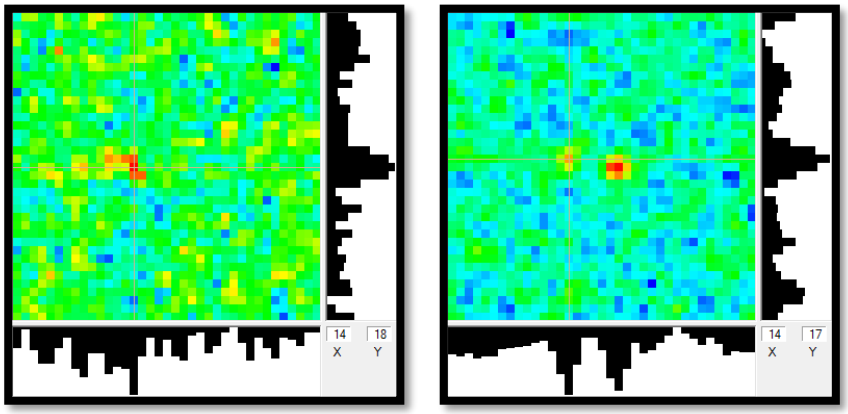

Figure 87. System7 E4/5M26 (Left) image cut on the Cs-137 photopeak, and (right) the image including the photopeak plus energy below the base of the Compton edge at 486 keV.

Measurement E4/5M27 run was the same basic configuration as the last one. However, with the time pressure between running the system, logging results, and getting video images, the system was only able to complete 3 full mask/anti-mask cycles for 3 minutes of data. That said, the overall spectrum looks very similar with clear photopeaks from ^{137}Cs and ^{60}Co. There is again a single source evident in the total image (13.2, 17.9) and it looks to be at approximately the location of the ^{137}Cs source last time.

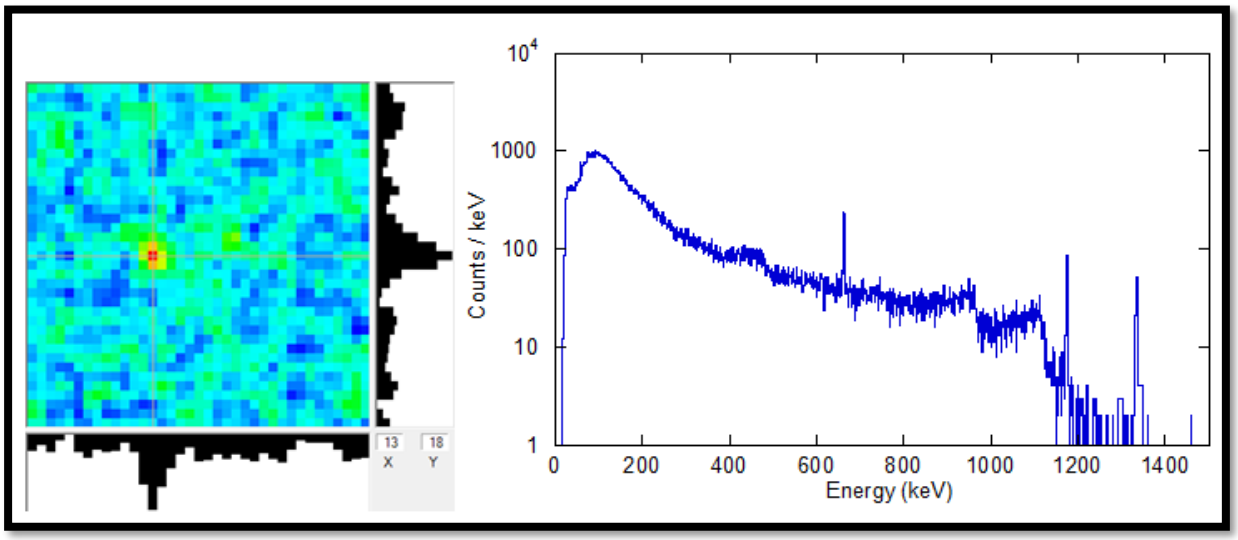

Figure 88. System7 gamma-ray image and spectrum from run E4/5M27.

Placing a tight cut on the 662-keV line does not reveal a single source location. This is not surprising given that there is only three-fourths of the data available last time. Taking the full spectral band below the Compton edge, plus the 662-keV peak does accentuate a second region to the right of the source (approximately where the ^{60}Co was located last time). A fit to the right region gives a location of (21.6, 16.8) for a source separation of 31.8 cm (33.7 with angular correction) with an uncertainty that has to be at least one pixel (3.8 cm).

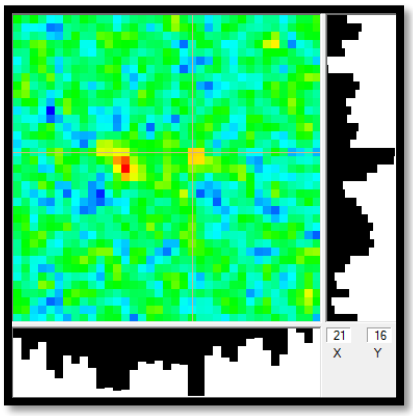

Figure 89. System7 gamma-ray image obtained using an energy window optimized for Cs 137.

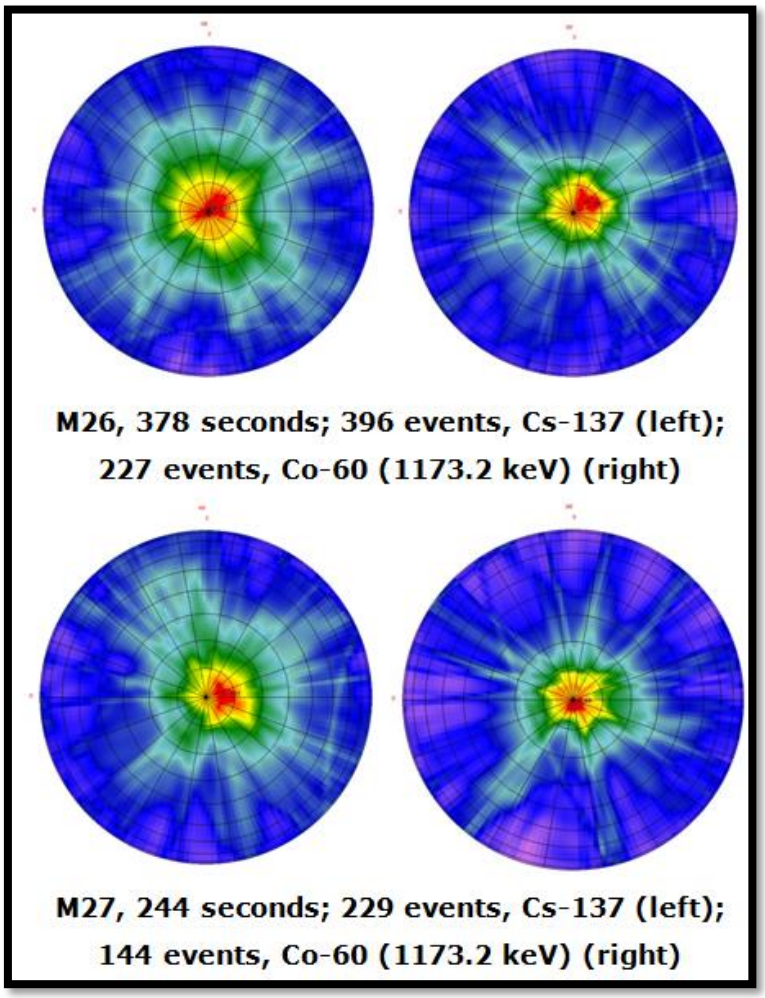

Figure 90. System4 imaging results for E4/5M26 and E4/5M27.

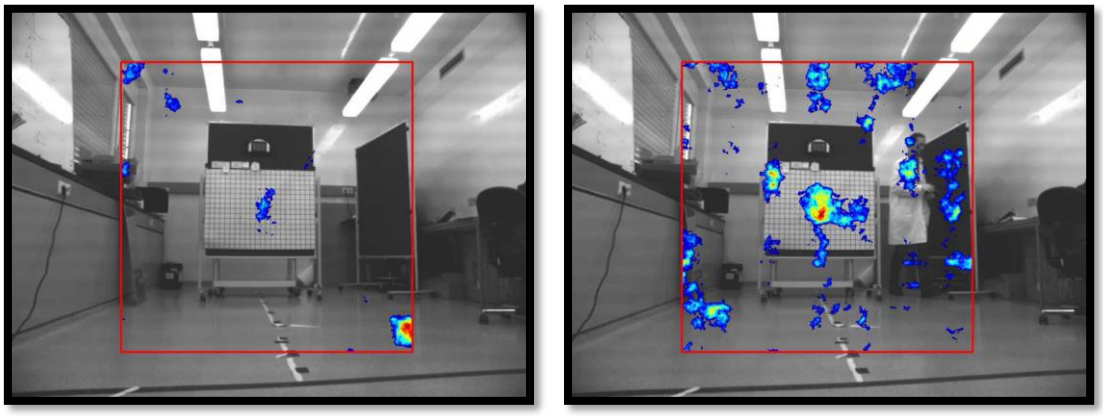

Figure 91. System6 imaging results E4/5M26 (left) and E4/5M27 (right)

For dynamic measurements, different geometry and less strong sources were used. Results of Volumetric Compton imaging are shown on Figure 92. Imaging results are followed by the comments from participants.

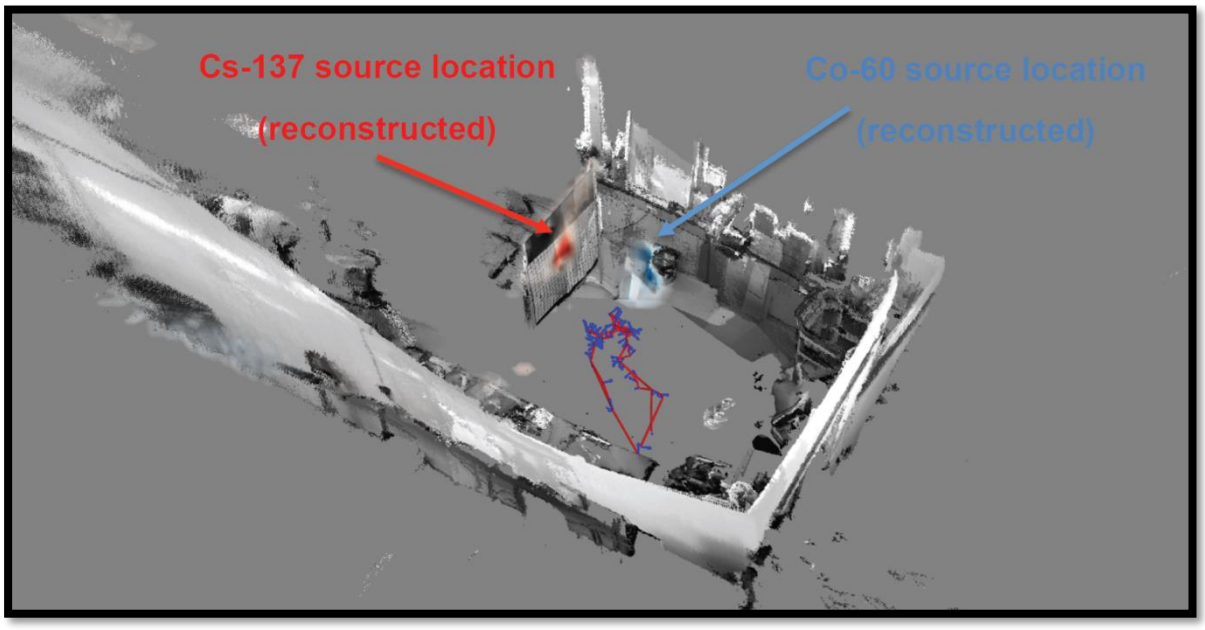

Figure 92. System5 real-time volumetric imaging results, two sources of different composition.

3D model is plotted in grayscale, while the gamma-ray source distributions are given by the colored maps: red for Cs-137 and blue for Co-60. ROI around 662 keV reconstructs a horizontal spread of sources near the top of the target screen board. One interesting result from this measurement is the Co-60 reconstruction, which identifies a hot spot near the black container. From subsequent measurements, we know this is the container in which the Co-60 source is transported. This result suggests the source may be present here as well, though if so, it must be heavily shielded. In a true unguided-search scenario, such a result could prompt an inspector to investigate the container. This result demonstrates the value of mobile imaging systems, which are able to overcome inverse r-squared and use proximity to increase the sensitivity of the imaging system.

5.5 Experiment 6: Extended Source

The goal of the experiment was to evaluate the capability of gamma-ray imagers to image detailed pattern of extended source distributed across wide area. 12 MTR plates were used to create basic geometry illustrated in Figure 93. In addition, point U sources were hidden behind target screen in the top and many high-energy point sources were added randomly. Geometry of measurements was not disclosed to the participants. Many high-energy sources had weak activity and it was not possible to image them.

Figure 93. Photograph of the geometry of measurements for E6M31.

Basic source geometry is imaged based on 150-200 keV (U-235) ROI. Source geometry is not clear (Figure 94).

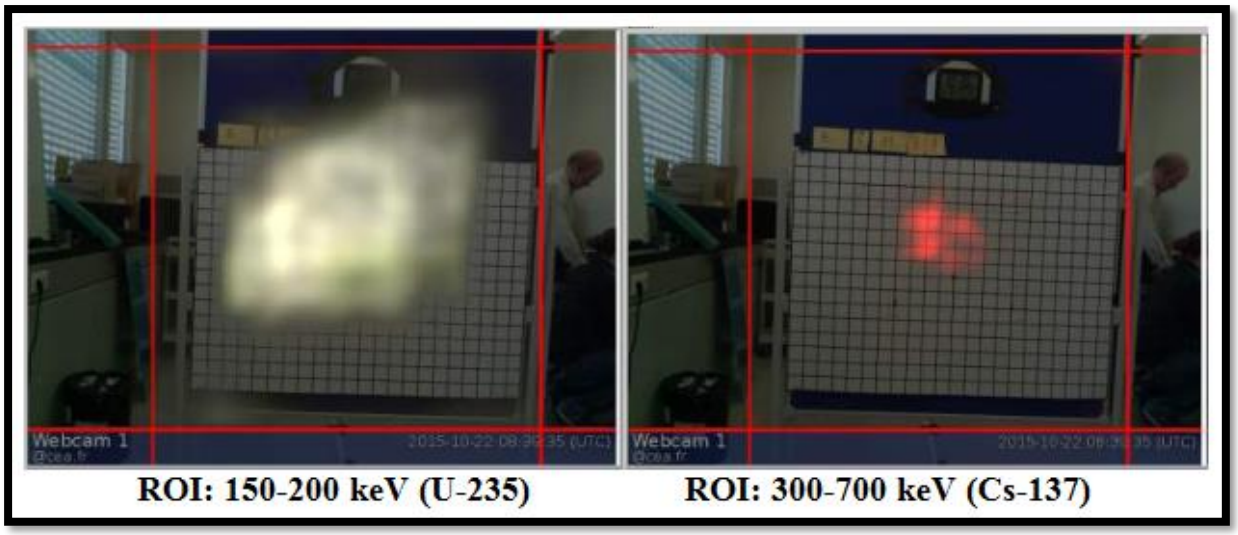

Figure 94. System3 imaging results for E6M31 – 11000 seconds.

Detailed extended source patter has been imaged (Figure 95) along with 3 point sources localized at the top of the screen (Figure 96).

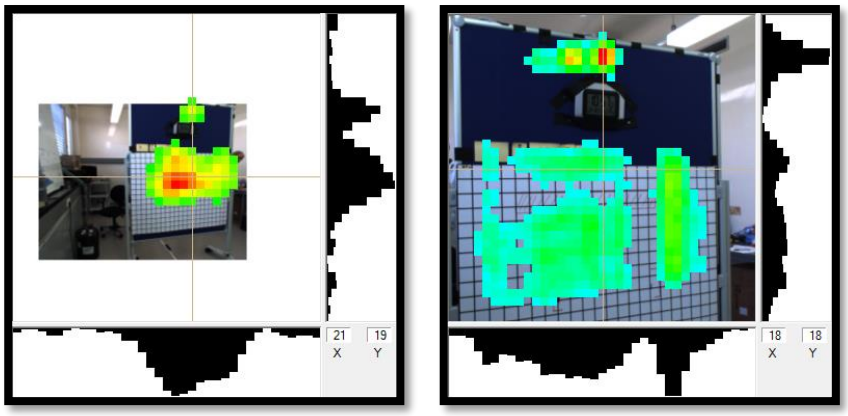

Figure 95. System7 wide field of view (left) and zoom image (right) for E6M31.

The line-out of intensity below the horizontal cursor shows a structure commensurate with 3 point sources of increasing strength from left to right. A spectrum from the peak pixel along the cursor is shown for each source, clearly showing each is EU. Examination of the high-energy portion of the spectrum shows no evidence of the 1-MeV line from ^{238}U daughters, indicating that this either very new low enriched ^{235}U, or it is highly enriched.

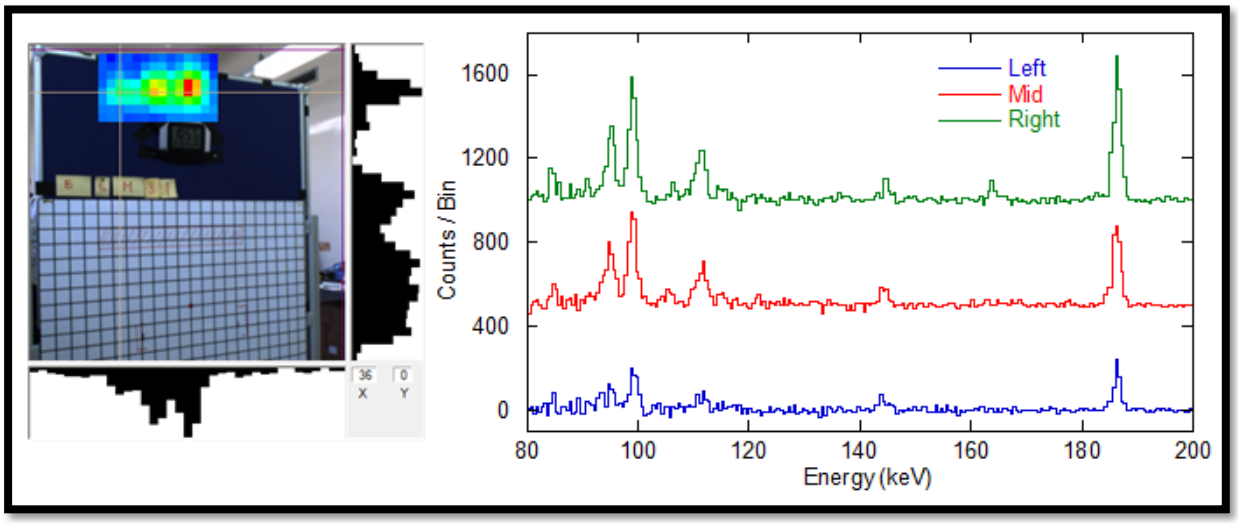

Figure 96. System7 video / gamma overlay image (left) and related spectra (right) for top sources of zoom-run E6M31. The mid and right spectra have been offset vertically by 500 and 1000 counts, respectively, to improve clarity.

Image in pinhole mode of operation (Figure 106) is generated based on 185.7 keV peak. Measurement time was 3605 seconds and 3721 events are imaged. Basic source geometry is clear.

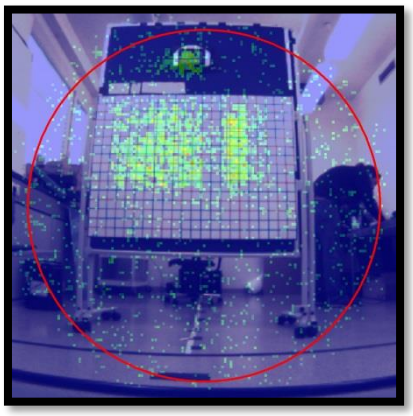

Figure 97. System4 (pinhole) imaging results for E6M31.

Image in Compton mode (Figure 107) is generated based on 185.7 keV (left), 661.6 keV (mid.) and 1173.2 keV (right) full-energy peaks. Measurement time was 5116 seconds. Images in inverted RGB color scheme are shown to improve contrast. Cs-137 and Co-60 sources are separated.

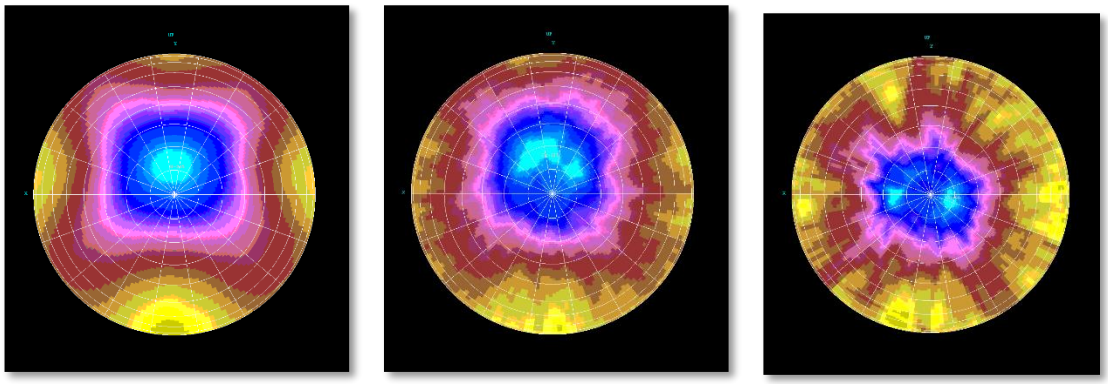

Figure 98. System4 imaging results in Compton mode for E6M31.

Images based on integral count rate (left) and on count rate in 185.7 keV peak (right) are shown on the Figure 99. 26x14 scans x 15 seconds were made.

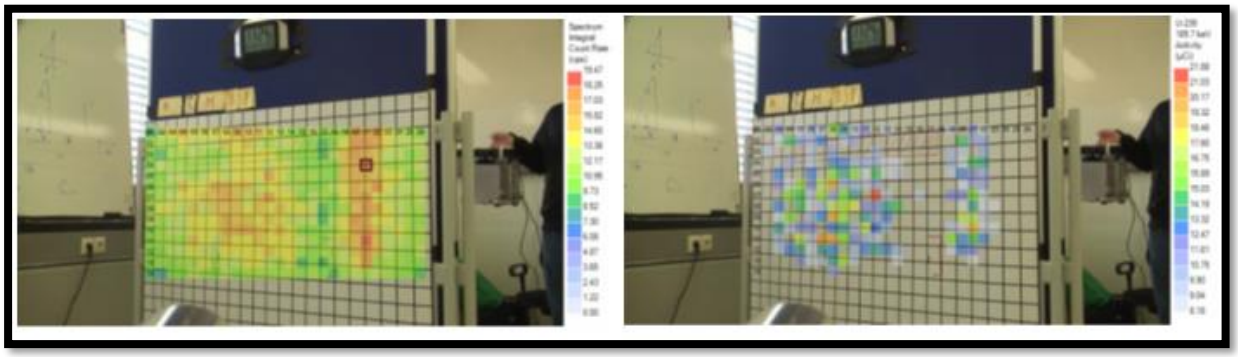

Figure 99. System8 imaging results for E6M31.

In this experiment to generate image (Figure 100) a mask was used. Data collected is near background / uniform activity levels. The use of other masks may have improved the collected data. System6 overheated after 21% of the acquisition time and automatically shut down.

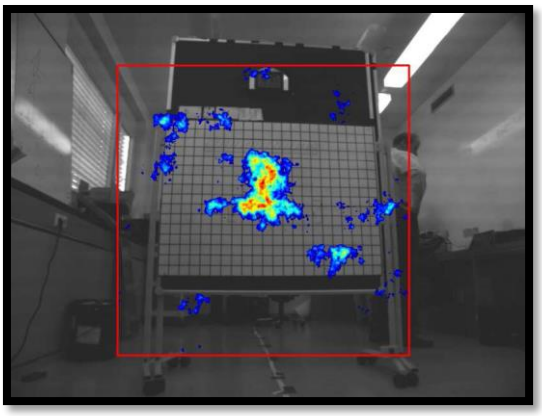

Figure 100. System6 imaging results for E6M31.

System1 was only able to image high-energy sources. Cs-137 sources are separated and Co-60 sources are not separated (Figure 101**Error! Reference source not found.**).

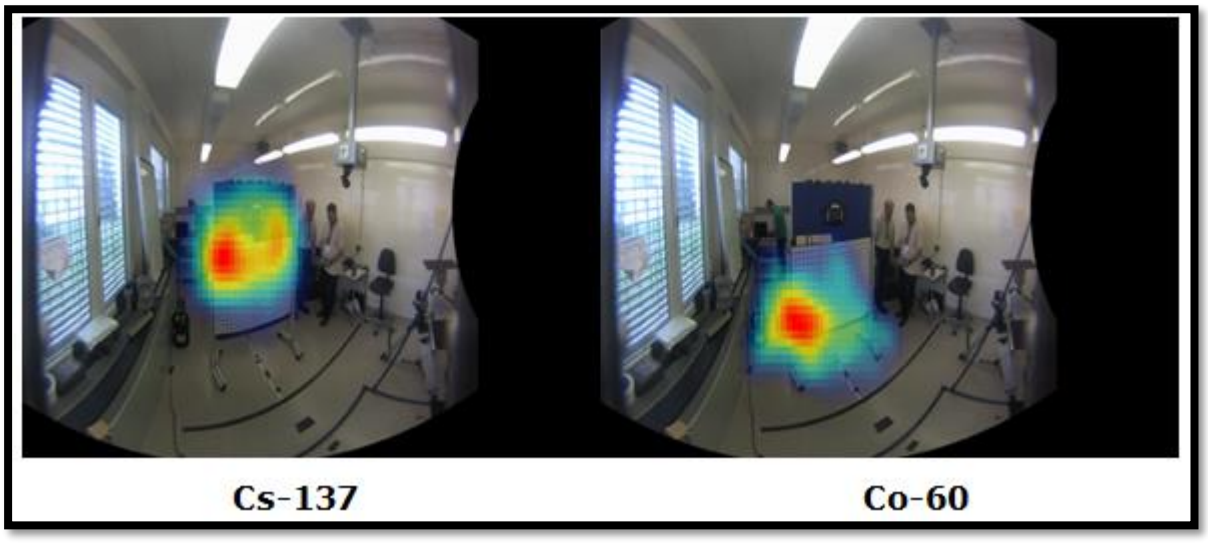

Figure 101. System1 imaging results for E6M31.

Table 18. Experiment 6: Summary of measurements results

Imager	**Extended source (pattern from MTR plates)**	**Uranium point sources (at the top)**	**Cs-137 and Co-60 point sources**
System3	Source area is correctly defined, missing part is not visible, detailed geometry is not clear	Not localized	Cs-137 sources are localized but not separated Co-60 sources do not localized
System1	Source area is not defined	Not localized	Co-60 sources are localized and separated Cs-137 sources are localized but not separated
System 3 (Compton)	Source area is correctly defined, missing part is not visible, detailed geometry is not clear	Sources are not localized	Sources are localized and separated
System4 (Pinhole)	Source area is correctly defined, missing part is visible, detailed geometry is not clear	Sources are localized but not separated	Not localized
System8	Source area is correctly defined, missing part is visible, detailed geometry is not clear	Area was not scanned	Not localized
System5	NP	NP	NP
System6	Source area is not defined	Not localized	Not localized
System7	Source area is correctly defined, missing part is visible, detailed geometry is clear	Sources are localized and separated	Not localized

5.6 Experiment 7a: False Alarm Rate

Overnight measurement (E7M37) was made without sources placed behind target screen. Information about presence (or absence) of sources was not disclosed to participants. The results are shown in the following figures.

For System8, the scan area was divided into 20 x 17 scan elements with a pitch 1.0°. Measurement time of each scan element was 170 seconds. Imaging results are shown in Figure 102.

Figure 102. System8 imaging results for E7M37

System1 produced the following spectrum in approximately 17 hours of measurements (Figure 103). Nothing apart from K-40 and Radon daughters (Pb-214 and Bi-214, peaks are marked by “unknown”) was detected.

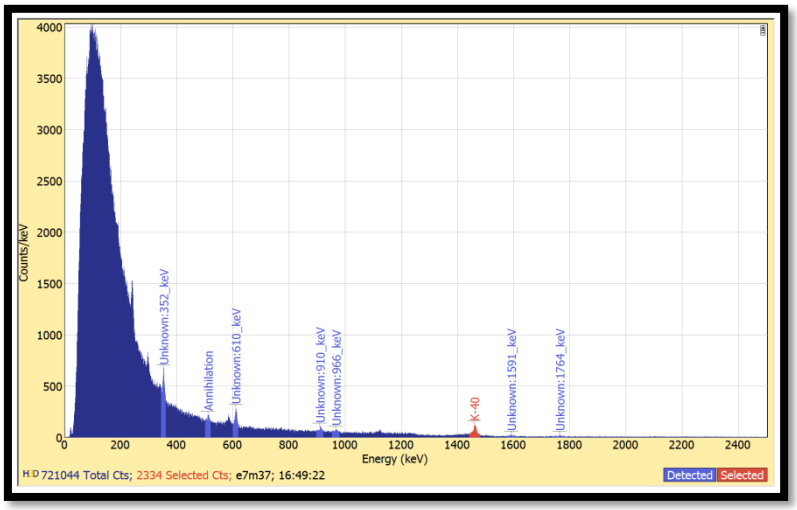

Figure 103. System1 spectrum results for E7M37

Overnight measurements were made in Compton mode of imager operation. Total measurements time was about 16 hours. U-235 was identified in the spectrum on the 3rd hour and localized on the 12th

hour (Figure 104). In the result of examination of localization image in scientific operator window (Figure 105, it is clear that source distribution is diffused all around imager.

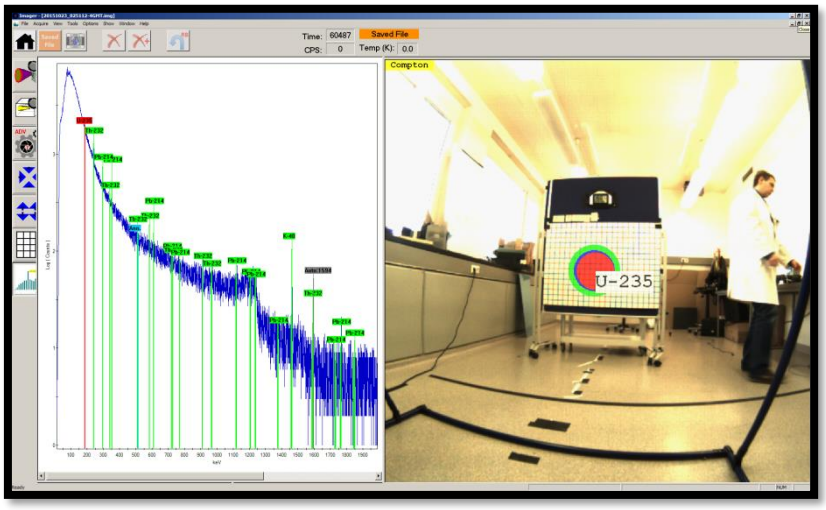

Figure 104. System4 spectrum results and image for E7M37

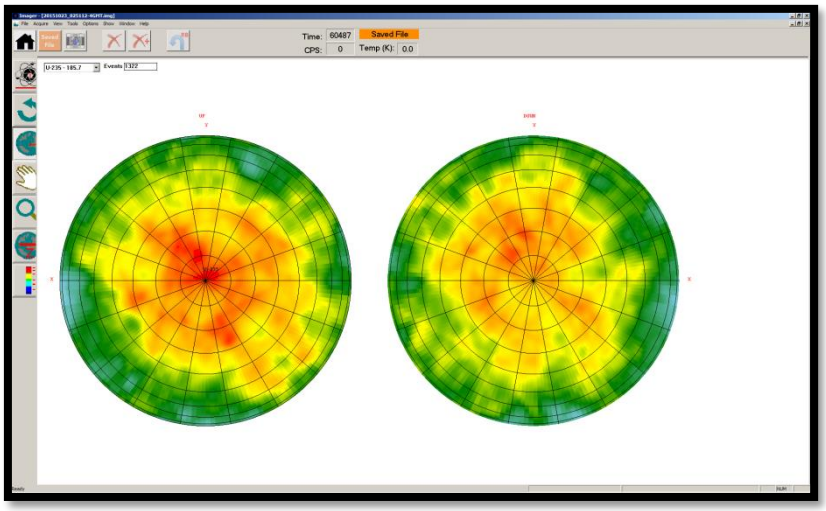

Figure 105. System4 resulting image in a different viweing mode for E7M37

System3 did not detect anything in the spectrum and there was no alarm on the image.

A total of 16 one-hour-long dwell periods were used. There is nothing obvious in the normalized image (Figure 106). A look at the low energy part of the spectrum (Figure 107) shows what appears to be a weak 186-keV line. There is no evidence of the 1-MeV line from ^{238}U daughters, nor is there evidence of Pu. A spectral cut on the 186-keV line (184-188 keV) reveals a hot spot with a significance of 4.6 sigma, which is below the normal alarm threshold.

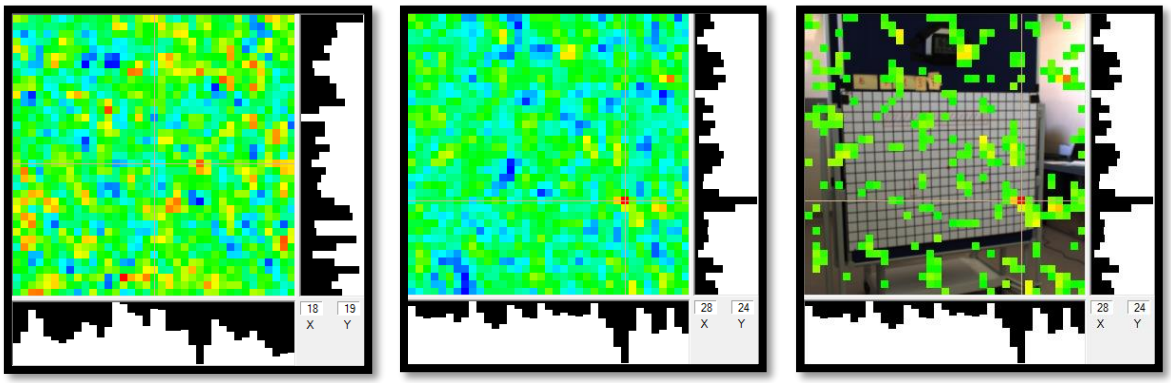

Figure 106. System7 measurement run E7M37; Total image (left) and images cut on the 186 keV line (center and right).

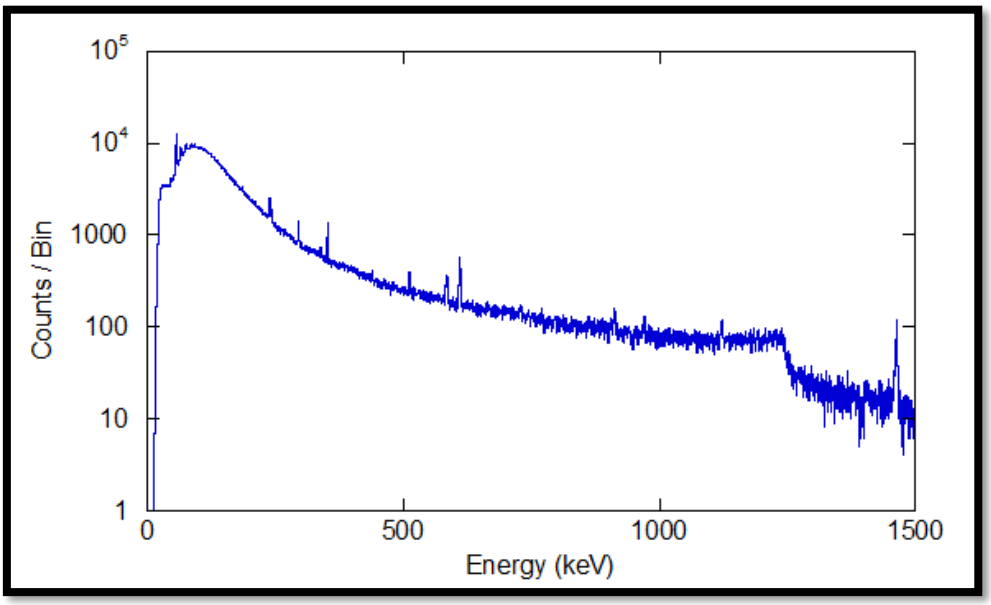

Figure 107. System7 spectrum for E7M37

5.7 Experiment 7b: High Background

The goal of experiment was to evaluate ability of gamma-ray imagers to localize source masked by other sources of similar composition (E7M32) and to localize Pu source masked by high-energy Co-60 source located in the field of view (E7M35) and behind gamma-ray imagers (E7M36). Results are shown in the figures below.

Geometry of measurements is illustrated on the Figure 108 and experimental setup is described in Table 19 below.

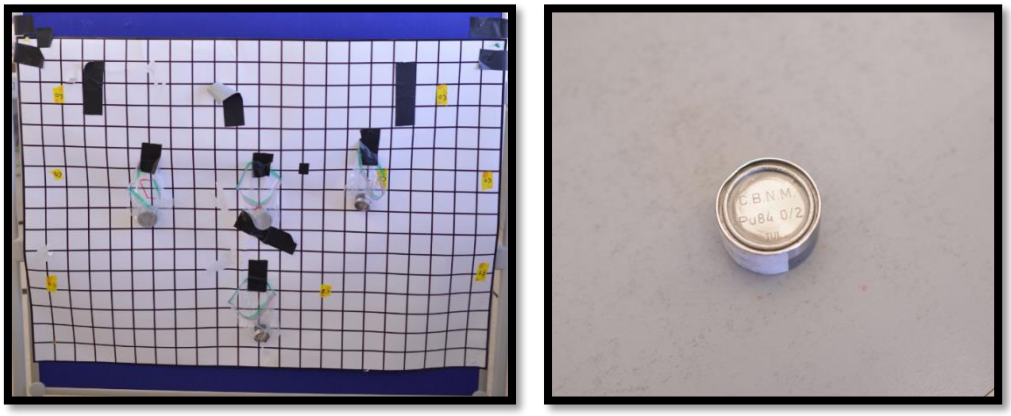

Figure 108. E7M32 – geometry of measurements (left), CBNM Pu84 source geometry (right)

Table 19. Description of experimental setup for E7M32

Position of source	Description of source type	Notes
HBPu source at (0; 0)	Steel cover towards gamma-ray imagers CBNM Pu64 source	Weak 59.5 keV emission in direction towards gamma-ray imagers
HBPu source at (-5; 0)	Entrance window with plastic cover towards gamma-ray imagers CBNM Pu70 source	Strong 59.5 keV emission in direction towards gamma-ray imagers
LBPu source at (5; 0)	Steel cover towards gamma-ray imagers CBNM Pu82 source	
LBPu source at (0; -6)	Entrance window with plastic cover towards gamma-ray imagers CBNM Pu93 source	

One of the sources used in this run had a fairly high rate and there were some issues in getting System7 started. This was resolved by using energy cuts to exclude the intense 60-keV line from the on-line image generation. For this configuration, the source-to-detector distance was 280 cm and focal length of 5 cm was used for a resolution and pixel size of 9.74 cm and 4.87 cm, respectively. A total of 4 60-s cycles of data were recorded and the final, normalized image is shown in Figure 109. From the video / gamma overlay image, it is clear that the imager aim was not optimal.

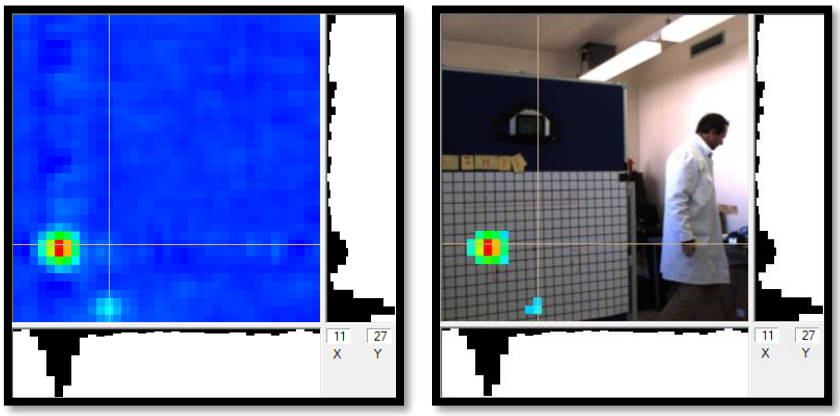

Figure 109. System7 E7M32 full-energy range image.

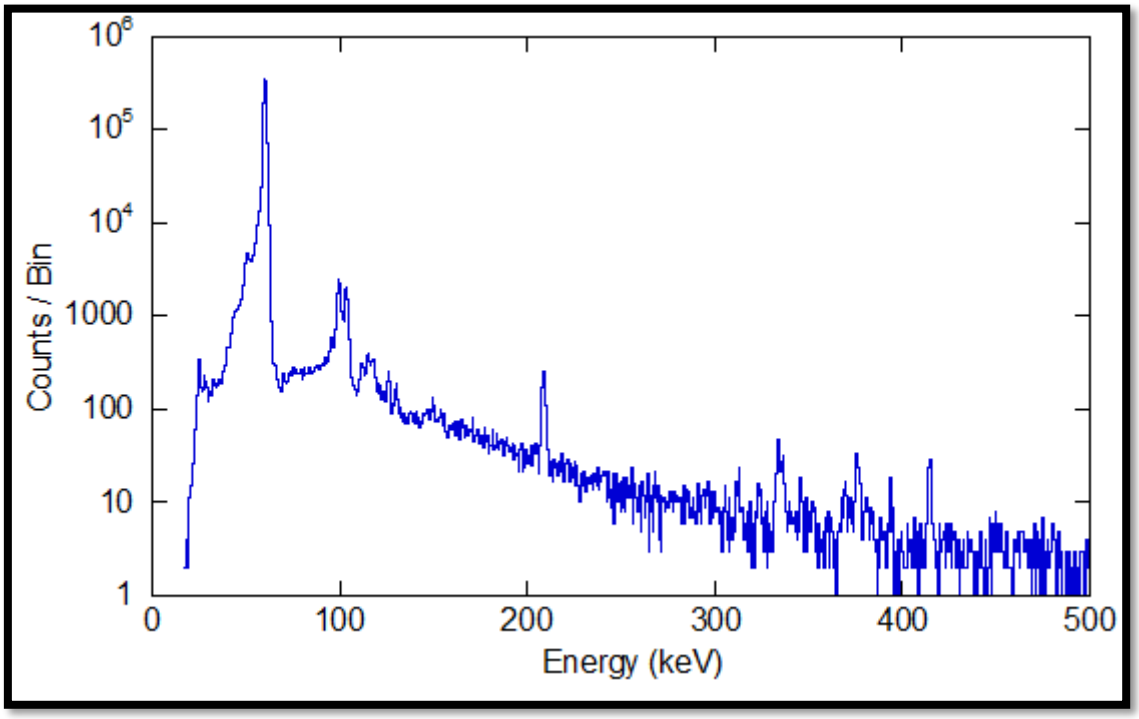

Figure 110. System7 total spectrum obtained from run E7M32.

Looking at the spectrum (Figure 110) there is clearly some Pu present. Based on the 208-keV line, some of this is from a HB source. If one looks at the spectra from the two obvious sources, then one sees that the weaker source has no 208-keV emissions. In fact, there are only 6 counts in the 208-keV line from that source region. On the other hand, the bright source has 337 counts for 569,824, 60-keV counts. The weak source has 98,961 60-keV counts so that one might expect 58 counts in the 208-keV peak. The uncertainty in counts per pixel in the peak ROI is 5.3 cnts so one would expect to see more events. In addition, if one generates an image based on a ROI for the 208-keV line, then a third source to the right of the strong peak and above the weak peak appears (Figure 111).

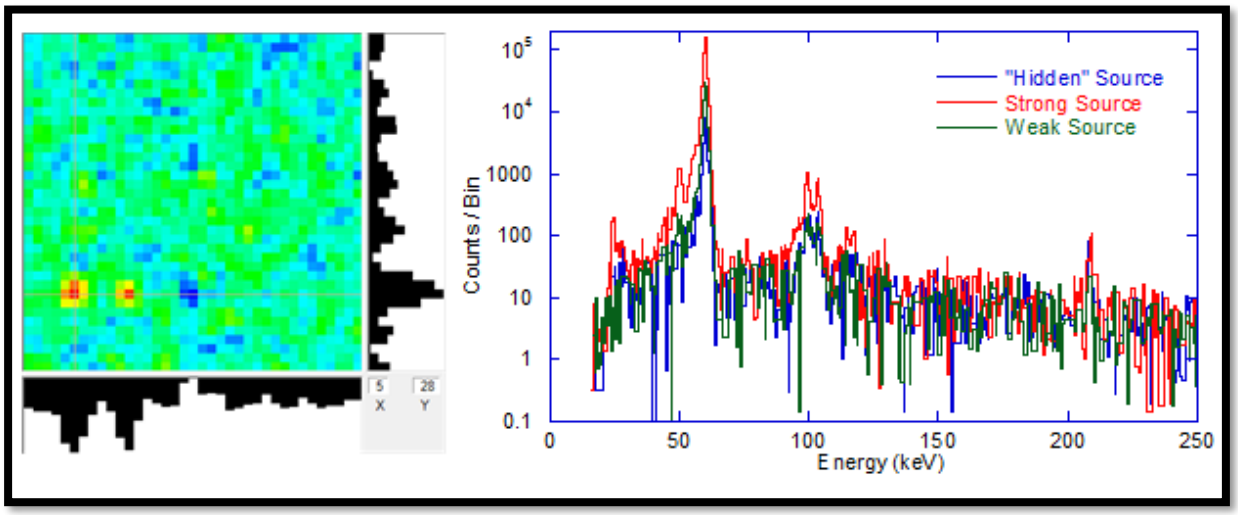

Figure 111. System7 image showing the location of the "hidden" source (left), and the spectra from the three different sources (right) from run E7M32.

This source has 197 208-keV counts with 27,607 counts in the 60-keV line indicating that the isotope responsible for the 208-keV line is present in greater abundance. All three sources do show K_α lines from Pu, although the mid-strength source has the weakest relative emissions from these lines.

The source locations are (5.16, 27.54), (10.92, 34.86), and (10.70, 27.93) for the strong, weak, and hidden sources, respectively. Assuming that the hidden source is in line with the strong and the weak sources this gives an x separation between the sources of 29.0 cm and a y separation of 36.2 cm; both after correction for angular projection.

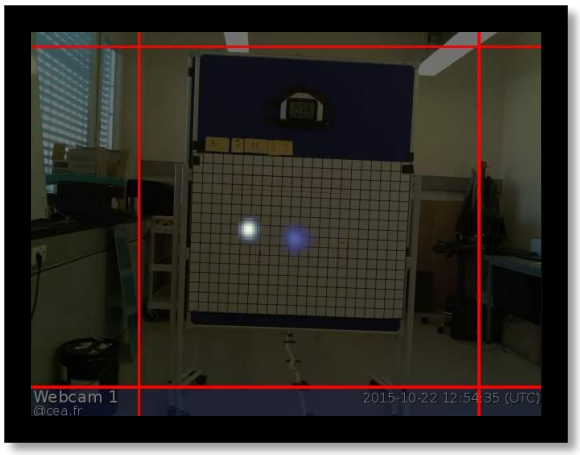

Figure 112. System3 resulting image with the strong Am-241 source in white and the weak Pu source in blue (E7M32)

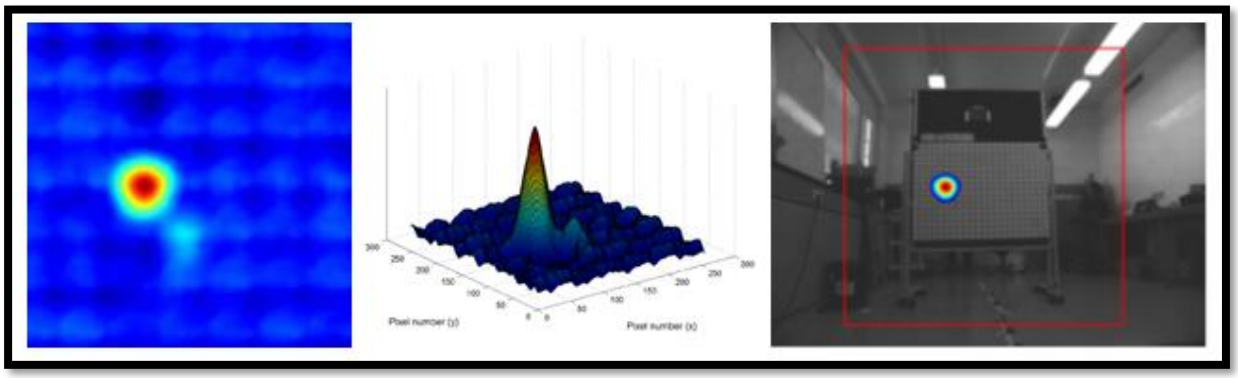

Figure 113. System6 resulting image for E7M32

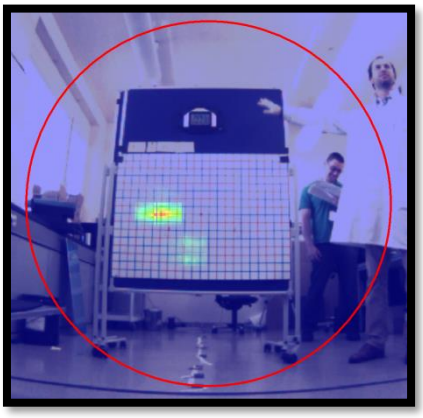

Figure 114. System4 resulting image for E7M32

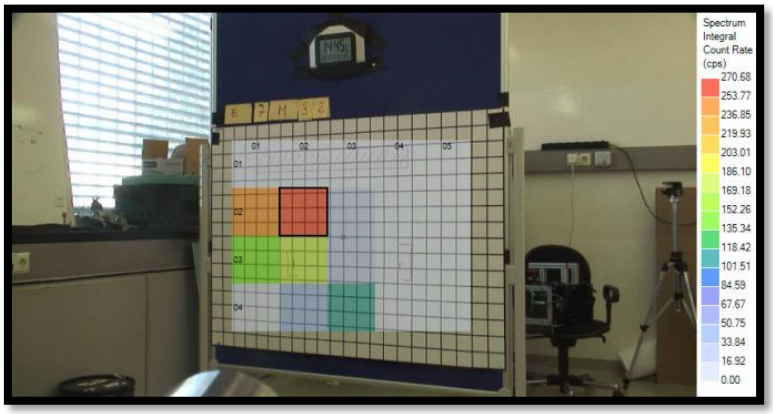

Figure 115. System8 resulting image for E7M32

The next set of figures is from the results received from measurements E7M35 and E7M36.

Two sources Pu (red) and Co-60 (green) are identified in 14 seconds and localized in 40 seconds (Figure 116).

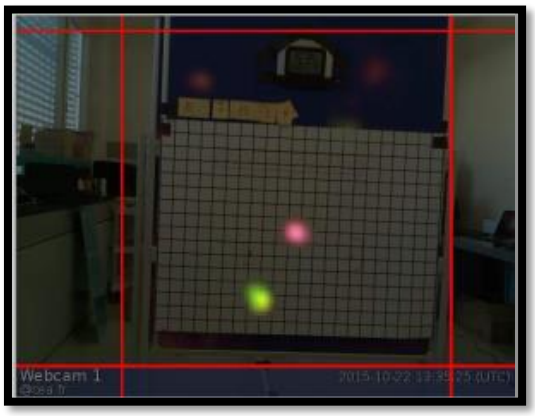

Figure 116. System3 resulting image for E7M35.

Pu source is identified (14 seconds) and localized in 140 seconds (Figure 117). Artifacts coming from Co-60 outside field of view are removed when image is built on a limited range (40-220keV).

Figure 117. System3 full range image (left) and 40-220keV image (right) for E7M36

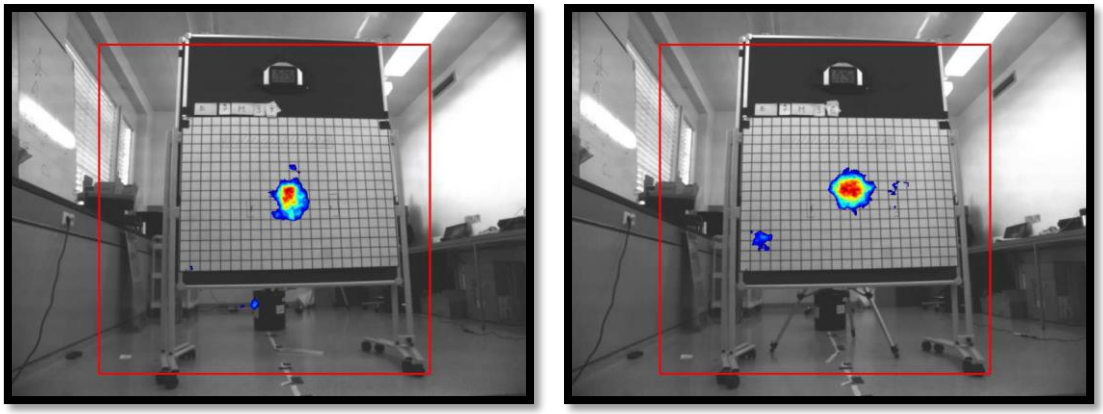

Figure 118. System6 imaging results for E7M35 (left) and E7M36 (right)

In the first scan conducted by System8, under E7M35, a Pu source was localized near localization threshold (blue square left image in Figure 119), so second scan was made to confirm localization of the source (red square right image in Figure 119).

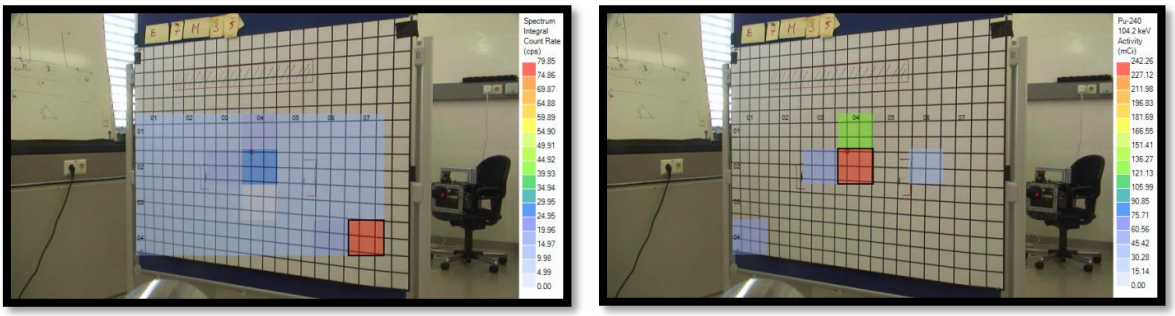

Figure 119. System8 imaging results for E7M35; first scan (left) second scan (right)

In E7M35 experiment (Figure 120) Pu source was imaged based on Am emissions in pinhole mode (left) and Co-60 source was imaged in front of gamma-ray imager in Compton mode (right). Measurement time was 600 seconds.

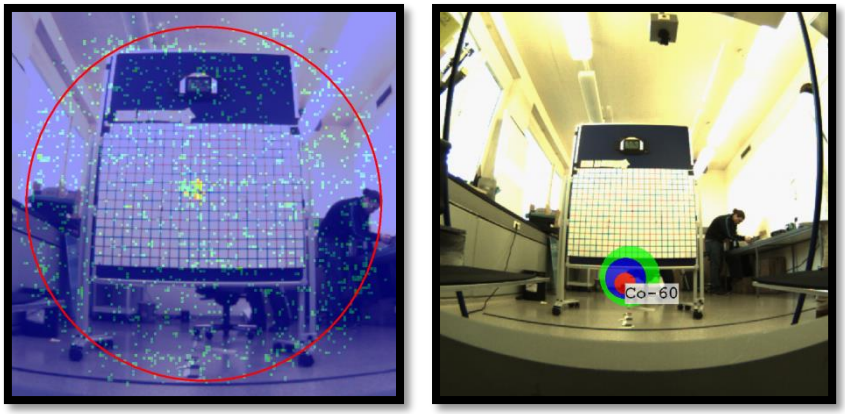

Figure 120. System4 imaging results for E7M35

In E7M36 experiment (Figure 121) Pu source was imaged based on Am emissions in pinhole mode (left) and Co-60 source was imaged behind gamma-ray imager in Compton mode (second hemisphere). Measurement time was 600 seconds.

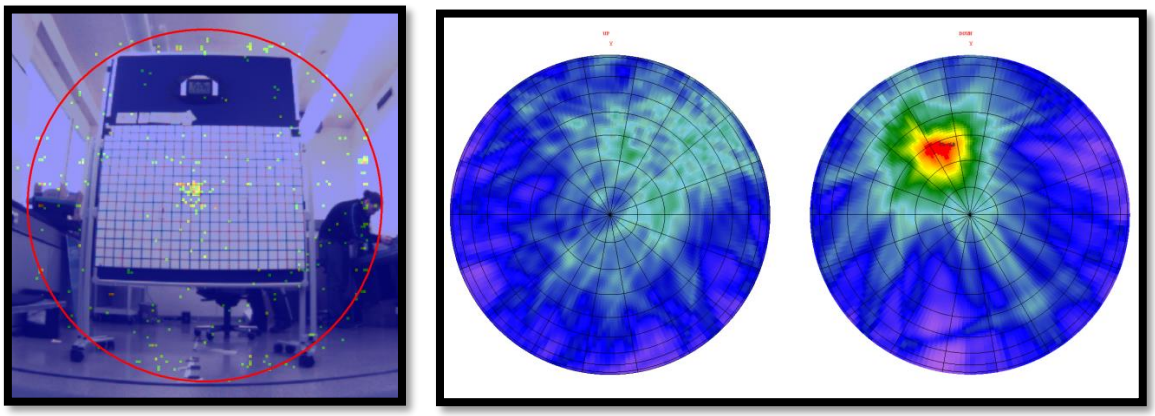

Figure 121. System4 imaging results for E7M36

Gamma-ray images from run E7M35 are shown on the Figure 132. Left image is based on all energies, middle on spectral cuts for HBPu (58-62, 98-106, and 207-210 keV), and right on spectral cut for Co-60 (above 500 keV).

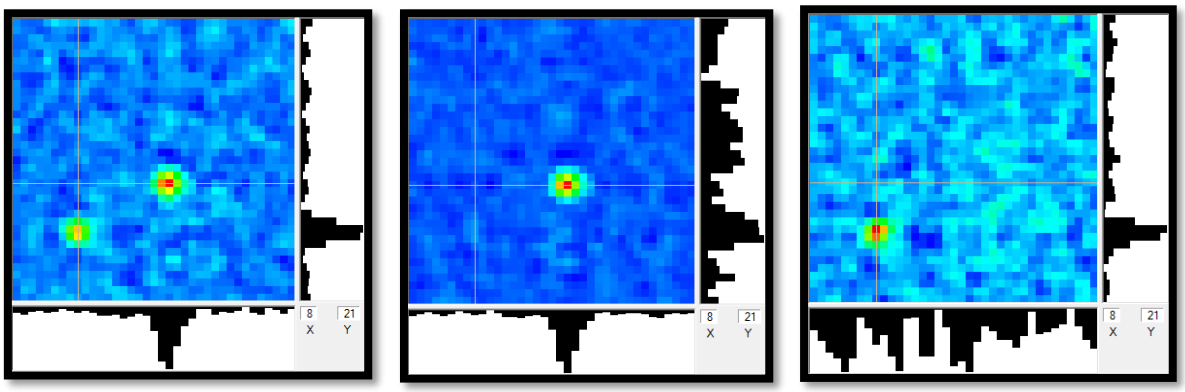

Figure 122. System7 imaging results for E7M35

Gamma-ray images from run E7M35 are shown on the Figure 123. The image on the left uses all of the data while the one on the right is generated with data in ROIs commensurate with the HBPu source. (58-62, 98-106, and 207-210 keV). This clearly improves the contrast.

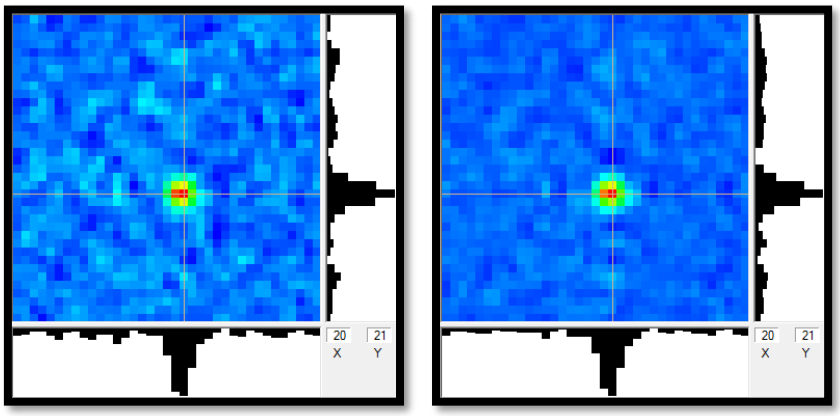

Figure 123. System7 imaging results for E7M36

Figure 124 shows total spectrum (left) and the low energy portion of the total spectrum compared to the spectrum from the source region of the image (right).

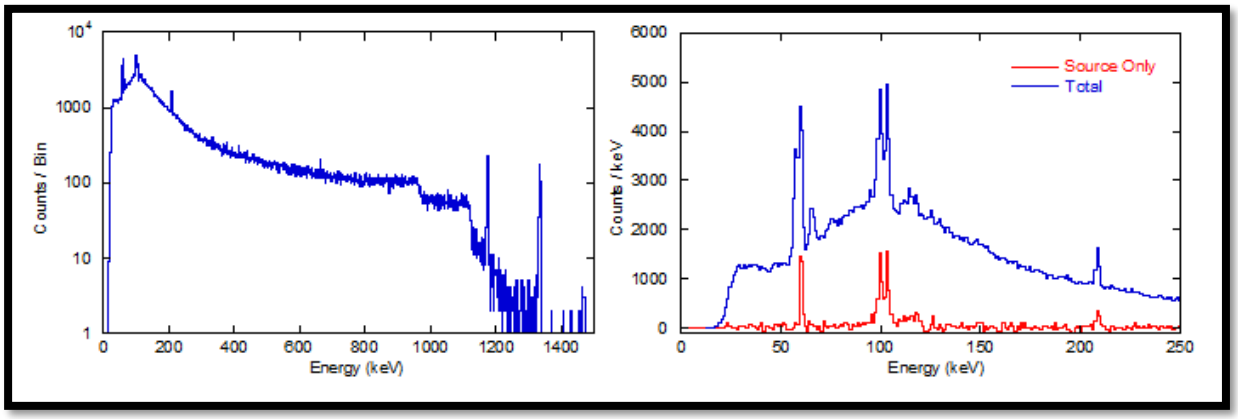

Figure 124. System7 spectrometric results for E7M36.

Table 20. Summary of measurements results for Experiment 7.

Imager	**CBNM Pu sources**	**Pu source masked by Co-60**
System4 (pinhole)	Two Pu sources are localized based on Am-241 emissions	Target source is localized in both cases
System5	NP	NP
System3	Two Pu sources are localized, one based on Am-241 emissions and second one based on Pu emissions	Target source is localized in both cases
System6	Two Pu sources are localized based on Am-241 emissions	Target source is localized in both cases
System7	Three Pu sources are localized and separated based on Pu emissions	Target source is localized in both cases
System1	NP	NP
System8	Major source is localized, other sources may present more detailed scan is needed	Target source is localized in both cases, additional scan was made

5.8 Experiment 8a: Angular Resolution for Extended Sources

The following figures illustrate the results for gamma-ray images for E8M39 and E8M40 from several systems.

5.8.1 Experiment E8 – extended HEU sources

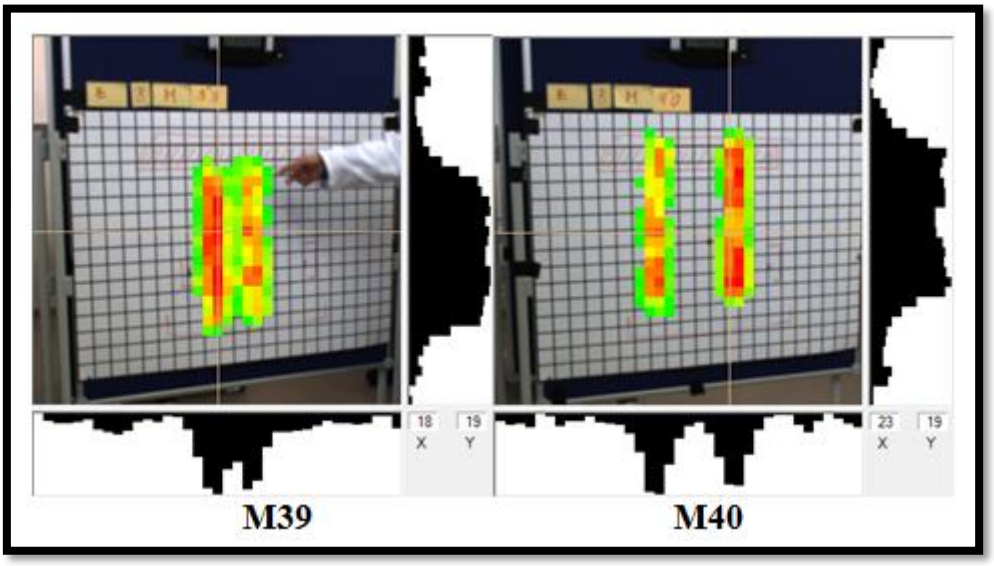

Figure 125. System7 imaging results after 900 seconds

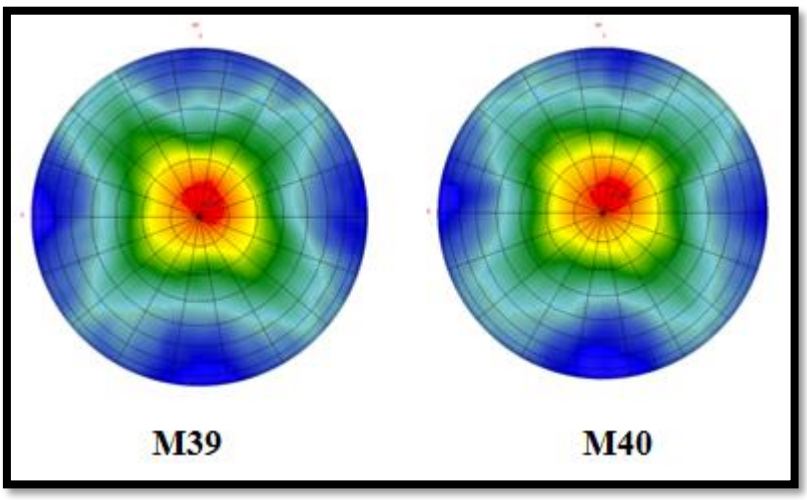

Figure 126. System4 imaging results after 600 seconds

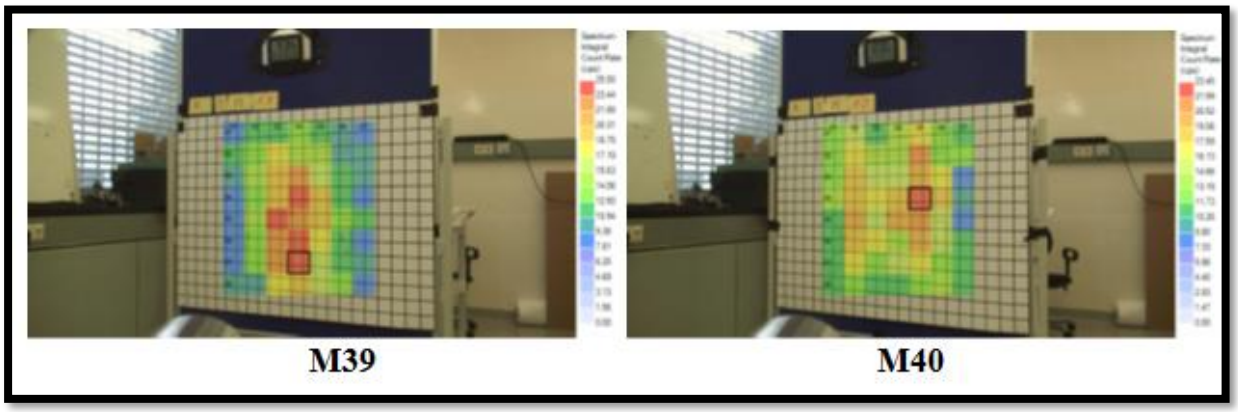

Figure 127. System8 imaging results after 600 seconds

5.8.2 Experiment E8 – HBPu sources

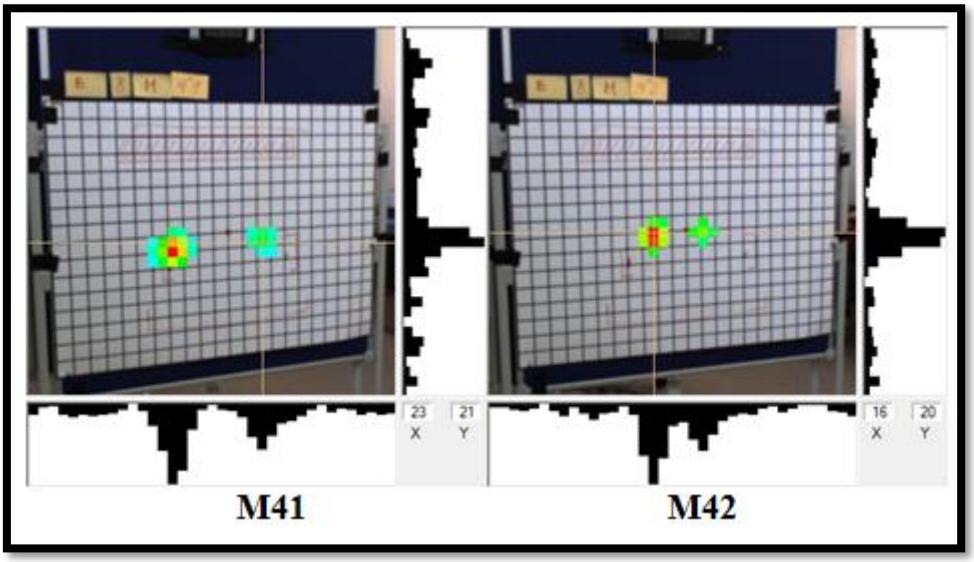

Figure 128. System7 gamma-ray images for E8M41 and E8M42 after 600 seconds (left), 400 seconds (right)

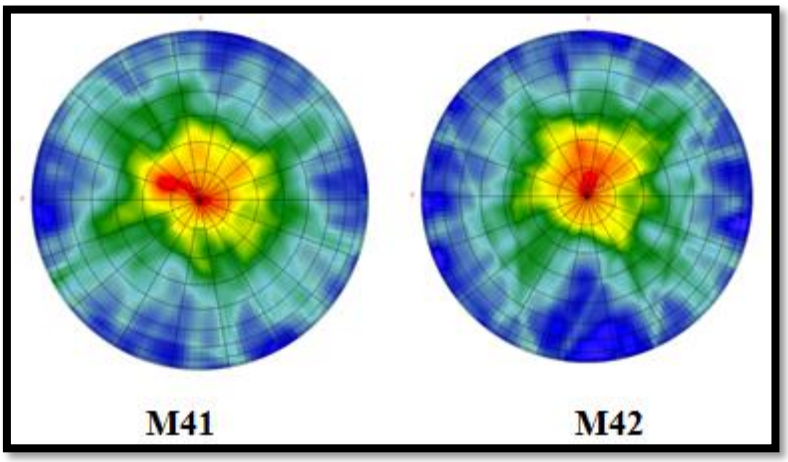

Figure 129. System4 gamma-ray images for E8M41 and E8M42 after 775 seconds (left), 680 seconds (right)

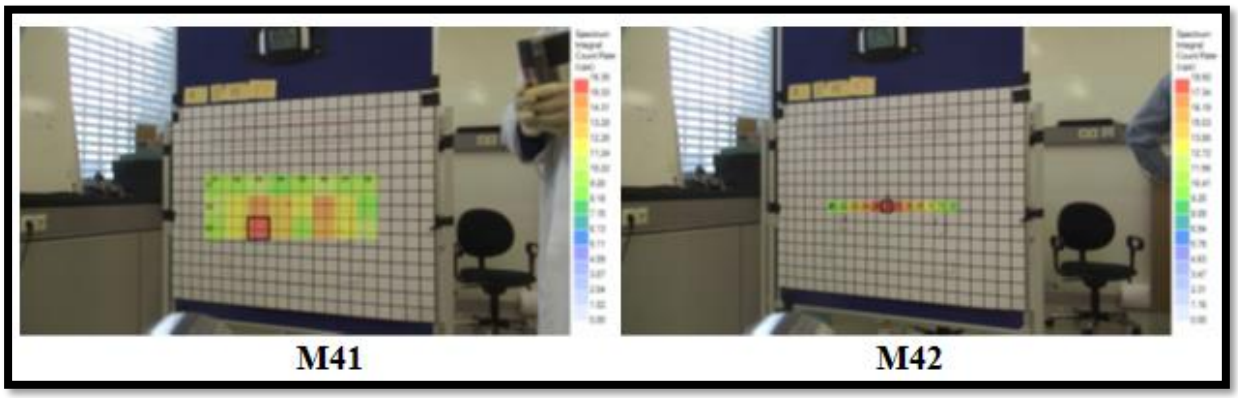

Figure 130. System8 gamma-ray images for E8M41 and E8M42 after 480 seconds (left), 528 seconds (right)

5.9 Experiment 8b: Glovebox Scenarios

5.9.1 Low-activity scenario

The following figures compare the results from several systems in the glovebox low-activity scenario.

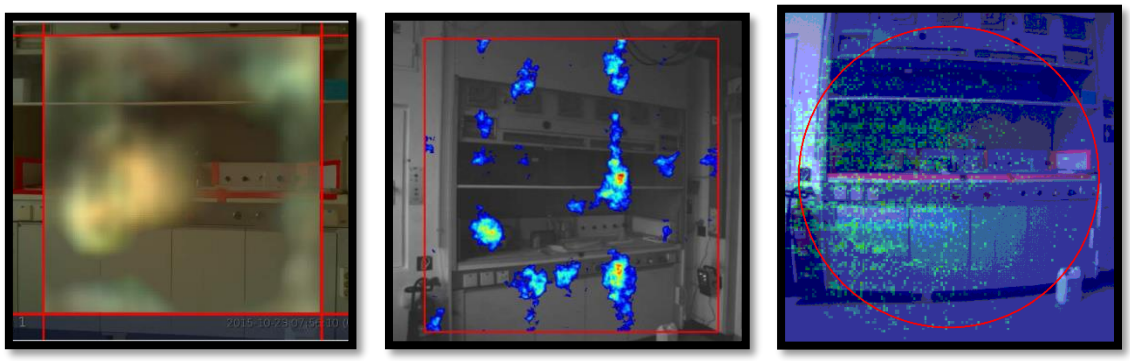

Figure 131. System3 (left), System6 (center), and System4 (right) gamma-ray images from the glovebox low-activity scenario.

Pu and Cs-137 were identified but localization is diffuse. A high part of the activity comes from outside the field of view. In the field of view, most of the activity seems to come from centre-left area.

5.9.2 High-activity scenario

The following figures compare the results from several systems in the glovebox high-activity scenario.

Figure 132. System3 gamma-ray images from the glovebox high-activity scenario.

Image based on 59.5 keV peak only (left) and dynamic range image based on 208 keV to 59.5 keV ratio (right); HBPu is imaged by green color.

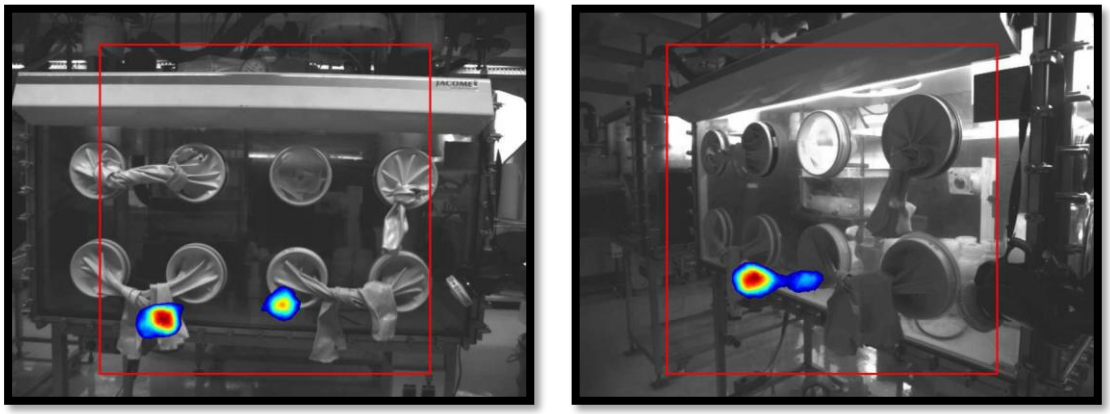

Figure 133. System6 gamma-ray images from the glovebox high-activity scenario, where two hot spots are localized.

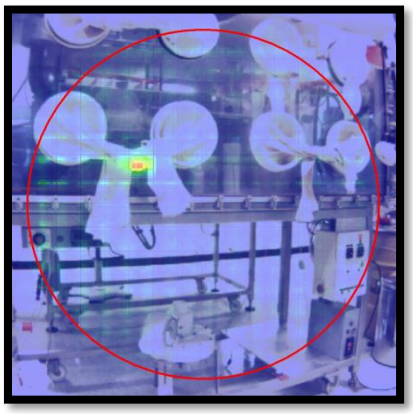

Figure 134. System4 gamma-ray images from the glovebox high-activity scenario, where one spot was localized based on the Am-241 low energy emission.

5.9.3 Fumehood high activity scenario

The following figures compare the results from several systems in the fumehood high-activity scenario.

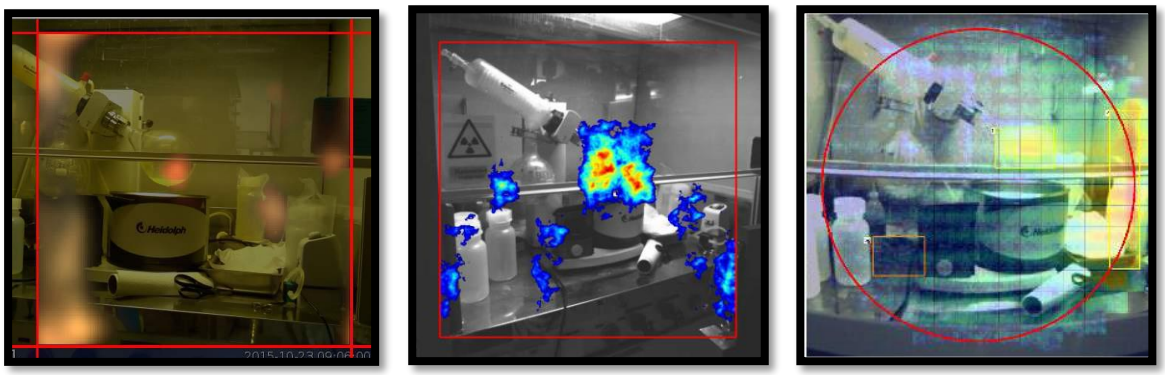

Figure 135. System3 (left), System6 (center), and System4 gamma-ray images for Fumehood high-activity scenario.

System4 identified Am-241 and Plutonium. A notable part of 59.5 keV emission comes from the round-bottom bottle. Peak around 310 keV is visible but his origin is unknown.

System6 identified one hot spot. System4, using the pinhole mode of operation identified one hot spot and extended source. Np-237 (311 keV) is localized behind gamma-ray imager in Compton mode of operation.

6 Performance vs. Contextual Usage Scenarios

In order to understand applicability of modern gamma-ray imagers to the nuclear safeguards applications, a set of Contextual Usage Scenarios (CUS) has been defined by the IAEA. General requirements for gamma-ray imagers are summarized in Table 21. Performance of the imagers against 18 IAEA CUS is summarised in Table 22. Evaluation of performance is based on the experimental results obtained at workshop.

Table 21. General requirements to gamma-ray imagers.

	General requirements	System4	System5	System3	System6	System7	System1	System8
1.	Good imaging efficiency for nuclear materials	**Yes**	**No***	**Yes**	**Yes**	**Yes**	**No***	**Yes**
2.	Identification of nuclear materials	**Yes**	**Yes**	**Yes**	**No**	**Yes**	**Yes**	**Yes**
3.	Wide field of view	**Yes**	**Yes**	**No**	**No**	**Yes**	**Yes**	**No**
4.	Low-weight portable, preferably hand-held operation	**No**	**Yes**	**Yes**	**Yes**	**No**	**Yes**	**No**
5.	Possibility to perform dynamic measurements	**No**	**Yes**	**No**	**No**	**No**	**No**	**No**
6.	Good imaging separation for different radionuclides	**Yes**	**Yes**	**Yes**	**No**	**Yes**	**Yes**	**Yes**
7.	Good angular resolution for the same radionuclides	**Yes**	**No**	**Yes**	**Yes**	**Yes**	**No**	**Yes**

* Uranium can’t be imaged based on 185.7 keV photon emissions; HBPu can’t be imaged based on 208 keV photon emissions.

Table 22. Performance vs. contextual user scenarios (CUS).

	System3	**System1**	**System4**	**System8**	**System5**	**System6**	**System7**
CUS 01	The inspector enters room/lab full of cupboards, containing several radioactive sources. While carrying out interviews, he captures a gamma image of the room. He is able to verify the presence of SNM that may be masked by other radioactive sources before leaving the room, and reorient his inspection accordingly.						
	Only static measurements could be done. Can determine presence of SNM. Can determine location of the SNM. Several measurements shall be done.	Only static measurements could be done. Can determine presence of SNM. Can't determine location of HEU based on 185.7 keV emission. One measurement could be sufficient.	Only static measurements could be done. Can determine presence of SNM as spectrometric HPGe detector is used. Can determine location of the SNM. One measurement could be sufficient. Imager is quite heavy.	Only static measurements could be done. Imager is not portable.	Dynamic measurements can be done. Can determine presence of SNM. Can determine location of Pu source. Can't localize U source based on 185.7 keV emissions. One measurement could be sufficient.	Only static measurements could be done. Imager is not spectrometric.	Only static measurements could be done. Can determine presence of SNM. Can't determine location of the SNM as instrument shall not be in movement. Couple of measurements could be sufficient. Imager is not portable.
CUS 02	The inspector enters room/lab full of cupboards. He leaves the camera operating during the rest of the CA and captures a gamma image of the room. He is able to verify the presence of NM before the end of the CA, and reorient his inspection accordingly.						
	Can determine presence of SNM. Can determine location of the SNM.	Can determine presence of SNM. Can't determine location of HEU based on 185.7	Can determine presence of SNM. Can determine location of the SNM. One measurement	Imager is not portable.	Can determine presence of SNM. Can determine location of Pu source.	Imager is not spectrometric. Can determine presence of radioactive material.	Can determine presence of SNM as spectrometric HPGe detector is used. Can't determine

	System3	**System1**	**System4**	**System8**	**System5**	**System6**	**System7**
	Several measurements shall be done.	keV emissions. One measurement could be sufficient.	could be sufficient. Imager is quite heavy.		Can't localize U source based on 185.7 keV emissions. One measurement could be sufficient.	Several measurements shall be done.	location of the SNM as instrument shall not be in movement. Couple of measurements could be sufficient. Imager is too big and heavy.
CUS 03	A gamma camera is used over a cascade hall, monitoring the centrifuges cylinders from the top, with a wide angle view, and possibly setup on rails so that it can randomly be moved across the warehouse. A gamma picture is taken, possibly with a very long integration time (24h). The visual imaging is optimally removed (to minimize the amount of information captured by the IAEA). The IAEA is able to visually confirm the presence of the absence of the accumulation of NM inside the enrichment process.						
	Capable. Good detection efficiency and relatively low background at 185.7 keV. Low detection efficiency at 1001 keV.	Not capable to make image based on 185.7 keV photon emissions. Capable to measure spectra. Good detection efficiency at 185.7 keV and at 1001 keV. Optimal energy resolution for room temperature.	Capable. Can be done. Good detection efficiency at 185.7 keV and relatively low detection efficiency at 1001 keV. Excellent energy resolution.	Capable. Good efficiency at 185.7 keV and good detection efficiency at 1001 keV.	Not capable to make image based on 186 keV emissions. Capable to measure spectra. Good efficiency at 185.7 keV and good detection efficiency at 1001 keV.	Imager is not spectrometric.	Capable. Good detection efficiency at 185.7 keV and relatively low detection efficiency at 1001 keV. Excellent energy resolution.

	System3	**System1**	**System4**	**System8**	**System5**	**System6**	**System7**
CUS 04	UF6 tail cylinders are stored in multiple layers. A gamma camera is setup on an automated robot that is able to automatically navigate between the cylinders. A gamma picture is captured for each cylinder while the inspector carries out other activities. An automated, recognition-software analyses the images, confirms the presence of UF6 material in each cylinder and identifies any potential anomaly for further manual verification.						
	Capable to image source pattern. Good detection efficiency and relatively low background a 185.7 keV. Low detection efficiency at 1001 keV.	Not capable to make image based on 185.7 keV photon emissions. Good detection efficiency at 185.7 keV and at 1001 keV. Optimal energy resolution for room temperature.	Capable to image source pattern. Low intrinsic detection efficiency at 185.7 keV and low detection efficiency at 1001 keV. Excellent energy resolution.	Capable to image source pattern. Multiple measurements are needed.	Not capable to make image based on 185.7 keV photon emissions. Good efficiency detection efficiency at 1001 keV.	Imager is not spectrometric. Capable to image source pattern.	Capable to image source pattern. Good detection efficiency at 185.7 keV and relatively low detection efficiency at 1001 keV. Excellent energy resolution
CUS 05	An inspector captures a gamma image from the top of a fresh fuel assembly (in air). He is able to pinpoint which assembly contain LEU at a pin level (partial defect, or H+ verification method).						
	Capable. Good detection efficiency at 185.7 keV. Good angular resolution.	Capable based on 1001 keV photon emissions. Limited angular resolution.	Capable. Low intrinsic detection efficiency at 185.7 keV. Good angular resolution.	Capable. Multiple measurements (scan elements) are needed to achieve good angular resolution.	Capable based on 1001 keV photon emissions. Good detection efficiency at 1001 keV. Limited angular resolution.	Imager is not spectrometric. Capable to image source pattern.	Capable. Excellent detection efficiency at 185.7 keV. Excellent angular resolution.
CUS 06	An inspector captures a gamma image from the side of a group of fresh fuel assemblies. He is able to pinpoint which assembly contains LEU.						

	System3	**System1**	**System4**	**System8**	**System5**	**System6**	**System7**
	Capable to image extended sources. Good detection efficiency at 185.7 keV. Good angular resolution.	Capable based on 1001 keV photon emissions. Limited angular resolution.	Capable. Due to pinhole usage low intrinsic detection efficiency at 185.7 keV. Good angular resolution.	Capable. Multiple measurements (scan elements) are needed to achieve good angular resolution.	Capable based on 1001 keV photon emissions. Good detection efficiency at 1001 keV. Limited angular resolution.	Imager is not spectrometric. Capable to image source pattern. Acceptable detection efficiency at 185.7 keV. Good angular resolution.	Capable to image extended sources. Excellent detection efficiency at 185.7 keV. Excellent angular resolution.
CUS 07	An inspector captures a gamma image lengthwise of an assembly/of several assemblies. He is able to measure and record in the report the actual active length of the assembly.						
	Capable to image extended sources. Good detection efficiency at 185.7 keV. Good angular resolution. Limited field of view.	Capable based on 1001 keV photon emissions. Limited angular resolution.	Capable. Long acquisition time.	Capable. Multiple measurements (scan elements) are needed to achieve good angular resolution.	Capable based on 1001 keV photon emissions. Good detection efficiency at 1001 keV. Limited angular resolution.	Imager is not spectrometric. Capable to image source pattern. Acceptable detection efficiency at 185.7 keV. Good angular resolution. Limited field of view.	Capable to image extended sources. Excellent detection efficiency at 185.7 keV. Excellent angular resolution. Wide field of view. Image can be zoomed if necessary. Lengths of extended source can be calculated (demonstrated at workshop).

	System3	**System1**	**System4**	**System8**	**System5**	**System6**	**System7**
CUS 08	Nuclear material is stored in a big difficult to access vessel. A gamma picture is taken, fill level is determined, geometry of different material layers inside the vessel are identified (e.g. sediment vs. liquid), or emptiness is verified.						
	Capable. Limited field of view. Many measurements could be needed. Limited performance at 1001 keV. Limited performance in imaging source pattern when source is distributed across the whole field of view.	Not capable to image U-235 based on 185.7 keV photon emissions. Capable based on 1001 keV photon emissions. Limited angular resolution.	Capable. Long acquisition time. Several measurements could be needed.	Multiple measurements (scan elements) are needed to achieve good angular resolution.	Optimal for characterisation of vessel. One volumetric measurement could be sufficient. Not capable to image U-235 based on 185.7 keV photon emissions.	Imager is not spectrometric. Not able to resolve different nuclear materials.	Capable. Several measurements could be needed. Limited performance at 1001 keV. Good performance in imaging source pattern when source is distributed across the whole field.
CUS 09	Multiple pipes/equipment may contain hold-up or in process nuclear material. A wide-angle gamma measurement is taken. The inspector looks at the superimposition of gamma and visual image, and is able to define the key spots where detailed measurement shall be made (ISOCS).						
	Capable. Limited field of view.	Not capable to image U-235 based on 185.7 keV photon emissions. Not capable to image HBPu	Capable.	Multiple measurements (scan elements) are needed to achieve good angular resolution.	Dynamic measurement could be made, distance between source and imager therefore could be greatly	Capable. Limited field of view.	Capable. Wide field of view.

	System3	System1	System4	System8	System5	System6	System7
		based on 208 keV photon emissions. Capable to image U based on 1001 keV photon emissions. Capable to image Pu based on 336 keV, 375 keV and 414 keV photon emissions. Limited angular resolution. Good separation of different radionuclides.			reduced and detection sensitivity increased. Not capable to image U-235 based on 185.7 keV photon emissions. Not capable to image HBPu based on 208 keV photon emissions. Capable to image U based on 1001 keV photon emissions. Capable to image Pu based on 336 keV, 375 keV and 414 keV photon emissions. Limited angular resolution. Good separation of different radionuclides.		
CUS 10	The inspector captures a gamma image from behind the curtain, in an area where the access has been managed by the operator. Without						

	System3	**System1**	**System4**	**System8**	**System5**	**System6**	**System7**
	capturing sensitive visual information, he is still able to verify the presence (or confirm absence) of nuclear material.						
	Capable to detect presence or confirm absence of nuclear material.	Capable to detect presence or confirm absence of nuclear material.	Capable to detect presence or confirm absence of nuclear material.	Multiple measurements (scan elements) are needed to achieve good angular resolution.	Capable to detect presence or confirm absence of nuclear material.	Imager is not spectrometric. Capable to detect presence or confirm absence of radioactive material.	Capable to detect presence or confirm absence of nuclear material.
CUS 11	The inspector captures a gamma image from a room containing sensitive equipment that is not safeguards relevant, or from a room that he cannot/ does not necessarily need to enter (clean room). He makes a gamma image, without capture sensitive visual information, or without entering the room. Inspector able to verify the presence (or confirm absence) of nuclear material.						
	Capable and well suited for localization of unshielded nuclear materials. Limited field of view, several measurements could be needed.	Capable Localization based on low-energy photon emissions can't be done. Imaging low-energy threshold is about 250 keV.	Capable with localization. limited angular resolution. Imaging low-energy threshold for Compton mode is about 150 keV.		Capable. Localization based on low-energy photon emissions can't be done. Imaging low-energy threshold is about 250 keV.	Imager is not spectrometric.	Capable and well suited for localization of unshielded nuclear materials. Wide field of view.
CUS 12	A gamma image of a whole glove box containing multiple small size containers is captured to assess the presence of special nuclear material.						
	Capable. Localization of unshielded SNM is optimal. Short counting time.	Localization of HEU based on 185.7 keV photon emissions is not possible.	Capable. Long counting time. Localization of shielded HEU	Multiple measurements (scan elements) are needed to achieve good	Localization of HEU based on 185.7 keV photon emissions is not possible.	Imager is not spectrometric.	Capable. Localisation of unshielded SNM is optimal. Short counting time.

	System3	**System1**	**System4**	**System8**	**System5**	**System6**	**System7**
	Localization of shielded HEU based on 1001 keV photon emissions is possible. Limited field of view.	Localization of shielded HEU based on 1001 keV photon emissions is possible. Localisation of LBPu is possible. Limited angular resolution.	based on 1001 keV photon emissions is possible.	angular resolution.	Localization of HEU based on 1001 keV photon emissions is possible. Localisation of LBPu is possible. Limited angular resolution.		Localization of shielded HEU based on 1001 keV photon emissions is possible.
CUS 13	During briefing or training, an image of the room along with the gamma sources is shown to inspectors. A map of the gamma radiation is provided to the inspectors. During site activities, inspectors remember more vividly the safe areas and are able to limit their dose rates.						
	Capable to generate image with hot spots (distributed sources).	Capable to generate image with hot spots (distributed sources) for energies of photons above 250 keV.	Capable to generate image with hot spots (distributed sources). Capable to estimate activities of localized sources.	Capable to image detailed dose-rate map.	Capable to generate 3D map with hot spots.	Capable to generate image with hot spots (distributed sources).	Capable to generate image with hot spots (distributed sources). Capable to estimate activities of localized sources.
CUS 14	A gamma camera is setup to monitor SF rods (Fukushima…), or any high activity sources. If one of the gamma sources disappear and alarm is raised.						
	Capable	Capable	Capable	Capable	Capable	Capable	Capable
CUS 15	A gamma camera is setup to monitor an entry/exit point. In the case of the appearance of a high-activity gamma source (Fukushima), an alarm is raised.						
	Capable	Capable	Capable	Capable	Capable	Capable	Capable
CUS 16	Various wastes containing nuclear material have been stored in a pit. A gamma picture is taken; spots with items containing nuclear						

	System3	**System1**	**System4**	**System8**	**System5**	**System6**	**System7**
	material are identified, enabling a general verification of nuclear material declarations. Further detailed verifications are then carried out.						
	Capable. Limited field of view.	Not capable to image U-235 based on 185.7 keV photon emissions. Not capable to image HBPu based on 208 keV photon emissions. Capable to image U based on 1001 keV photon emissions. Capable to image Pu based on 336 keV, 375 keV and 414 keV photon emissions. Limited angular resolution. Good separation of different radionuclides.	Capable.	Multiple measurements (scan elements) are needed to achieve good angular resolution.	Not capable to image U-235 based on 185.7 keV photon emissions. Not capable to image HBPu based on 208 keV photon emissions. Capable to image U based on 1001 keV photon emissions. Capable to image Pu based on 336 keV, 375 keV and 414 keV photon emissions. Limited angular resolution. Good separation of different radionuclides.	Imager is not spectrometric	Capable. Wide field of view.
CUS 17	Wastes containing nuclear material have been stored in a pit. A gamma picture is taken establishing a reference fingerprint used as a containment and surveillance measure; the image is compared to a previous one and documents any significant change that occurred between the inspections.						
	Capable.	Not capable to	Capable.	Multiple	Not capable to	Imager is not	Capable.

	System3	**System1**	**System4**	**System8**	**System5**	**System6**	**System7**
	Limited field of view.	image U-235 based on 185.7 keV photon emissions. Not capable to image HBPu based on 208 keV photon emissions. Capable to image U based on 1001 keV photon emissions. Capable to image Pu based on 336 keV, 375 keV and 414 keV photon emissions. Limited angular resolution. Good separation of different radionuclides.		measurements (scan elements) are needed to achieve good angular resolution.	image U-235 based on 185.7 keV photon emissions. Not capable to image HBPu based on 208 keV photon emissions. Capable to image U based on 1001 keV photon emissions. Capable to image Pu based on 336 keV, 375 keV and 414 keV photon emissions. Limited angular resolution. Good separation of different radionuclides.	spectrometric	Wide field of view.
CUS 18	An inspector captures a gamma image profile of a transport container of fresh fuel assemblies. He is able to visually confirm the presence (or absence) and number of fresh fuel assemblies.						

	System3	**System1**	**System4**	**System8**	**System5**	**System6**	**System7**
	Capable, but performance is limited by the relatively narrow field of view.	Not capable	Capable. Long acquisition time.	Capable, but multiple measurements are needed to achieve good angular resolution.	Not capable	Capable.	Capable.

7 Conclusion

In the result of research and development work over the past decade, a technology breakthrough in gamma-ray imaging has happened. It is associated with application of position sensitive semiconductor radiation detectors, which are combined with coded-aperture and Compton imaging methods. Gamma-ray imagers presented at workshop could be suitable for nuclear safeguards and closely related applications.

The following features of modern gamma-ray imagers have been demonstrated:

- Application of semiconductor radiation detectors
- High-level of segmentation of CZT, CdTe and HPGe detectors
- Application of coded-aperture and Compton imaging methods

In most gamma-ray imagers presented at the workshop, 3D-position sensitive semiconductor radiation detectors are deployed making the application of both coded-aperture and Compton imaging technologies in a single device possible. Due to relatively low energies of photons emitted by U and Pu coded-aperture imaging, it could be considered as a necessary mode of operation of gamma-ray imager for nuclear safeguards, however Compton mode may be useful as well. 3D volumetric Compton imaging has been demonstrated and it provides the possibility of making dynamic measurements for what is of importance for a variety of safeguards contextual usage scenarios.

Features of individual gamma-ray images demonstrated at workshop are summarized below.

System4

This system combines pinhole/Compton imaging methods. U and Pu sources could be successfully imaged in Compton mode of operation, however angular resolution in this operation mode is limited. For imaging of a pattern of extended sources pinhole mode of operation is used. For a detector having diameter 90mm sensitivity of pinhole imaging method could be greatly improved in case, if single pinhole will be replaced with coded aperture. Short system start-up time for electrically cooled HPGe detector has been demonstrated. Excellent values of energy resolution have been measured. In order to decrease weight of the instrument development of the version of portable imager with conventional liquid nitrogen cooling system may be considered.

System5

3D volumetric Compton imaging has been successfully demonstrated and it provides possibility of making dynamic gamma-ray imaging, which is essential for nuclear safeguards and close related application. As soon as CZT detector is used U Compton imaging based on registration of scattering and absorption of 186 keV photons is not possible, so U imaging is limited to the imaging of incident photons with energies 1001 keV (Pa-234m) however Pu Compton imaging has been successfully demonstrated. Active coded mask imaging is under development. Volumetric active coded-mask imaging would be of interest for nuclear safeguards and would solve problem U imaging based on low

energy emissions. Another alternative could be in the development of Volumetric Compton Imager based on relatively low-Z detector such as HPGe detector.

System6

Current version of the System6 coded-aperture imager utilizes a non-spectrometric CdTe detector. Good results have been demonstrated in terms of localization of U and localization of Pu based on Am-241 emissions. Localization capabilities could be improved if spectrometric information will be available, so the image could be constructed based on the particular ROI. Real benefit of usage of CdTe detector could be associated with its spectrometric characteristics, but the detector should be cooled. As it was demonstrated here for a highly pixelated CdTe detector already at detector temperature -10 °C good values of energy resolution could be achieved and in general thermoelectric cooler could be used. Relatively high operating temperature, shortens requirements to thermal insulation system. Further improvement of CdTe crystals growth may be expected in the future and potentially more thick CdTe detectors could be available.

System3

Coded-mask imager has shown excellent performance on point sources and non-complex extended source patterns. 5 mm thickness of room temperature CZT detector array having sensitive volume of 6 cm3 is well suited for U and Pu imaging. For distributed source when it “fills” practically the entire field of view, application of mask/anti-mask imaging method could be considered. HURA mask is used with hexagonal pattern, it may be replaced with mask having rectangular pattern in order to fit detector geometry. As soon as 3D position sensitive CZT detectors are used application of Compton imaging method could be considered as well. Some engineering work is required in order to replace relatively heavy enclosure with more ergonomic and lighter one. In terms of spectrometric capabilities, number of channels of multichannel analyzer needs to be increased.

System7

Coded-aperture imager has been demonstrated. Imager performed well against all tests and scenarios. Mask/anti-mask acquisition strategy was especially useful for imaging of extended source patterns. Variable focal length which allows make gamma-ray image in wide field of view first and then zoom specific areas of interest is an important feature. Availability of spectra of each imaging pixel allows operator to get complete information about radiological composition of localized gamma-ray sources. Applied 3 mm thick Tantalum mask is rather transparent for high-energy photons (Cs-137 and Co-60), so application of Compton imaging method in addition to coded aperture could be essential. Some engineering work is required in order to make automated mask positioning and rotating system more compact.

System1

Compton imaging by means of single 3D position sensitive CZT detector has been successfully demonstrated. Good values of imaged to full-energy peak events have been demonstrated at high energies (Cs-137 and Co-60). Large volume (6 cm3) single crystal room temperature CZT detector is utilized in the imager and excellent values of energy resolution have been obtained (1% at 662 keV).

Coded-aperture imaging is under research. Development of Compton imager based on array of 4 CZT detectors (24 cm3 total sensitive volume) with coded aperture imaging package has been highlighted and it should be suitable for nuclear safeguards applications.

System8

This system could be classified as a gamma-ray scanner. In order to obtain a gamma-ray image multiple measurements needs to be performed. The system is fully automated and could be especially useful for the search and localization of hot spots in high-background radiation environment, as well as on the creation of radioactivity map of the scanned area. As soon as localization of source is made using variations of radiation signals between individual scan elements and in order to obtain good values of angular resolution LaBr3 detector is well collimated what makes system heavy. In order to overcome this difficulty implementation of active collimator operating in anti-coincidence mode with main detector could be considered.

7.1 Conclusion to measurement campaign

The goal of the workshop was to evaluate technologies utilized in gamma-ray imaging systems and make a review and definite conclusion about current status and perspectives of the development of this emerging field with application for nuclear safeguards. In order to achieve this goal, different types of static measurements with radioactive sources and nuclear materials were conducted.

Measurements were submerged into sets of the following eight Experiments:

- Experiment 1 – Measurements of sensitivity in wide energy range of imager operation
- Experiment 2 – Overnight localization and identification of weak source in the presence of masking source
- Experiment 3 – Measurements of sensitivity to nuclear materials, time to detect, identify and localize nuclear materials
- Experiment 4/5 – Angular resolution measurements
- Experiment 6 – Localization performance for extended sources
- Experiment 7 (a) – False alarm rate
- Experiment 7 (b) – High-background masking scenario
- Experiment 8 (a) – Angular resolution for extended sources
- Experiment 8 (b) – Glove box scenarios

In addition dynamic measurements have been made to reveal performance characteristics of 3D volumetric Compton imager.

Tests under experiments 1 and 3 were focused on the estimation of total sensitivity and sensitivity in full-energy peaks. Experiments were conducted with Am 241, Cs-137 and Co-60 to cover wide energy range of imager operation and with HBPu, LBPu, HEU and LEU to evaluate sensitivity to nuclear materials. Sensitivity measurements allowed to evaluate and compare suitability of gamma-ray imagers for both imaging modes.

Test under Experiment 2 and 7 (b) have revealed the importance of having spectrometric information for coded-aperture imaging in order to enhance imaging capabilities, which is achieved by imaging the

events from selected region of interest in the spectrum. In Compton imaging full-energy peak events are imaged, therefore Compton imager shall be spectrometric.

As soon as nuclear materials such as HEU and LBPu are characterized by relatively low energies of emitted photons coded-aperture imaging could be considered as a necessary mode of imager operation for the tasks associated with activities of nuclear safeguards.

Angular resolution and field of view of coded aperture imaging is a function of mask pattern, distance between mask and detector and spatial resolution of the detector. Therefore, basic tests under experiments 4/5 and 8b were aimed to reveal performance of coded-aperture imagers and in particular to evaluate level of segmentation of semiconductor radiation detectors.

Tests under Experiment 6 have demonstrated, an advantage of using mask/anti-mask imaging method for imaging of a pattern of widely distributed source.

Tests under Experiment 7 (b) and Experiment 8 (b) have demonstrated, an advantage of having combined coded-aperture/Compton imager.

Tests under Experiment 2 and 8 (a) have demonstrated an independence of gamma-ray imagers in their ability to detect and localize radioactive source from necessity in having background measurements.

Some Pu experiments with coded-aperture imagers were affected by low-energy Am-241 emissions as imagers were able to localize unshielded Pu sources very fast, however availability of spectrometric information allowed mitigate this difficulty performing further analysis based on the regions of interests characteristic for LBPu and HBPu and excluding low-energy photon emissions.

Methodology of measurements of such basic imaging parameters as field of view and angular resolution as well as such derived parameters as time to alarm, time to identify and time to localize needs to be developed.

Field of view and its uniformity is estimated measuring sensitivity of gamma-ray imager to the point source positioned at different angles with reference to the detector.

Angular resolution is estimated accumulating gamma-ray image of point source; when a necessary number of imaged events is obtained with full-widths of half maximum of imaged peak is measured.

Time to alarm algorithm utilized in one system and based on N*sigma comparisons of a radiation signal amplitude in individual pixels with mean value of signal obtained in all imaged pixels, allows to control false alarm rate and avoid background measurements, in the meantime this algorithm is more suitable for point rather than distributed sources. Time to alarm could be estimated based on accumulation of a gamma-ray image of two point sources separated across the field of view.

Time to localize algorithm could be based on N*sigma comparison of mean radiation signal amplitude obtained in the cluster of imaged pixels with mean value of signal obtained in all imaged pixels. Time to localize may be estimated accumulating gamma-ray image of two point sources separated across the field of view and could be linked to the angular resolution measurements.

Time to identify may be linked to spectrometric performance. As soon as full-energy peak is identified in the spectrum detection flag (independent from background measurements) may be raised what could alert an operator about presence of the source within imager field of view.

At the workshop a majority of tests were made with unshielded nuclear materials, which clearly indicated advantages of using coded-aperture imaging method. Tests with shielded nuclear materials may reveal advantages of Compton imaging method as with increase of energies of incident photons improvement of imaging efficiency and angular resolution could be expected.

In the result of the analysis of experimental results it can be concluded that new generation of gamma-ray imagers having the following essential features already demonstrated by participants at this workshop:

- Application of semiconductor radiation detectors
- High-level of segmentation of CdTe, CZT and HPGe detectors
- Application of 3D position sensitive semiconductor detectors
- Combination of coded-mask/Compton imaging methods
- Performing dynamic gamma-ray imaging – 3D volumetric Compton imager has been successfully demonstrated.

Gamma-ray imagers demonstrated at workshop can be suitable for nuclear safeguards and are capable to address majority of the contextual user scenarios defined by the IAEA.

8 References

[1] A. N. Sudarkin et al. *HERV - High Energy Radiation Visualizer, A New System for Imaging in X-Ray and Gamma Regions.* IEEE Transactions on Nuclear Science, Volume 43, Issue 4, pg. 2427 – 2433, 1996

[2] O. Gal et al. *CARTOGAM – a portable gamma camera for remote localisation of radioactive sources in nuclear facilities.* Nuclear Instruments and Methods in Physics Research A 460 (2001) 138–145

[3] O. P. Ivanov et al. *New Portable Gamma-Camera for Nuclear Environment and Its Application at Rehabilitation Works.* IEEE 2004.

[4] O. Gal et al. Development of a portable gamma camera with coded aperture Nuclear Instruments and Methods in Physics Research A 563 (2006) 233–237

[5] K.A. Hughes et al. *RadScan 600 - A Portable Instrument for the Remote Imaging of Gamma Contamination: Its Design and use in Aiding Decommissioning Strategy*. IEEE 1997

[6] Klaus-Peter Ziock. *Gamma-ray Imaging Spectrometry. Science and Technology Review*. October 1995.

[7] Peter E. Vanier. *Analogies between neutron and gamma-ray imaging.* Brookhaven National Laboratory. 2006

[8] L. J. Schultz et al. *Hybrid coded aperture and Compton imaging using an active mask.* Nuclear Instruments and Methods in Physics Research A 608 (2009) 267–274

[9] John A. Mason et al. *DEVELOPMENT AND TESTING OF A NOVEL GAMMA RAY CAMERA FOR RADIATION SURVEYING, CONTAMINATION MEASUREMENT AND RADIATION DETECTION.* 12-A-409-INMM

[10] John A. Mason et al. *Testing and Performance Validation of a Sensitive Gamma Ray Camera Designed for Radiation Detection and Decommissioning Measurements in Nuclear Facilities.* WM2013 Conference, February 24 – 28, 2013, Phoenix, Arizona, USA

[11] L. Mihailescu et al. *SPEIR: A Ge Compton camera.* Nuclear Instruments and Methods in Physics Research A 570 (2007) 89–100

[12] P. N. Luke et al. *Amorphous Ge Bipolar Blocking Contacts on Ge Detectors.* IEEE TRANSACTIONS ON NUCLEAR SCIENCE. VOL. 39, NO. 4.1992

[13] Free-piston Stirling-cycle cryocoolers. http://sunpowerinc.com/

[14] Pulse tube Stirling-cycle cryocoolers. http://www.thales-cryogenics.com/

[15] RATZLAFF, CHELSEA ROBYN. *Detector Response Function for a Germanium Strip Type Detector/Imager*. Master of Science Thesis, 2014.

[16] Bruks et al. *A 4-π Field of View Compton Imager Based on a Single Planar Germanium Detector*. IEEE

[17] Ethan Hull. *Germanium Gamma-Ray Imager*. Presentation, IAEA October 2015.

[18] GeGI - Graphical User Interface. http://phdsco.com/news/view/14/gegi-performs-at-iaea-workshop-

[19] Klaus Ziock. *Coded-aperture Gamma-Ray Imaging.* Presentation. IAEA October 2015

[20] Klaus Ziock. *ORNL Gamma-Ray Imager Results from the IAEA TDW on Gamma-Ray Imaging*. ORNL/LTR-2015/679. November 2015

[21] Christopher G. Wahl et al. *The Polaris-H imaging spectrometer.* Nuclear Instruments and Methods in Physics Research A 784 (2015) 377 – 381

[22] F. Zhang et al. *Events Reconstruction in 3-D Position Sensitive CdZnTe Gamma-ray Spectrometers (Ph. D. Thesis).* University of Michigan, 2005.

[23] W. Kaye. *Energy and Position Reconstruction in Pixelated CdZnTe Detectors (Ph. D. Thesis).* University of Michigan, 2012.

[24] Sonal Joshi. *Coded Aperture Imaging Applied to Pixelated CdZnTe Detectors (Ph. D. Thesis)*, University of Michigan, 2014.
[25] Willy Kaye. *Polaris and Orion 3D CdZnTe Gamma-Neutron Imaging Spectrometers.* Presentation at IAEA, October 2015.
[26] G. Montemont. *CEA Portable Gamma-Ray Imagers.* Presentation, IAEA October 2015.
[27] H. Lemaire et al. *Implementation of an imaging spectrometer for localization and identification of radioactive sources.* Nuclear Instruments and Methods in Physics Research A 763 (2014) 97-103.
[28] M. Gmar et al. *GAMPIX: A new generation of gamma camera.* Nuclear Instruments and Methods in Physics Research A 652 (2011) 638-640.
[29] Mark Amman et al. *Detector Module Development for the High Efficiency Multimode Imager*. IEEE Nuclear Science Symposium Conference Record, 2009.
[30] R. Barnowski, A. Haefner, K. Vetter. *LBNL's High Efficiency Multimodal Imager (HEMI) and Demonstration of Hand-Held Volumetric Imaging.* December 2015.
[31] Michelle Lee Galloway. *Characterization and Applications of a CdZnTe-Based Gamma-Ray Imager, (Ph. D. Thesis).* University of California, Berkeley, 2014.
[32] S. Dubos et al. *ORIGAMIX, a CdTe-based spectro-imager development for nuclear applications.* Nuclear Instruments and Methods in Physics Research A 787 (2015) 302-307.

9 Technical Contacts

Dimitri Finker — d.finker@iaea.org

Andrey Sokolov — a.sokolov@iaea.org

10 Document Revision History

Revision History		
Version No.	Release Date	Description of changes
1		New Document.